

2015

Effects of regulatory light chain phosphorylation on mutant and wild-type cardiac muscle myosin mechanochemistry

<https://hdl.handle.net/2144/13939>

"Downloaded from OpenBU. Boston University's institutional repository."

BOSTON UNIVERSITY
SCHOOL OF MEDICINE

Dissertation

**EFFECTS OF REGULATORY LIGHT CHAIN PHOSPHORYLATION ON
MUTANT AND WILD-TYPE CARDIAC MUSCLE MYOSIN
MECHANOCHEMISTRY**

by

ANASTASIA SMARO KARABINA

B.S., University of Michigan, 2008

Submitted in partial fulfillment of the
requirements for the degree of
Doctor of Philosophy

2015

Approved by

First Reader

Dr. Jeffrey Moore, Ph.D.
Professor of Physiology and Biophysics

Second Reader

Dr. William Lehman, Ph.D.
Professor of Physiology and Biophysics

DEDICATION

To Zach

Because of you I am a better version of myself

ACKNOWLEDGEMENTS

The work presented in this dissertation would not have been possible without the support and guidance of my advisor, Jeffrey Moore. His enthusiasm for science, eagerness to determine the unknowns, and creativity in problem solving foster an environment that is both stimulating and motivating. I especially appreciate Jeff's willingness and dedication to helping me (and all of his students) learn the skills necessary to become a successful scientist, both in the pursuit of scientific research and a professional career. Jeff's excitement for science is infectious and is matched by his excitement for undertakings outside the lab; it has made working in the lab something that I look forward to from day to day throughout the years.

**EFFECTS OF REGULATORY LIGHT CHAIN PHOSPHORYLATION ON
MUTANT AND WILD-TYPE CARDIAC MUSCLE MYOSIN
MECHANOCHEMISTRY**

ANASTASIA SMARO KARABINA

Boston University School of Medicine, 2015

Major Professor: Jeffrey R. Moore, Ph.D., Professor of Physiology and
Biophysics

ABSTRACT

Cardiac muscle contraction is responsible for pumping blood throughout the body. The cyclical, ATP-hydrolysis dependent interaction of the myosin motor protein with filamentous actin drives muscle contraction. During this process the α -helical neck region of myosin acts as a lever arm, transmitting contractile force between thick and thin filaments by amplifying small conformational changes in the myosin motor domain. The resulting relative displacement of thick and thin filaments causes muscle shortening. The regulatory light chain (RLC) of myosin mechanically supports the lever arm by binding to the myosin heavy chain neck region; this is a crucial interaction in maintaining myosin's ability to produce force and motion. We investigated the role of N-terminal modifications of the RLC in modulating actomyosin contractility at the molecular level. Phosphorylation of the RLC is a naturally occurring post-translational modification of the RLC N-terminus that is important for cardiac function and has been shown to enhance contractility at the cellular level. In contrast, genetic mutations of the RLC that lead to familial

hypertrophic cardiomyopathy (FHC) disrupt cardiac function and trigger remodeling of the cardiac muscle structure. We studied two FHC-linked mutations, N47K and R58Q, located in the N-terminus of the RLC in close proximity to the phosphorylation site. Using *in vitro* motility assays we examined how RLC modifications affect the mechanochemical properties of cardiac β -myosin. We found that the FHC mutations reduced myosin force and power generation, in contrast to RLC phosphorylation which increased myosin force and power for WT and mutant myosins. Phosphorylation of mutant RLC resulted in a restoration of the mutation-induced decreases in contractility to WT dephosphorylated levels. These results point to RLC phosphorylation as a general mechanism to increase force production of the individual myosin motor and as a potential target to ameliorate the fundamental contractile FHC-induced phenotype.

TABLE OF CONTENTS

TITLE PAGE.....	i
COPYRIGHT	ii
APPROVED BY	iii
DEDICATION	iv
ACKNOWLEDGEMENTS.....	v
ABSTRACT	vi
TABLE OF CONTENTS	viii
LIST OF TABLES	xii
LIST OF FIGURES	xiii
LIST OF ABBREVIATIONS	xv
CHAPTER 1 – INTRODUCTION.....	1
1.1 Significance and Scope of Thesis.....	1
1.2 Muscle Contraction	3
1.2.1 Cardiac Muscle Histology	4
1.2.2 Sarcomere: The Contractile Unit	7
1.2.3 Myosin	12
1.2.4 Acto-Myosin Biochemical Cycle.....	17
1.2.5 Load Dependence	20
1.3 Heart Physiology	21
1.3.1 Gross Anatomy and Function	23

1.3.2 Modulation of Contraction via RLC Phosphorylation	29
1.3.3 Familial Hypertrophic Cardiomyopathy	35
CHAPTER 2 – METHODS AND MATERIALS.....	42
2.1 Purification of Proteins	42
2.1.1 Porcine Cardiac Myosin.....	42
2.1.2 Regulatory Light Chains	43
2.1.3 Myosin Light Chain Kinase	44
2.2 Preparation of Proteins	46
2.2.1 RLC Phosphorylation.....	46
2.2.2 RLC Depletion and Exchange	48
2.2.3 TRITC Phalloidin Actin.....	49
2.3 Polyacrylamide Gel Electrophoresis (PAGE)	49
2.3.1 SDS-PAGE	49
2.3.2 Native-PAGE	50
2.4 Actin-Activated ATPase	52
2.5 <i>In Vitro</i> Motility Assays	53
2.5.1 Epifluorescence	54
2.5.2 Standard Motility Assay Protocol.....	57
2.5.3 Unloaded Motility Assays.....	59
2.5.4 Frictional Loading Motility Assays.....	60
2.5.5 Power Output Transformation.....	68
2.5.6 Inhibition of Loaded Motility by ADP	70

CHAPTER 3 – RESULTS: Studies of Physiological and Pathological RLC

Modifications	73
3.1 RLC Phosphorylation.....	75
3.2 RLC Depletion and Reconstitution	77
3.3 Actin-Activated ATPase	78
3.4 <i>In Vitro</i> Motility Assays	79
3.4.1 Myosin Maximal Sliding Velocity.....	80
3.4.2 Myosin Isometric Force.....	81
3.4.3 Myosin Power Output	86
3.4.4 Effect of Exogenous ADP on Loaded Velocity.....	90
CHAPTER 4 – DISCUSSION AND PERSPECTIVES.....	92
4.1 Molecular Effects of RLC Modifications on Myosin Mechanochemistry .	95
4.2 Higher Order System Function.....	104
4.2.1 Correlating RLC Phosphorylation Effects to Cellular and <i>In Vivo</i> Function .	104
5.2.2 Familial Hypertrophic Cardiomyopathy-linked Mutations	106
CHAPTER 5 – FUTUTRE DIRECTIONS	112
5.1 Optical Trapping	112
5.1.1 Basic Principles	112
5.1.2 Optical Layout.....	116
5.1.3 Calibrations.....	119
5.1.4 Three Bead Assay	122
5.2 Towards Thick Filaments.....	127

5.2.1 Contribution of Thick Filament Backbone to <i>In Vitro</i> Measurements	127
5.2.2 Thick Filament Motility Assays.....	132
5.3 Summary	135
CHAPTER 6 – REFERENCES.....	138
CURRICULUM VITAE	155

LIST OF TABLES

Table 1: Actin-Activated Myosin ATPase Rates	79
Table 2: Loaded Parameters of Cardiac β -Myosin Predicted from Model Fitting	88

LIST OF FIGURES

Figure 1.1: RLC Binds to S1-S2 Junction of Myosin	1
Figure 1.2: Cellular Arrangement of Cardiac Muscle Tissue	5
Figure 1.3: Components of Cardiac Muscle Cells	6
Figure 1.4: Sarcomere Structure	8
Figure 1.5: Thick and Thin Filament Structure	9
Figure 1.6: Three State Model of Regulation	12
Figure 1.7: Myosin Structure	13
Figure 1.8: Myosin Powerstroke	14
Figure 1.9: Regulatory Light Chain	16
Figure 1.10: Actomyosin Cross-bridge Cycle	18
Figure 1.11: Blood Flow through the Heart	23
Figure 1.12: Ventricular Pressure During Heartbeat	25
Figure 1.13: Anatomy of the Left Ventricle	28
Figure 1.14: FHC Pathology	36
Figure 2.1: Comparison of Glycerol versus Urea as Gel Medium	51
Figure 2.2: Illustration of the <i>In Vitro</i> Motility Assay	54
Figure 2.3: Fluorescence Microscope and Filter Cube Schematic	56
Figure 2.4: Diagram of the Frictional Loading Motility Assay	61
Figure 3.1: Phosphorylation of hvRLCs by MLCK	75
Figure 3.2: RLC Exchange on PC β -Myosin	77
Figure 3.3: Linear Regression Fit to Solution Absorbance Data	78

Figure 3.4: Maximal Actin Sliding Velocity	81
Figure 3.5: Frictional Loading Motility Assay of WT and Mutant Myosins	82
Figure 3.6: Frictional Loading Assays Comparing Phosphorylation State	83
Figure 3.7: Trend of Increased Isometric Force Production	84
Figure 3.8: Average Myosin Isometric Force	86
Figure 3.9: Transformation of Data and Fits to Hill Equation for Power	87
Figure 3.10: Comparison of Myosin Power Output	88
Figure 3.11: Model Fitting to the Physiological Range of Loads	89
Figure 3.12: Effect of Exogenous ADP on Loaded Actin Sliding Velocity	91
Figure 4.1: Effect of Lever Arm Stiffness	99
Figure 5.1: Optical Trapping Force Diagram	113
Figure 5.2: Optical Trapping Design	117
Figure 5.3: Detection Optics Schematic	118
Figure 5.4: AOD Calibration	120
Figure 5.5: QD Calibration	121
Figure 5.6: Optical Trap Stiffness Calibration	122
Figure 5.7: Illustration of the Three Bead Assay	123
Figure 5.8: Actin Dumbbell Linkage Calibration	124
Figure 5.9: Sample Data Trace of Myosin Stiffness Measurement	125
Figure 5.10: Single Myosin Thick Filament	128
Figure 5.11: Purification of LMM Rod from Full Length Myosin	130
Figure 5.12: Fluorescence Microscopy of LMM Thick Filament Backbone	131

LIST OF ABBREVIATIONS

<i>ABP</i>	actin binding protein
<i>ADP</i>	adenosine diphosphate
<i>ANOVA</i>	analysis of the variance
<i>AOD</i>	acousto-optic deflector
<i>ATP</i>	adenosine triphosphate
<i>AV</i>	atrioventricular
<i>BES</i>	N,N-Bis(2-hydroxyethyl)-2-aminoethanesulfonic acid
<i>BSA</i>	bovine serum albumin
<i>CaM</i>	calmodulin
<i>CCD</i>	charge coupled device
<i>CDTA</i>	1,2-cyclohexylenedi nitrilo-tetraacetic acid
<i>ddH₂O</i>	double distilled water
<i>DEAE</i>	diethylaminoethyl cellulose
<i>DTT</i>	dithiothreitol
<i>EDTA</i>	ethylenediaminetetraacetic acid
<i>EGTA</i>	ethylene glycol tetraacetic acid
<i>ELC</i>	essential light chain
<i>ELIPA</i>	enzyme linked inorganic phosphate assay
<i>EM</i>	electron microscopy
<i>EMCCD</i>	electron multiplying charge coupled device
<i>FHC</i>	familial hypertrophic cardiomyopathy

hvRLC	human ventricular regulatory light chain
<i>LMM</i>	light meromyosin
MESG	2-amino-6-mercapto-7-methylpurine ribonucleoside
<i>MHC</i>	myosin heavy chain
<i>MLCK</i>	myosin light chain kinase
<i>MOPS</i>	3-(N-morpholino)propanesulfonic acid
MyBP-C	myosin binding protein C
MYPT2	myosin phosphatase targeting subunit 2
PAGE	polyacrylamide gel electrophoresis
<i>PC</i>	porcine cardiac
PIPES	piperazine-N,N'-bis(2-ethanesulfonic acid)
<i>PMSF</i>	phenylmethylsulphonyl fluoride
PNP	purine nucleoside phosphorylase
PP1c- δ	protein phosphatase 1 catalytic subunit delta
P-V	pressure-volume
QD	quadrant detector
<i>RLC</i>	regulatory light chain
<i>S1</i>	subfragment 1
<i>S2</i>	subfragment 2
SCD	sudden cardiac death
<i>SDS-PAGE</i>	sodium dodecyl sulfate polyacrylamide gel electrophoresis
TEMED	tetremethylethylenediamine

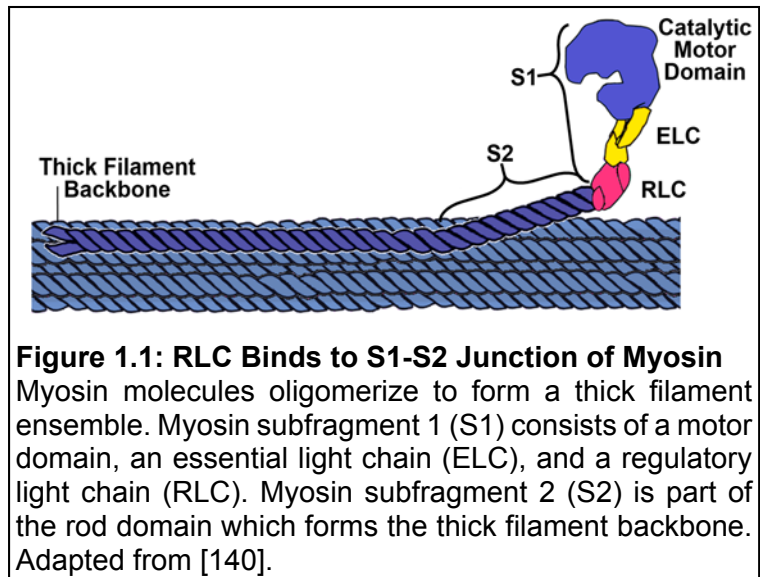
<i>Tris</i>	tris(hydroxymethyl)aminomethane
<i>TRITC</i>	tetramethyl rhodamine isothiocyanate
<i>WT</i>	wild type

CHAPTER 1 – INTRODUCTION

1.1 Significance and Scope of this Thesis

My overall goal as a researcher in basic science is to understand the mechanisms of cardiac muscle contraction and how these processes are altered in disease. The studies presented in this thesis are focused on the regulatory light chain (RLC) of myosin. Myosin is the motor protein directly responsible for generating the force and motion of muscle contraction by using the chemical energy from ATP

hydrolysis to translocate actin thin filaments. The RLC binds to the S1-S2 junction of myosin in a position where it can interact with and influence the thick filament ensemble of myosins, as



well as the individual myosin protein (Figure 1.1). The aim of my dissertation is to understand how modifications of the RLC modulate cardiac muscle contraction at the molecular level. Specifically, I studied phosphorylation of the RLC and two genetic mutations of the RLC which lead to cardiac disease.

Phosphorylation of the RLC is a naturally occurring post-translation modification that is critical to the proper functioning heart. RLC phosphorylation is constitutively maintained at about 50% in the heart and modulates cardiac contraction; however, the mechanism by which it exerts its effects is not fully understood. In skeletal muscle fibers, RLC phosphorylation is correlated with potentiation of the isometric force response [134], and *in vitro* studies indicate that it alters myosin thick filament structure presumably by repelling myosin heads away from the thick filament [69]. Phosphorylation of the RLC has also been associated with changes in the stiffness of the lever arm and/or hinge region in skeletal [42] and smooth [64] muscle myosins. Understanding the molecular mechanism of RLC phosphorylation is important because phosphorylation levels are often altered in disease [56, 86, 142, 146].

Cardiomyopathy is a condition where the heart muscle is structurally or functionally abnormal. Two cardiomyopathy-linked mutations, N47K and R58Q, located in the RLC N-terminus are studied in this work. Previously, both mutations have been shown to disrupt the load-dependent behavior of cardiac myosin [41]. Because of the opposing effects of phosphorylation and the RLC mutations, I have tested the hypothesis that phosphorylation of the mutant RLC rescues mutation-induced defects in the myosin molecule.

I investigated the effect of RLC mutations and phosphorylation on myosin contractility at the molecular level using *in vitro* motility assays with an applied exogenous load to gain a better understanding of how RLC modifications can

lead to the effects and phenotypes that are observed at the organ level. I found that RLC mutations reduced the force generating capabilities of isolated cardiac myosin, while phosphorylation of the RLC enhanced the force producing ability of WT myosin, as well as that of the mutant myosins. The enhanced force production of mutant myosins in the phosphorylated state resulted in a restoration of force production to WT dephosphorylated levels.

Note to the reader: Unless otherwise noted, the information provided in sections 1.2.1, 1.2.2, and 1.3.1 can be found in the following textbooks: “Muscle Contraction” by Bagshaw 1993, and “Physiology of the Heart & Circulation” by Little 1981. The reader is referred to these texts for further information.

1.2 Muscle Contraction

There are three types of muscle tissue in the human body: skeletal, smooth, and cardiac muscle. Regardless of the type, all muscles contract, producing force and motion. Skeletal muscle is attached to bones by tendons, and is responsible for moving the skeleton. Although skeletal muscle has many functions ranging from rapid body movement to maintaining posture, it is voluntarily controlled. Smooth muscle is found lining the walls of many hollow organs, blood vessels and respiratory passageways and is responsible for changes in organ shape and internal organ movements such as peristaltic contractions during digestion and pupil dilation. Cardiac muscle is found

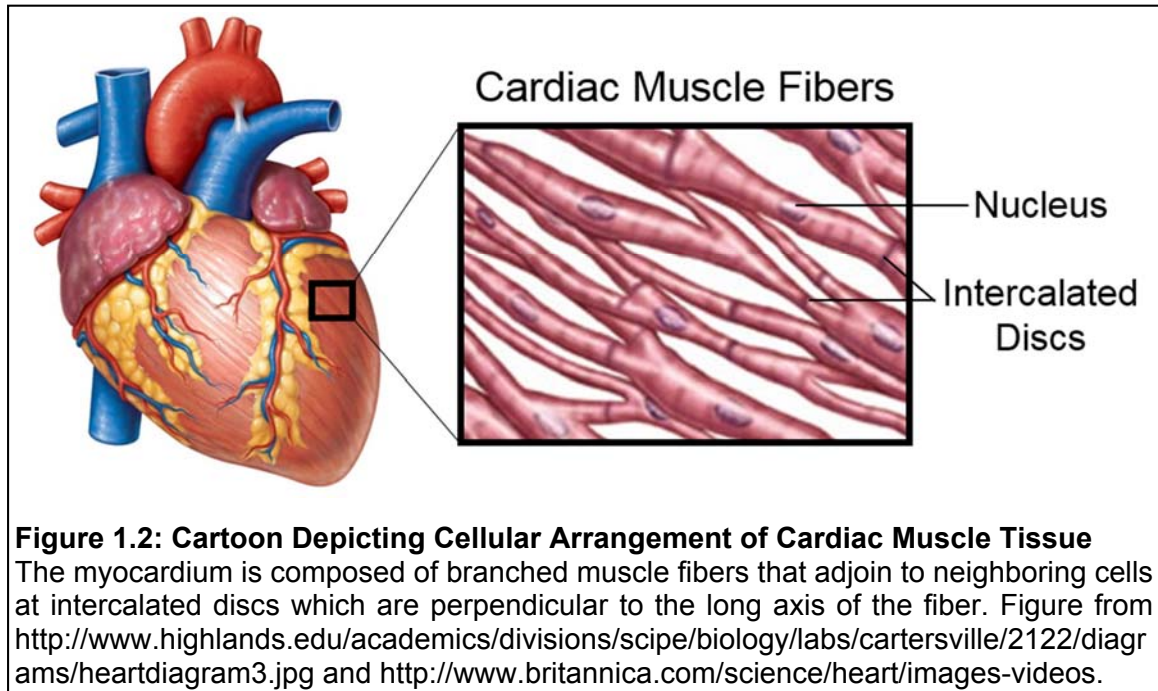
exclusively in the walls of the heart, and is responsible for pumping blood through the circulatory system. Smooth and cardiac muscle contraction is involuntary.

The focus of this thesis is on contractile proteins isolated from cardiac muscle. In the following sections of this chapter, I will introduce the cardiac muscle cell, basic properties of muscle contraction, the structure-function relationship of the heart and how it is affected by RLC phosphorylation and FHC mutations.

1.2.1 Cardiac Muscle Histology

Cardiac muscle cells, also called fibers or myocytes, are elongated, thin and branched. Due to their branched nature and end-to-end connections cardiac muscle cells form an intertwined directional fibrous mesh that comprises the muscle tissue of the heart (Figure 1.2). The sarcolemma is the cell membrane that surrounds each fiber and is responsible for the end-to-end connection by forming intercalated discs at the junction of two cells. Intercalated discs consist of overlapping finger-like protrusions of the sarcolemma that contain desmosomes which create strong cell-cell adhesions, fascia adherens which anchor internal cellular structures to the membrane, and numerous gap junctions which directly connect the cytoplasm of neighboring cells facilitating the rapid spread of an electrical signal from cell to cell. Intercalated discs are only found in cardiac muscle cells, and allow depolarization to spread throughout the cardiac tissue to create the synchronized pumping action of the tissue while preventing adjoining

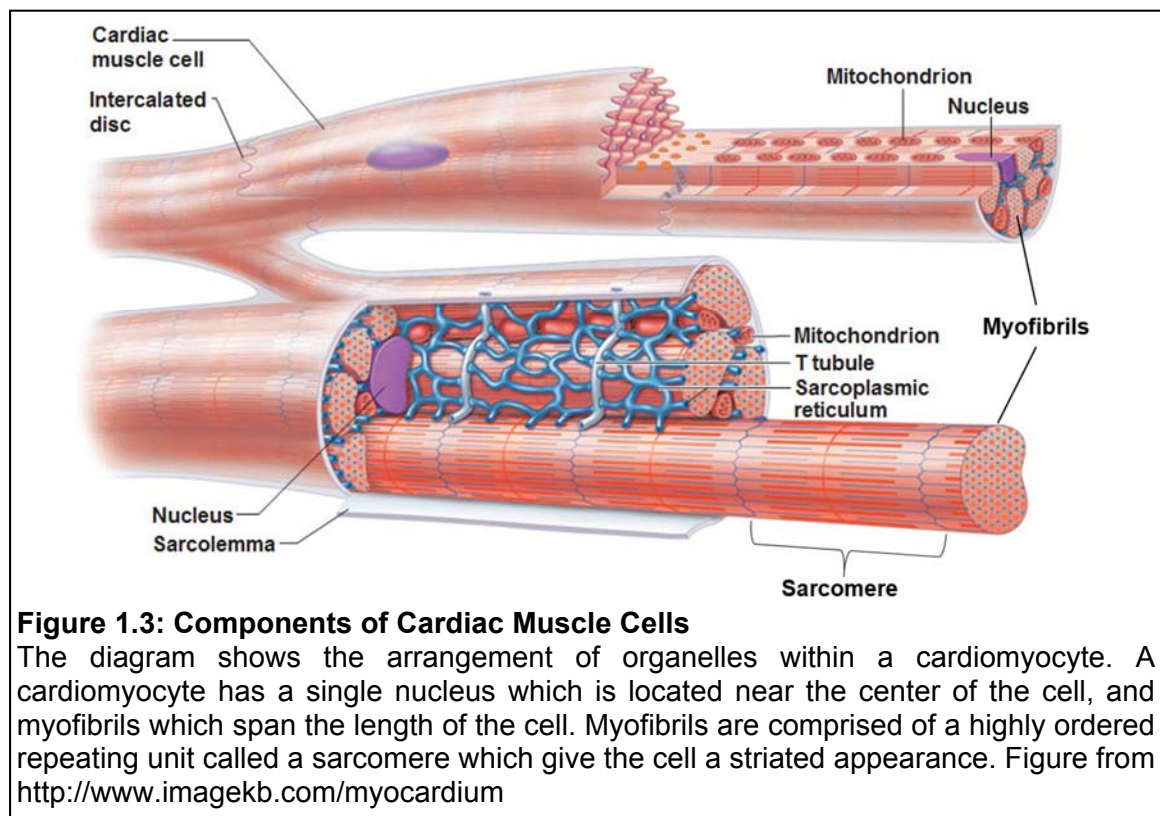
cells from separating under the shear stress of contraction.



The cytoplasm of cardiac muscle fibers largely consists of myofibrils, highly specialized cylindrical organelles that span the length of the cell. Myofibrils are responsible for the physical contraction of muscle cells (Figure 1.3). The characteristic light and dark banding pattern of single myofibril results from a repeating structural unit called a sarcomere (Figure 1.3). Each sarcomere is a highly organized array of overlapping thick and thin filaments that shortens and lengthens as the thick and thin filaments slide relative to each other. Synchronized contraction of sarcomeres within the myofibrils results in the large scale contraction of the muscle fiber.

Muscle contraction is activated by calcium binding to the thin filament (Figure 1.6). The simultaneous contraction of parallel-arranged myofibrils within a

muscle fiber is triggered by a large scale release of calcium into the cytoplasm. When an action potential is initiated in a cardiac muscle cell, calcium is released into the cytoplasm from regularly spaced invaginations in the sarcolemma known as t-tubules (Figure 1.3). The calcium released from t-tubules is not sufficient to activate the muscle, but this initial calcium release triggers the release of large stores of calcium from within the sarcoplasmic reticulum, an extensive network of tubules that surrounds each myofibril and is responsible for storing, releasing, and sequestering calcium in the course of the activation-relaxation cycle during the heartbeat (Figure 1.3). The sarcoplasmic network assures that calcium is released throughout the whole cell thus activating contraction simultaneously along the entire length of the fiber.



The heart is the most worked muscle in the body, continually contracting to pump blood ~70 times/min over a lifetime, and therefore requires a constant source of energy. For this reason, cardiac muscle cells have an extremely high mitochondrial density in between myofibrils which allow the cell to quickly supply large amounts of ATP to adjacent sarcomeres, where the chemical energy from the hydrolysis of ATP is converted into kinetic energy in the form of muscle contraction.

1.2.2 Sarcomere: The Contractile Unit

The banding pattern observed in striated muscle results from the series arrangement of cylindrical structures called sarcomeres, the fundamental contractile units of muscle. Each sarcomere consists of a parallel lattice of interdigitated thick and thin filaments held in place between two Z-discs, which form boundaries between neighboring sarcomeres (Figure 1.4). Thin filaments contain primarily actin and are anchored directly to the Z-disc, which is comprised primarily of α -actinin, an actin binding protein. Actin filaments extend from the Z-disc towards the center of the sarcomere. The motor protein myosin forms bipolar thick filaments, the center of which attach to a protein scaffold at the midline of the sarcomere. Each end of the thick filament is tethered to the nearest Z-disc by a large elastic protein called titin. Opposite ends of thick filaments are inserted into the lattice of thin filaments that attach and extend from the nearest Z-disc. The array of thick and thin filaments reveals a highly defined

myofilament lattice when viewed in cross-section. In the overlapping region of myofilaments, the thin filaments form a hexagonal arrangement around each thick filament, and in turn thick filaments form a triangular arrangement around each thin filament (Figure 1.4).

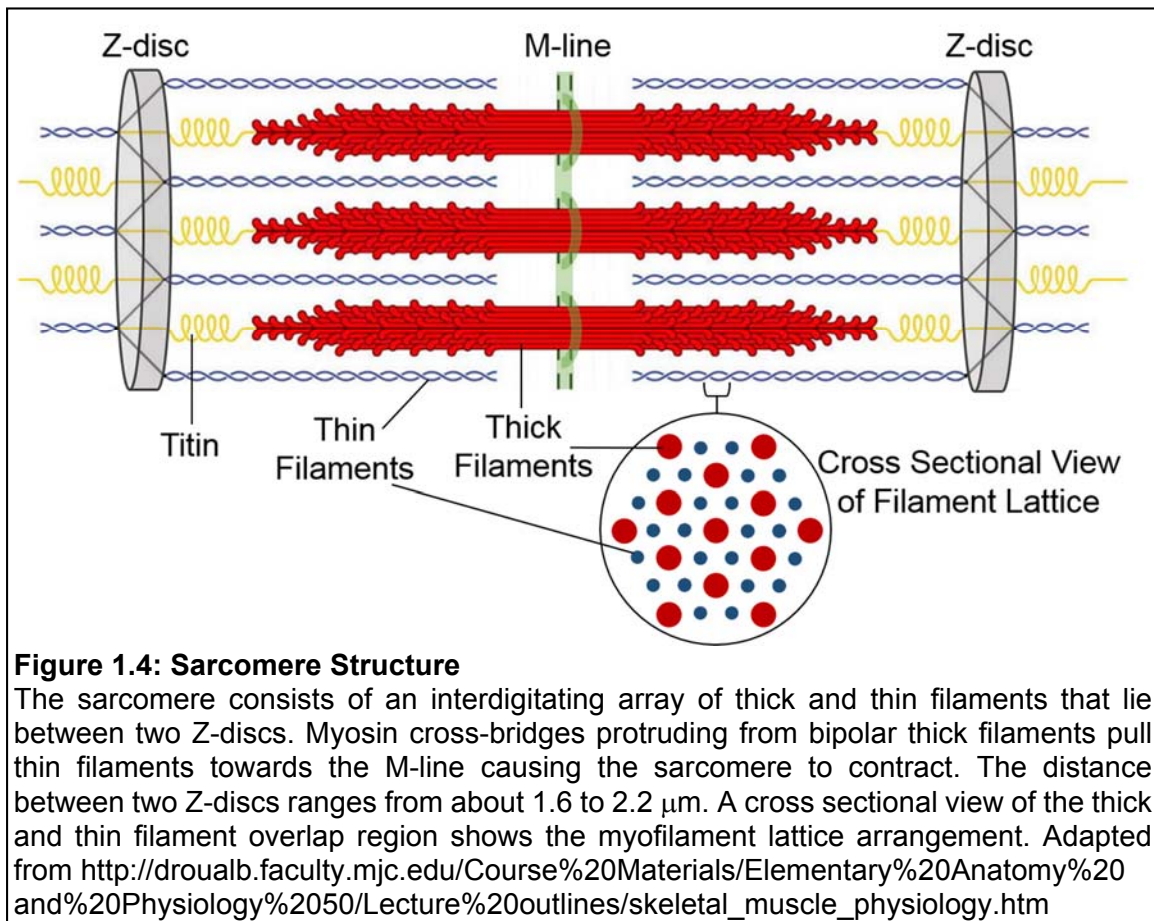
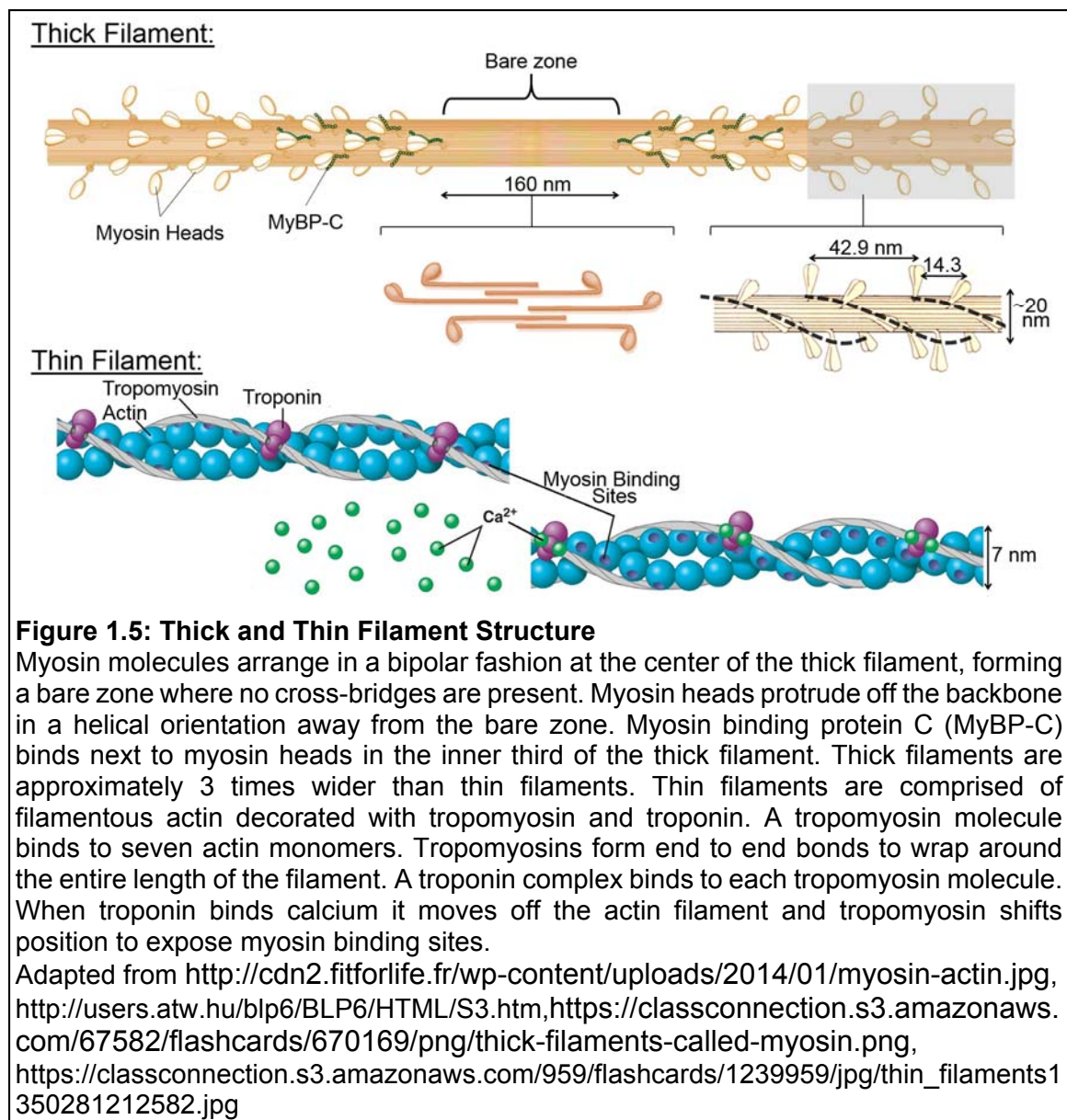


Figure 1.4: Sarcomere Structure

The sarcomere consists of an interdigitating array of thick and thin filaments that lie between two Z-discs. Myosin cross-bridges protruding from bipolar thick filaments pull thin filaments towards the M-line causing the sarcomere to contract. The distance between two Z-discs ranges from about 1.6 to 2.2 μm . A cross sectional view of the thick and thin filament overlap region shows the myofilament lattice arrangement. Adapted from http://droualb.faculty.mjc.edu/Course%20Materials/Elementary%20Anatomy%20and%20Physiology%2050/Lecture%20outlines/skeletal_muscle_physiology.htm

Myosin forms cross-bridges that extend from the thick filament backbone which interact with actin in the thin filaments to shorten the sarcomere. Thick filament cross-bridges pull the thin filaments towards the center of the sarcomere, increasing the level of filament overlap and moving both Z-discs closer together. Thick filaments are 1.6 μm long, thin filaments are 0.8 μm long,

and the sarcomere is approximately 2 μm long at rest [112]. During cardiac contraction the sarcomere will shorten by up to 20% [14] or about 400 nm. Given that sarcomeres in a single myofibril are connected in series, a small sarcomeric length change will produce a significant shortening of the myofibril and muscle fiber.



Thick Filament Structure

Myosin is composed of a long rod-like domain connected to a globular domain at one end. Myosin rod domains oligomerize in a parallel, staggered fashion to form the thick filament backbone while the globular domains sit at the surface of the thick filament and form the cross-bridges. Myosin molecules arrange in a bipolar fashion at the center of a thick filament with their rod domains aligned in an anti-parallel orientation; this creates a bare zone at the mid-region of the filament that is devoid of cross-bridges (Figure 1.5). Another protein associated with the thick filament is myosin binding protein C (MyBP-C), which binds next to myosin cross-bridges along the inner third of the thick filament. MyBP-C also extends off the thick filament to interact with actin and is thought to have a modulatory role in muscle contraction.

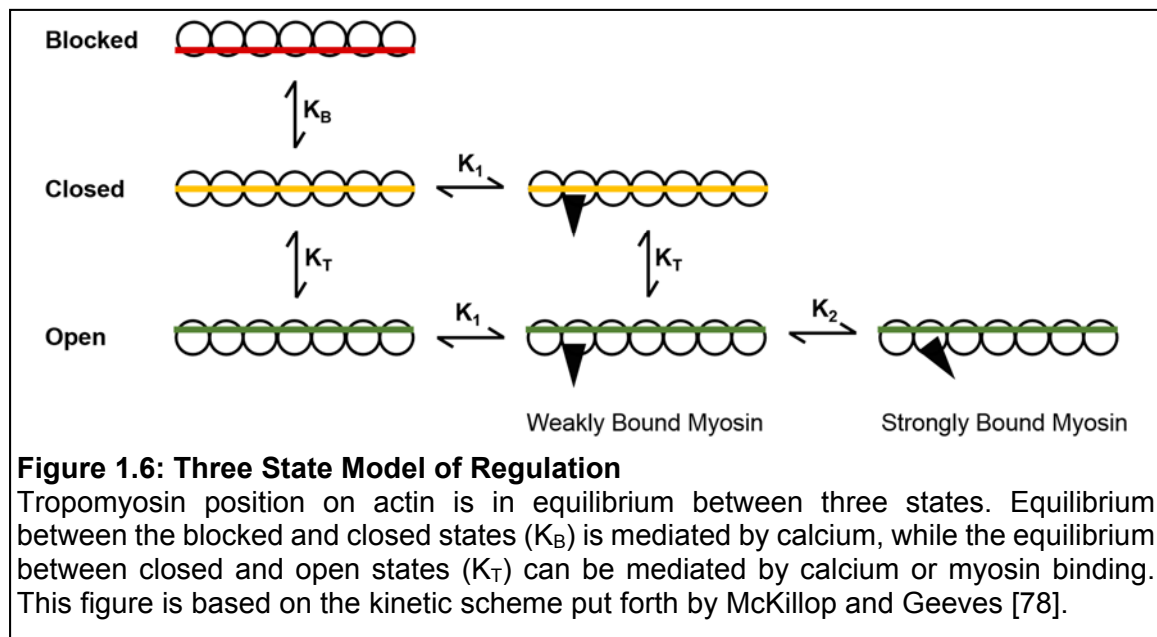
Thin Filament Structure

There are three main proteins that comprise the thin filament: actin, tropomyosin, and troponin (Figure 1.5). Actin monomers polymerize into a filament which forms the core of the thin filament. Tropomyosin is an α -helical coiled-coil protein that binds along the actin filament spanning seven consecutive actin monomers. Tropomyosins form end to end bonds to create a ropelike structure that winds around the entire actin filament [105]. Troponin is a calcium binding protein that, together with tropomyosin, regulates the activation of muscle contraction. A troponin complex binds along each tropomyosin and spans the

junction of two tropomyosin molecules [131]. In the absence of calcium, troponin also binds to actin such that it forces tropomyosin to assume a position on actin that sterically blocks myosin binding sites [101]. When troponin binds calcium during muscle activation, it dissociates from actin which allows tropomyosin to assume its preferred position on actin, exposing myosin binding sites and allowing muscle contraction to proceed (for review see [39]).

The above regulatory scheme is known as the steric blocking model (Figure 1.6), where tropomyosin position on actin is in equilibrium between three states (a blocked, closed, and open state) [78]. In the absence of calcium, tropomyosin assumes a “blocked” position on actin and prevents myosin-binding. In the presence of calcium, tropomyosin favors a “closed” position on actin that partially exposes the myosin-binding site and allows the myosin cross-bridge to weakly bind actin. When myosin weakly binds the thin filament, the tropomyosin strand shifts even further to fully expose myosin-binding sites, such that tropomyosin assumes an “open” position on actin. In an open state, the myosin cross-bridge is able to undergo a weak to strong binding transition [24]. By moving tropomyosin to a fully open state, myosin binding lowers the energy barrier for neighboring myosins to bind actin, and therefore increases the probability that successive cross-bridges will bind to the thin filament. The effects of myosin binding are more pronounced when the thin filament is only partially activated by calcium. This provides an influential role for the strong binding of myosin in regulating muscle contraction, although calcium activation of the thin

filament remains a requirement of regulation. While thin filament regulation may be the dominant control process in striated muscle, the focus of this thesis is on thick filament-based regulation, which modulates muscle contractility further.

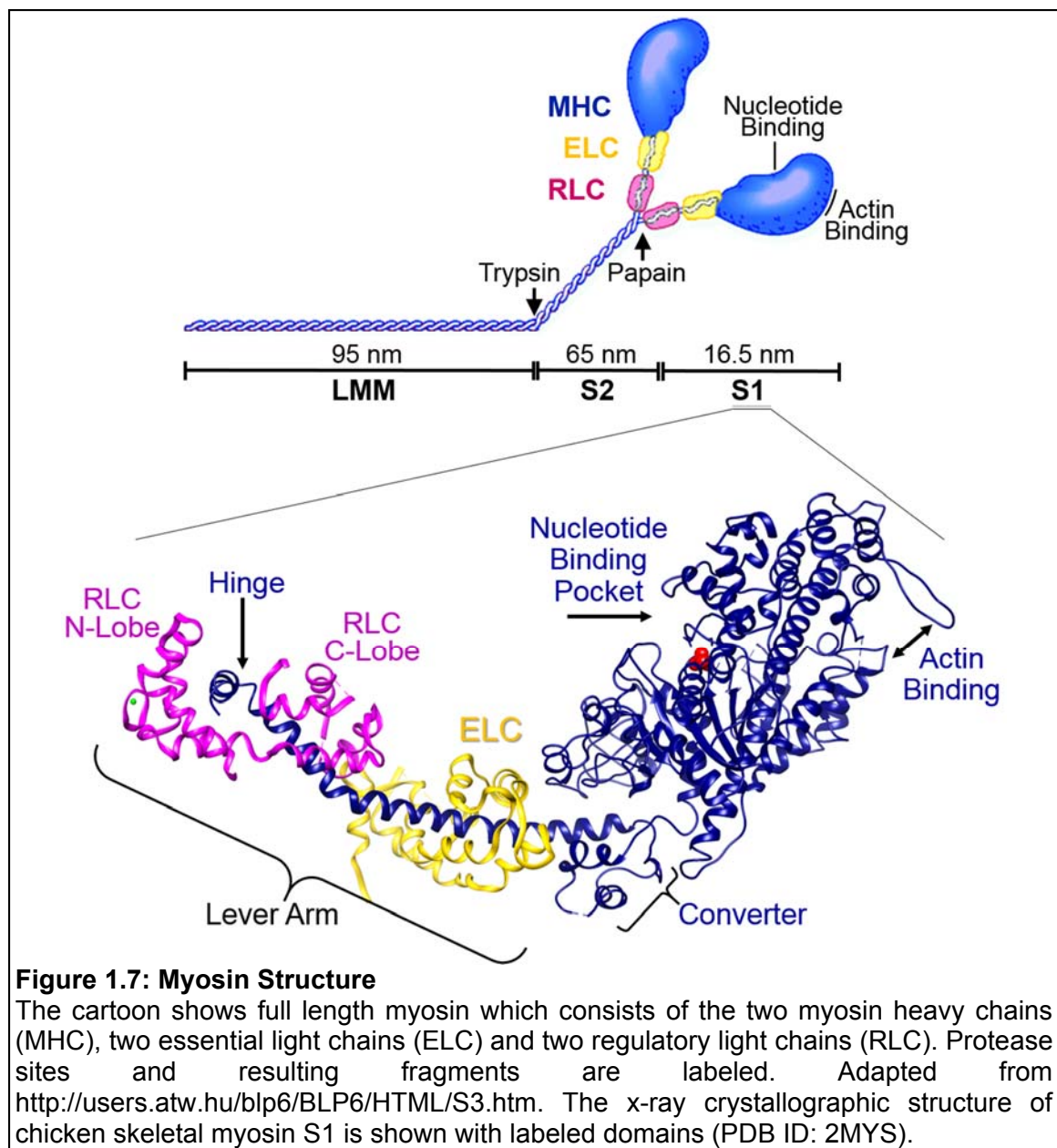


1.2.3 Myosin

Myosin motors are the molecular machinery responsible for converting the energy from ATP hydrolysis into the force and motion of muscle contraction.

Myosin is a hexameric protein made up of two myosin heavy chains (MHC), two essential light chains (ELC) and two regulatory light chains (RLC). The MHC has an N-terminal globular head domain, an α -helical neck region and a C-terminal tail domain (Figure 1.7). The tail domain is responsible for dimerization of the MHCs, forming an α -helical coiled-coil rod that composes the backbone of myosin thick filaments. The ELC and RLC bind to the α -helical neck region of each MHC. The myosin heavy chain globular head along with the light chain

bound neck region constitute the myosin cross-bridge that protrudes off the filament backbone, and is commonly referred to as subfragment 1 (S1) due to proteolytic digestion sites (Figure 1.7). The globular head comprises the catalytic motor domain of myosin which contains an actin binding site and an ATP binding site.



Myosin binds to actin, displaces actin, and dissociates from actin as it hydrolyzes ATP [73]. The light chain bound neck region of myosin acts as a lever arm to amplify small conformational changes that occur in the catalytic site and generate a large scale displacement of actin [145]. The converter domain is a small compact structure that sits at the junction of the catalytic motor domain and the lever arm. The converter rotates relative to the motor domain as myosin occupies different nucleotide bound states (Figure 1.8). The lever arm, linked directly to the converter, swings through a $\sim 70^\circ$ angle to produce a displacement of actin that is proportional to the length of the lever arm [107]. This conformational rearrangement of the myosin cross-bridge is called the myosin powerstroke. The lever arm must be somewhat rigid to transmit contractile force from the actin-bound head to the thick filament backbone. Binding of the ELC and RLC to the single α -helix of the MHC neck region mechanically stabilizes the lever arm [84]. In the absence of bound light chains, the α -helical neck is insufficient to transmit contractile force, and the lever arm is essentially reduced to the length of the converter-catalytic domain linkage, resulting in significantly decreased actin displacements [144].

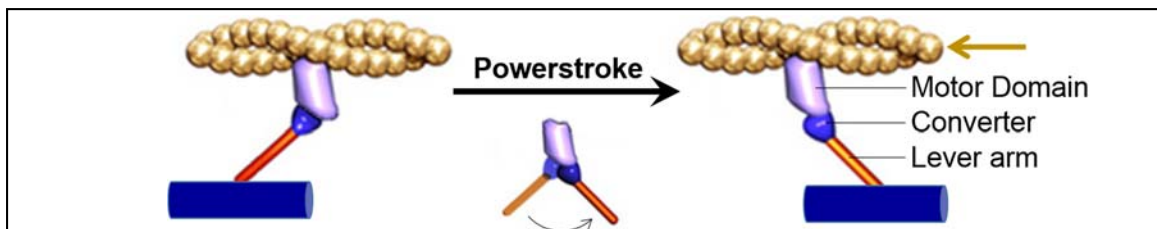


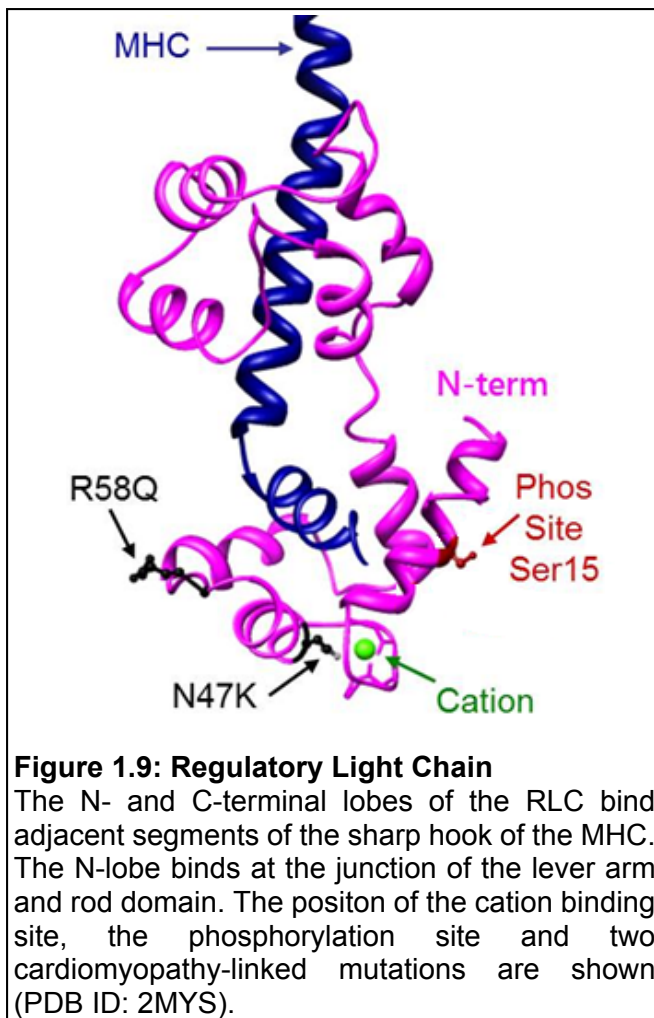
Figure 1.8: Myosin Powerstroke

A $\sim 70^\circ$ rotation of the converter domain relative to the motor domain results in a structural rearrangement of myosin that displaces the bound actin filament. The myosin lever arm rotates with the converter domain to amplify the displacement of actin. Adapted from [33].

In mammalian hearts there are two genes (MYH6 and MYH7) that encode the MHC which results in the expression of two distinct MHC isoforms (α and β , respectively) [92]. In the human myocardium, the β -MHC isoform is dominantly expressed. Each light chain of myosin is also encoded by two genes in cardiac tissue. The ELC is encoded by the MYL3 and MYL4 genes, and the RLC is encoded by the MYL7 and MYL2 genes. The MYL3 and MYL7 genes are exclusively expressed in the atrial myocardium while the MYL4 and MYL2 genes are exclusively expressed in the ventricular myocardium; this results in an atrial and ventricular isoform for each light chain. Genetic mutations linked to cardiomyopathies have been identified in the genes that encode the MHC isoforms and the ventricular light chain isoforms [79, 89]. It is of note that cardiomyopathy-linked mutations associated with the MYH6 gene are rare with a total of 5 documented cases [15, 94] while mutations in the MYH7 gene are the most frequent cause of hypertrophic cardiomyopathy [3]. The work carried out in this thesis was focused on the β -MHC and ventricular RLC isoforms.

The ELC and RLC are calmodulin homology proteins, each containing two globular domains connected by a flexible linker that wraps around the α -helical neck forming a dumbbell shape [9, 19]. Both light chains contain four EF hand motifs however in each light chain only one of the EF hands is capable of cation binding. The ELC binds to a conventional IQ motif allowing overlap of its two lobes when bound to the MHC, however the RLC binds to a modified IQ motif that allows each lobe to bind in tandem, expanding the range of the MHC that is

stabilized by the RLC [51]. The RLC binds to the C-terminus of the lever arm, sitting at the junction of the lever arm and rod domain of the filament backbone (Figure 1.9). The MHC α -helix forms a hook at this junction, and the modified IQ motif allows the RLC to bind both sides of the sharp bend [51]. This region acts as a pivot to allow the lever arm to change orientations relative to the filament backbone as myosin performs its powerstroke. Therefore in addition to providing structural support to the lever arm, the RLC also binds to a critical hinge region of the lever arm and interfaces with the thick filament backbone.



The RLC N-terminal lobe binds to the C-terminus of the lever arm surrounding the hinge region (Figure 1.9), and the C-terminal lobe binds further up the lever interfacing with the ELC [106]. New evidence suggests that the functional pivot point of the lever arm may lie between the RLC N- and C-lobes [61]. Studies in this thesis focus on N-terminal modifications of the ventricular myosin RLC. The RLC contains an EF hand motif

capable of binding Ca^{2+} - Mg^{2+} and a highly conserved phosphorylation site at serine15 in its N-terminal lobe. The RLC undergoes structural changes upon cation binding [108, 139]. The cation binding site could be involved in regulating Ca^{2+} levels in muscle cells [1] or possibly serve a structural role [108]. The RLC phosphorylation site is in close proximity to the cation binding site, and in skeletal muscle phosphorylation induces a conformational change of the RLC [111]. In smooth muscle, RLC phosphorylation activates muscle contraction, but in striated muscle it is thought to exert a modulatory role. The role of RLC phosphorylation in the heart will be discussed in detail in section 1.3.3.

1.2.4 Acto-Myosin Biochemical Cycle

The classic Lymn-Taylor model [73] correlates the biochemical and mechanical intermediates of the actomyosin cross-bridge cycle (Figure 1.10). The time it takes to complete one biochemical cycle is the inverse of the actin-activated ATPase rate of myosin, k_{ATP} ($=1/t_{cycle}$). Myosin is detached from actin when it has ATP bound in its active site. The myosin cross-bridge hydrolyzes ATP which primes the head for actin-binding allowing myosin to weakly interact with the thin filament. The myosin head undergoes a weak to strong binding transition which is coupled to the release of inorganic phosphate and a conformational rearrangement of the lever arm. This is known as the myosin powerstroke and results in actin filament displacement by a distance, d (Figure 1.10). ADP is released from the cross-bridge and myosin remains tightly bound

to actin in a post-powerstroke rigor state until ATP binding causes rapid dissociation of the actomyosin complex.

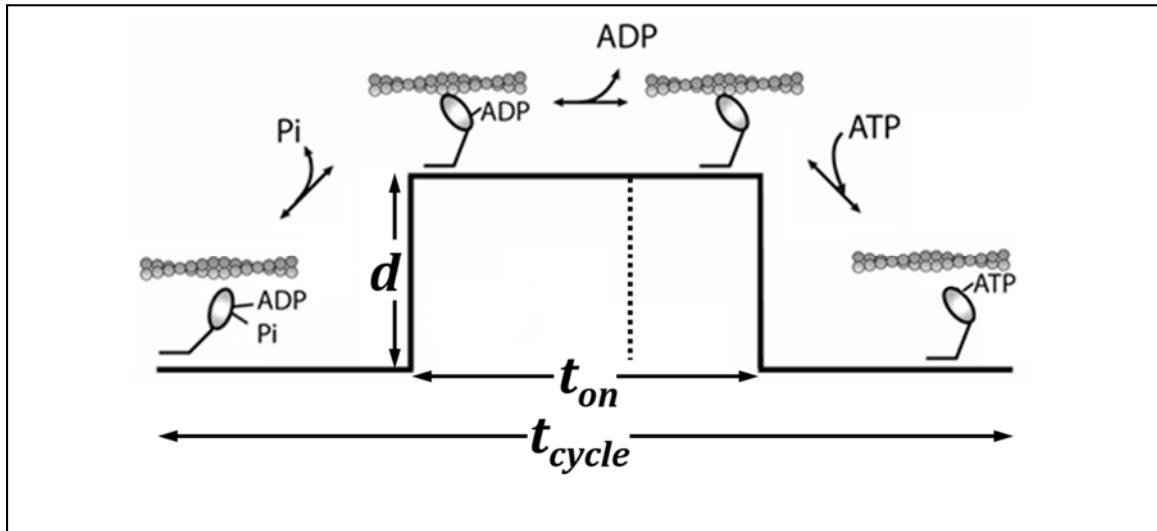


Figure 1.10: Actomyosin Cross-bridge Cycle

Myosin weakly binds an actin filament when ADP and phosphate occupy the nucleotide binding pocket. The myosin powerstroke is coupled to the release of phosphate, and results in the displacement of actin by a distance, d . Myosin is strongly bound to actin in the ADP bound and rigor states. The time myosin spends strongly bound to actin during one cycle is t_{on} . Figure from Jeff Moore.

The rate limiting step of actomyosin detachment is ADP release. EM reconstructions and crystal structures of S1 with different nucleotides bound suggest that ADP release is associated with a continuation of the lever arm swing of the myosin powerstroke [10, 59, 113, 114, 157], albeit much smaller in magnitude than the lever arm swing associated with phosphate release. The amount of time that myosin spends in the ADP-bound and rigor states determines how long it is strongly attached to actin, t_{on} . Myosin can only produce force in a strongly bound state. The fraction of time that myosin spends strongly attached during one biochemical cycle is known as the duty cycle, $f (=t_{on}/t_{cycle})$. Force production can be tuned by changing the rates of cross-bridge attachment

or detachment to influence the population of myosin cross-bridges occupying a strong binding state.

Mammalian hearts express α - and β - MHC isoforms. In humans, the atrial myocardium predominantly expresses α -MHC, while in the ventricular myocardium β -MHC is dominantly expressed at a 9:1 ratio over the α -isoform, although the ratios of α - and β -MHC shift during disease [82, 109]. The difference in isoform expression is significant because the MHC isoforms exhibit different functional properties. The α -MHC displays faster ATPase rates and shortening velocities, however, slower cross-bridge cycling of the β -MHC allows for higher levels of force generation in a more energetically efficient manner [47, 117, 147]. Single molecule optical trapping studies have shown that β -myosin has a prolonged rate of detachment [99], consistent with data from fiber studies which also show slower rates for detachment of β -myosin [70]. A decrease in the rate of detachment would result in an increased time spent for strongly bound myosin allowing for increased recruitment of myosin cross-bridges to the thin filament which could account for the increased force production observed for β -myosin. This demonstrates a role for thick filament regulation via myosin strong binding in muscle contraction, and shows that myosin isoform composition may influence the contractile properties and energetics of the muscle tissue.

1.2.5 Load Dependence

A load is a resisting force that is applied to an object. Under physiological conditions, cardiac muscle always experiences a load as it contracts. When there is no load imposed on a muscle, it will contract at maximal shortening velocity. When a load imposed on muscle is equal to the force producing capabilities of the muscle, the muscle will generate tension equal to the load but will not shorten. This is called isometric contraction because the muscle remains at a constant length. Muscle produces no work at either of these two extremes since work is the exertion of force over a distance. The ability of the heart to pump blood depends on its ability to produce work (i.e. shorten against a load), and therefore it is important to understand how load affects the biochemical and mechanical processes of muscle contraction.

In 1923, Fenn showed that the rate of heat production from a contracting muscle decreases as the load increases [31]. This was the first evidence to show that load slows the rate of energy release during muscle contraction. This slower rate of energy release stems from a decrease in the actomyosin ATPase rate [50]. A slowing of the chemical turnover from ATP hydrolysis allows the muscle to conserve energy under higher loads. Load can only be transmitted to the myosin motor when it is bound to actin, therefore load can only affect the biochemical transitions that are associated with a strongly bound state.

There is ample evidence that load affects the rate of ADP release from myosin. For example, measurement of MgADP accumulation using fluorescent

probes demonstrated a significant increase in the steady-state rate of MgADP release during fast shortening velocities compared to isometric contractions [49, 133]. Without any other changes in the ATPase cycle, a slower ADP release rate would result in a higher duty cycle for myosin under load. This could serve to increase the population of myosin cross-bridges bound to actin at higher loads, and thus allow a greater force to be produced by the muscle.

It has been proposed the load-sensitive mechanism affecting ADP release involves an isomerization (i.e. molecular rearrangement with no change in chemical structure) of the myosin molecule in the ADP bound state. The isomerization is the above described continuation of the lever arm swing which results in the opening of the nucleotide-binding pocket. This would shift myosin to a conformation that facilitates nucleotide exchange from the binding pocket. Loading the myosin would cause an inhibition of the lever arm swing in the ADP bound state, thus preventing the isomerization and inhibiting ADP release [36, 95]. Thus load can alter the mechanical and chemical properties of myosin. In the experiments presented in chapter 3, we use a non-motor actin-binding protein to introduce a load in the motility assay in order to provide a more physiologically relevant measure mimicking native actomyosin mechanochemistry.

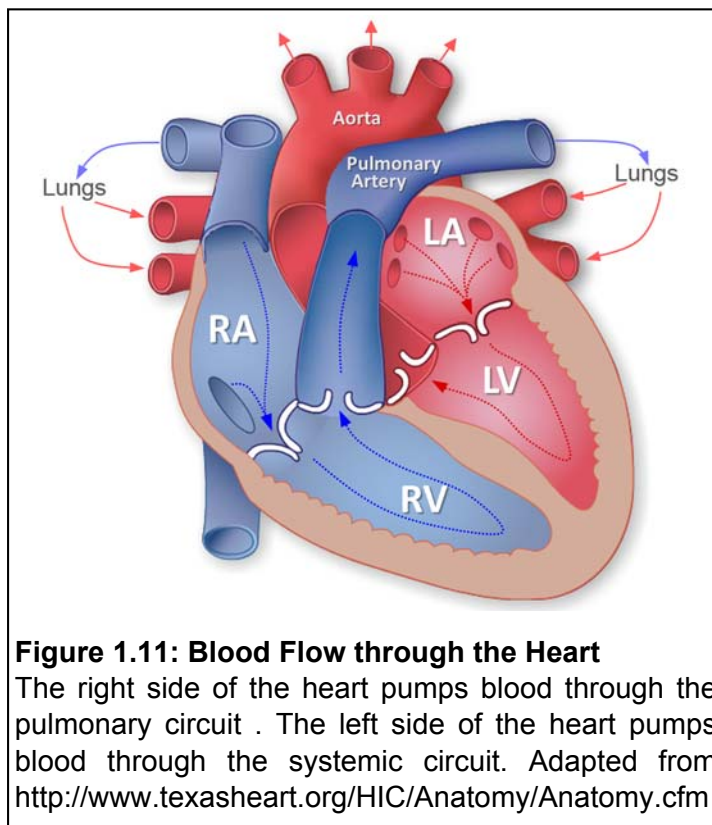
1.3 Heart Physiology

The heart works as a pump to circulate blood throughout the cardiovascular system, a vast network of blood vessels that form a closed loop to

carry blood from the heart to all the peripheral tissues and organs of the body and back to the heart. Blood is the aqueous transportation medium of our body that delivers oxygen, hormones, antibodies, cellular building blocks for growth and repair, and various nutrients to bodily tissues and removes carbon dioxide and metabolic waste products while distributing heat throughout our body, all serving to maintain homeostasis. Arteries carry oxygen and nutrient rich blood from the heart to all of our cells and veins carry deoxygenated blood back to the heart. The largest diameter blood vessels connect directly to the heart and then repeatedly branch into smaller vessels until they reach all of the cells in our body. The arterial and venous systems are connected by capillaries, the smallest of the blood vessels which are a short distance from cells and allow for the efficient exchange of nutrients and waste products via diffusion. The heart is responsible for maintaining the circulatory needs of the body by continually pumping blood from the venous network to the arterial network (Figure 1.11). The effects of the RLC mutations and phosphorylation on muscle contraction ultimately affect the pump function of the heart. In the remainder of this chapter I will describe general structure-function aspects of the heart (section 1.3.1) and how these aspects are affected by RLC phosphorylation (section 1.3.2) and cardiomyopathy-linked mutations (section 1.3.3).

1.3.1 Gross Anatomy and Function

The heart is composed of four chambers, the top two chambers are atria which collect blood coming into the heart, and the bottom two chambers are ventricles which pump blood out of the heart. The heart functions as two pumps in series, the right atrium and right ventricle forming one pump and the left atrium and left ventricle forming the second pump (Figure 1.11). Each pump contains an atrioventricular (AV) valve which allows the one-way flow of blood from the atrium to the ventricle. The right side of the heart is a low pressure pump. It pumps deoxygenated blood from the vena cava through the pulmonary arteries to the lungs. The left side of the heart is a high pressure pump. Oxygenated blood from



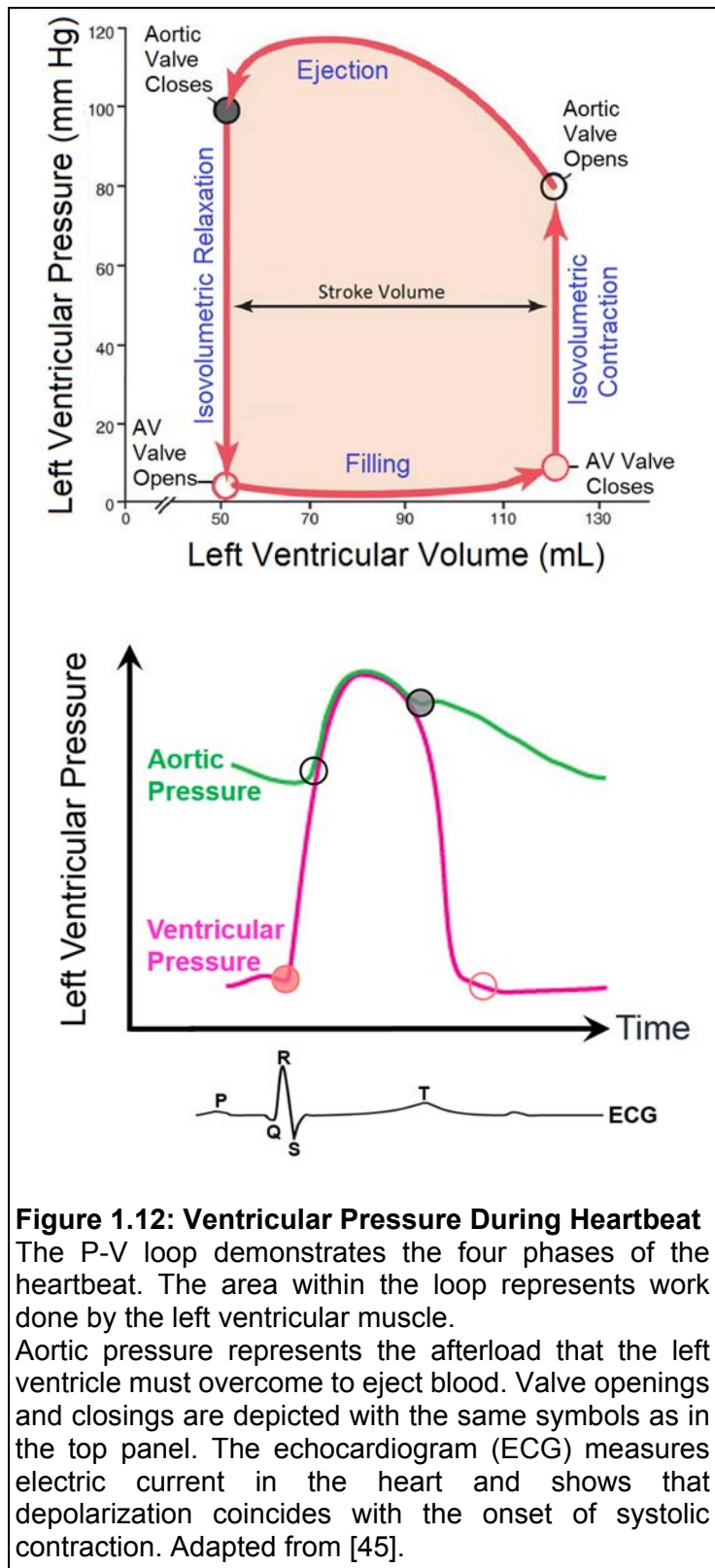
the lungs flows through the pulmonary veins into the left atrium. The left ventricle is responsible for pumping blood into the aorta and through the entire systemic circulation back to the right side of the heart.

The heartbeat occurs in two phases, diastole and systole. During diastole the muscle relaxes and the

chambers fill with blood. During systole the muscle contracts and blood is ejected. The diastolic and systolic periods are synchronized between the right and left sides of the heart, and in order to ensure proper filling of all four chambers atrial contraction precedes ventricular contraction. Cardiac contraction is initiated by depolarization of specialized cardiac cells that exhibit autorhythmicity, the ability to fire action potentials on their own. These cells are called pacemaker cells and form a conduction system in the heart through which electrical impulses spread rapidly to initiate a timed contraction of the myocardium. The heart rate (beats per minute) is determined by the pacemaker cells with the fastest firing rate. Cardiac output is the volume of blood pumped by the heart per minute. It is the product of heart rate and the stroke volume, the amount of blood pumped per heartbeat. Cardiac output must be maintained at a sufficient rate to deliver adequate and continuous supply of oxygen and other nutrients to the body. As bodily demand varies, such as during exercise, so must cardiac output.

Ventricular contractility during one heartbeat cycle can be visualized by plotting ventricular pressure versus ventricular volume (Figure 1.12). The ventricular cardiac cycle is divided into four phases: diastolic filling, systolic isovolumetric contraction, systolic ejection, diastolic isovolumetric relaxation. During diastole the AV valve opens and blood from the atrium fills the ventricle. Systole begins just prior to AV valve closure. At this point the ventricle contracts

isovolumetrically because blood cannot be ejected from the left ventricle until the ventricular pressure reaches or exceeds the pressure in the aorta. When left ventricular pressure reaches aortic pressure, the aortic valve opens, and ejection begins. The end of systole is marked by closure of the aortic valve. At this point the ventricle will relax isovolumetrically until the AV valve opens once again. The stroke volume of contraction is represented by the difference between end diastolic volume and end systolic volume. The work



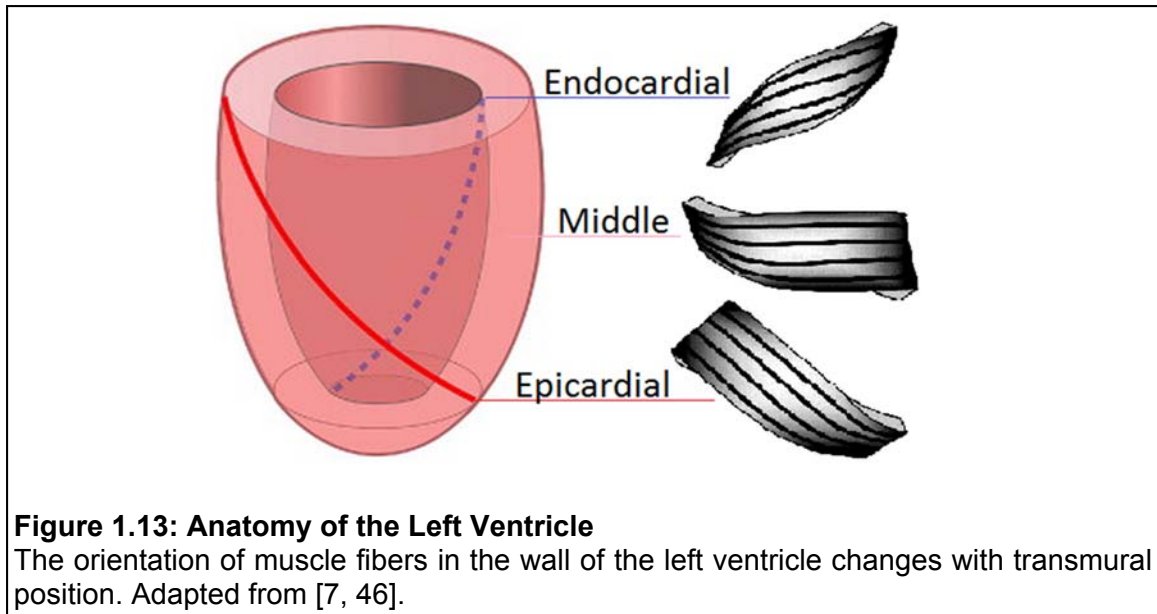
capacity of the ventricle is represented by the area within the P-V loop.

Work capacity is essentially the amount of the energy that the ventricle can expend during one heartbeat cycle. One major factor that determines the energy requirement for blood ejection is the afterload. Afterload is the force that opposes ventricular contraction, and is represented by aortic pressure for the left ventricle. The higher the afterload, or aortic pressure, the more energy the ventricle must expend to build the pressure needed to open the aortic valve. This leaves less energy for the next phase of contraction where muscle shortens to eject blood. The work capacity of the muscle is an important determinant of stroke volume and relies on how much force the muscle can produce. The P-V loop shows the work capacity for one heartbeat cycle, however the heart must be able to beat repetitively. Therefore, not only does the ventricle have to perform sufficient work, but it must do so at a sufficient rate. Cardiac power output is the rate at which the ventricle can perform work, and it represents the heart's ability to efficiently pump blood [4, 80, 85, 128].

The same amount of blood flows through the left and right sides of the heart but the left ventricle has to work much harder to pump blood because it experiences a higher afterload. Blood entering the aorta travels through the entire systemic circulation back to the right side of the heart, whereas blood in the pulmonary circuit travels to the lungs, a low resistance circuit, before returning to the left side of the heart. The pressure in the aorta is five times greater than the pressure in the pulmonary artery to accommodate the greater

resistance in the systemic circulation. The two genetic mutations of the RLC studied in this work lead to a remodeling of the left ventricle which disrupts its ability to function properly.

The left ventricle is anatomically suited to pump against the higher pressures of the systemic circuit. The left ventricle has a conical shape with its base at the interface with the atrial chamber and aortic valve. The myocardium is an entangled web of muscle fibers and the gross nature of the tissue structure is still debated. The ventricular tissue is often discussed in terms of layers comprising the wall assigned as epicardial (outer), middle, and endocardial (inner). It is important to note that these are not distinct or separated layers within the ventricular wall as fibers interconnect transmurally to form a continuum. However, it is clear that fiber orientation changes transmurally through the wall. The endocardial and epicardial fibers are arranged in opposing oblique orientations, while those in the middle are to those found to be circumferentially aligned (Figure 1.13). The contrasting orientation of fibers allows the ventricle to generate torsion as it contracts to “wring out” blood [7, 46]. During contraction the longitudinal axis of the left ventricle varies only slightly in length as the chamber circumference significantly decreases. Ventricular torsion places different contractile requirements on fibers found in different regions of the wall, such as more forceful contractions for epicardial fibers [30]. In the following section I will discuss mechanisms of RLC phosphorylation that modulate cardiac contraction, including a potential role in maintaining ventricular torsion.



The left ventricular myocardium must work against the afterload imposed on the heart by aortic blood pressure and peripheral resistance. Ejection is further constrained to the duration of systole for each heartbeat. Therefore the shortening velocity of contraction under load will determine the volume of blood ejected from the ventricle per heartbeat. Power can be calculated as the product of force and velocity. Subtle changes to the force-velocity relationship of muscle contraction will have profound effects on cardiac power output, and subsequently heart function. In chapter 3 we introduce exogenous loads to the *in vitro* motility assay to mimic a more physiological, loaded experimental system and calculate the effects of the mutations and phosphorylation on actomyosin power.

1.3.2 Modulation of Cardiac Contraction via RLC Phosphorylation

Cellular Effects

The pump function of the heart must be finely tuned to maintain sufficient cardiac output over a wide range of physiological conditions. The dominant regulatory control of cardiac contraction is the binding of calcium to the thin filament which exposes binding sites on actin and permits myosin cross-bridges to engage the thin filament. As calcium levels rise during an activating transient, so does the rate of ATP hydrolysis from the actomyosin biochemical cycle along with tension generation in muscle fibers. The calcium sensitivity of muscle to ATPase or force is commonly measured by determining the amount of calcium necessary to reach half maximal activation; a greater sensitivity to calcium means that less calcium is required to reach half maximal activation. Myosin strong binding to actin at submaximal calcium is a mechanism that modulates the activation of cardiac contraction (see Figure 1.7). RLC phosphorylation, while regulatory for invertebrate and smooth muscle, has a modulatory role in cardiac muscle contraction, subtly modifying and fine tuning the rates of cross-bridge attachment to and detachment from actin [120].

Various *in vitro* fiber studies have shown that phosphorylation of the RLC increases the calcium sensitivity of force for skeletal fibers [81, 104] and cardiac fibers, including those from mouse, rat, rabbit, pig and human [22, 86, 87, 115, 130, 135]. This leftward shift of the tension-pCa relationship acts to increase the duration of muscle contraction due to an early onset of activation and delayed onset of relaxation. An increase in the calcium sensitivity of a muscle cell, as seen with RLC phosphorylation, would most likely arise from an increase in

myosin strong binding at submaximal calcium as opposed to increased calcium binding to troponin to activate the thin filament. Myosin is more likely to occupy a strong binding state when the spacing between myofilaments is decreased [74]. In fact, it is well established that decreased interfilament lattice spacing of muscle fibers increases the calcium sensitivity of force [77, 153]. An in depth study by Colson et al. [23] directly confirmed the notion that RLC phosphorylation decreases lattice spacing to increase Ca^{2+} sensitivity using a combination of X-ray diffraction and mechanical fiber techniques to study murine trabeculae.

Colson and colleagues observed a second structural alteration induced by RLC phosphorylation in the mouse fibers. The distribution of mass from myosin cross-bridges showed a net movement away from the thick filament and closer to the thin filament, as determined from 1,0 and 1,1 equatorial reflections in resting fibers. This phenomenon has been widely studied in skeletal muscle, and demonstrated using electron microscopy [69] and fiber diffraction techniques [98], however the study mentioned above was first to demonstrate the structural change in cardiac muscle. It has been proposed that phosphorylation induces a charge repulsion of myosin heads away from the thick filament, and this is supported by charge replacement studies of the RLC [137]. Importantly, the net transfer of cross-bridge mass is a separate effect from the decreased lattice spacing of myofilaments as determined from x-ray fiber diffraction experiments. Phosphorylation of MyBP-C, another thick filament associated protein, but not RLC, also resulted in a net transfer of cross-bridges away from the thick filament

with no corresponding decrease in lattice spacing, and subsequently there was no change in the calcium sensitivity for these fibers [23].

The disposition of myosin heads off the thick filament backbone manifests as an increase in the rate of force development of the fiber, which is seen for muscle fibers containing phosphorylated RLC (and also phosphorylated MyBP-C) [23]. Mechanical studies on skeletal and cardiac fibers have demonstrated increased rates of force development upon phosphorylation of the RLC [23, 88, 130, 136]. By lifting the myosin cross-bridges off the thick filament backbone, RLC phosphorylation orients myosin heads in a more optimal position to bind the thin filament which presumably leads to an increase in the rate of cross-bridge attachment. Increasing the rate of attachment to actin will increase the number of myosins occupying a strongly bound state through two mechanisms: (1) it decreases the time spent in a detached state for the population of phosphorylated myosin, and (2) it increases the rate of exposure of actin-binding sites for neighboring myosins.

It is evident that phosphorylation of the RLC has the ability to markedly alter cardiac contraction. RLC phosphorylation alters the sarcomeric lattice and thick filament structure to fine tune activation and increase recruitment of myosin motors via changes in strong binding kinetics. Each effect contributes to the pump function of the heart. By increasing the calcium sensitivity to force, it follows that RLC phosphorylation allows the muscle more time to contract during systole by initiating contraction at an earlier stage of the activating calcium

transient. Increasing the rate of force development allows the muscle to develop pressure faster. During the isovolumetric contraction phase of systole, the faster left ventricular pressure reaches the afterload, the more time it can spend ejecting blood during systole.

Global Tissue Effects

RLC phosphorylation levels in the heart are determined by the relative activity of kinases and phosphatases. A cardiac specific myosin light chain kinase (cMLCK) has been identified [17]. It is exclusively expressed in cardiac tissue and the myosin RLC is its only known substrate. Changes in the expression level of cMLCK result in changes to RLC phosphorylation levels; however, this is not seen for other kinases in the heart. RLC phosphorylation is maintained at a steady state level of approximately 45% due to the competitive actions of cMLCK and myosin light chain phosphatase holoenzyme [18]. The phosphatase is known to have a multiple substrates in cardiac tissue. However, when myosin phosphatase target subunit 2 (MYPT2) binds to the phosphatase, the holoenzyme becomes RLC specific for the RLC [83, 97]. The specificity of control exerted over RLC phosphorylation and its sustained presence suggests it is an important contributor to basal cardiac function.

While RLC phosphorylation levels in the human heart are maintained at about 45%, the pattern of RLC phosphorylation is not uniform in the heart. Given that RLC phosphorylation is constitutively maintained in a specific pattern, it is likely to infer regional influences over the heart. RLC phosphorylation is present

at higher levels in the epicardium and near the apex of the heart in humans, rabbits and rodents [25, 48, 123, 154]. It was also found in higher levels in the specialized Purkinje fibers of the mouse heart [154]. Evidence suggests that this gradient is functionally significant in maintaining left ventricular torsion and untwisting necessary for proper left ventricular ejection and relaxation [26]. Muscle fibers that are required to perform at enhanced levels to create torsion correlate with areas of increased RLC phosphorylation in the heart [25]. Gene targeted knock in mice bearing non-phosphorylatable RLC showed a loss of left ventricular torsion and untwisting compared to WT mice. Computational models that mimicked this effect also predicted that uniform phosphorylation of the ventricle could not maintain torsion to the same degree as measured in WT mice [123]. These findings suggest that basal heart function is sustained through regional mechanical differences caused by RLC phosphorylation.

Thin filament regulation is extremely cooperative and acts as an on/off switch for muscle contraction on a beat to beat basis. However the dynamic environment experienced by the heart and the demand for optimal performance requires more than a simple on/off mechanism. The heart is constantly adapting to the circulatory needs of the body as it experiences a broad range of conditions including rest, exercise, fight or flight, injury, etc. Thick filament regulation via RLC phosphorylation represents a possible mechanism to finely tune heart function as it experiences varying conditions over longer time scales.

The levels of phosphorylation can be regulated to adapt to the demands placed on the heart under varying conditions. For example, isolated rat hearts subjected to differing levels of left ventricular passive stretch were shown to have phosphorylation levels in the endocardium that were significantly reduced compared to those in the epicardium under diastolic pressure of 15 mmHg. In contrast, phosphorylation levels were equal between endocardial and epicardial tissue under a diastolic pressure of 0 mmHg [48]. Muscle hypertrophy is an enlargement of the muscle tissue due to an increase in the size of the component cells. Exercise conditioning in mice results in physiological hypertrophy, however increased RLC phosphorylation in transgenic mice resulted in an attenuation of physiological hypertrophy following treadmill exercise [52]. In addition, the expression of cMLCK was upregulated in mice that underwent swimming exercise, which lead to an increase in RLC phosphorylation levels from 33 to 39% [154]. These studies support the idea that RLC phosphorylation levels are dynamic and regulated in response to the demands placed on the heart.

The level and pattern of RLC phosphorylation has proved to be critical to the basal function and adaptive properties of the heart. It is therefore not surprising that non-physiological and pathological changes resulting in reduced levels of RLC phosphorylation are correlated with poor cardiac performance *in vivo*. Multiple studies of transgenic mice expressing non-phosphorylatable RLC exhibited myocyte structure abnormalities, cardiac remodeling, and left ventricular dysfunction including decreased pressure, stroke volume and power

output ultimately leading to heart failure [115, 118, 123]. Similar studies in which cMLCK expression was ablated lead to decreased or complete loss of RLC phosphorylation in transgenic mice which resulted in an inability to adapt to external stresses, hypertrophy and severe heart failure [29, 154]. Likewise, decreased RLC phosphorylation resulting from increased expression of the myosin phosphatase holoenzyme lead to left ventricular remodeling and impaired function [83]. Consistent with findings in the murine animal model, genetic screening of 490 patients with cardiac hypertrophy revealed a mother and son bearing mutations in MLCK [25]. RLC phosphorylation is critical to cardiac function, and alterations in the levels of RLC phosphorylation have been linked to heart failure in human patients [142].

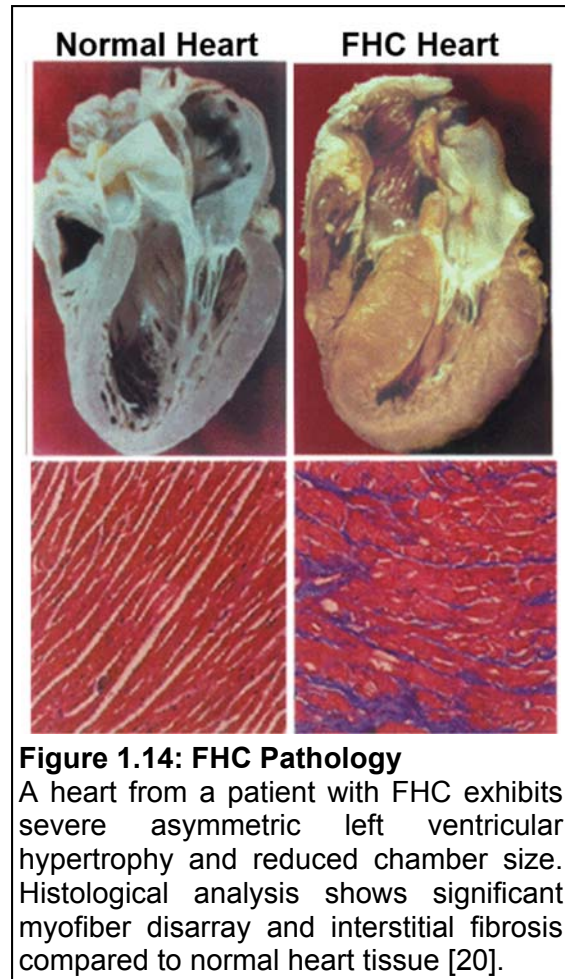
1.3.3 Familial Hypertrophic Cardiomyopathy

Familial hypertrophic cardiomyopathy (FHC) is the most common type of genetic heart disease in United States [35]. It affects about 1 in 500 people and is a leading cause of sudden cardiac death in adolescents. The condition is characterized by asymmetric ventricular hypertrophy, usually in the left ventricle or ventricular septum, and is often accompanied by myocyte disarray and fibrosis (Figure 1.14). Decreased chamber size and increased wall stiffness are symptoms of hypertrophy which commonly lead to diastolic relaxation and filling abnormalities [21]. FHC is caused by autosomal dominant mutations in genes that encode sarcomeric proteins. There are hundreds of known mutations in at

least 11 genes that are expressed in the heart [121]. However, it remains unclear how the disease manifests, and the clinical presentation, prognosis and treatment for FHC are extremely heterogeneous [150].

Many patients that exhibit hypertrophy have an otherwise normal functioning heart and remain symptom free, while for others the disease may manifest in diastolic dysfunction, progressive heart failure, atrial fibrillation, or sudden cardiac death (SCD). Other symptoms may include

chest pain, dizziness, shortness of breath, and lethargy [21]. There is no cure for FHC; treatment options are limited and focus exclusively on treating the most severe symptoms rather than the cause of the disease [76]. This is in part due to the fact that it is hard to detect FHC before cardiac remodeling occurs, at which point treatment relies on management of the disease and assessment of the risk for SCD. For individuals who are at high risk of SCD, a defibrillator may be surgically implanted to reduce their risk of SCD [58]; however, often times SCD is the first obvious manifestation of the disease. Early detection of FHC is



necessary in order to invest in preventative therapies and intervene at a stage when the disease can be attenuated. For this reason there has been a major push in recent years to develop more robust genetic screening technologies and increase their availability [13].

Early diagnosis is only one part of the battle in developing successful therapeutic measures. Not only does the clinical presentation of FHC vary widely, but the pathophysiology is unique to the specific disease-causing mutation [20, 58]. Development of therapeutic strategies requires knowledge of the molecular defects posed by the causal mutation as well as how these underlying defects trigger hypertrophy. This is the motivation behind much of the basic research that is carried out on FHC-linked mutations today, including studies performed here aimed at characterizing the molecular phenotype of mutations in the myosin RLC and potential rescue mechanisms (section 3.5). Hopefully our work can potentially pave the way for treatments that correct dysfunction before significant hypertrophic remodeling.

Familial hypertrophic cardiomyopathy is a disease of the sarcomere, most likely stemming from impaired muscle contraction, structure and/or energetic consumption. Mutations can arise in almost any component or region of the sarcomere, exerting a wide range of effects at the molecular level, yet leading to a seemingly shared phenotype. This suggests that mutations with varying defects may share common functional consequences that trigger hypertrophy. For example, a mutation that reduces force production might trigger compensatory

hypertrophy in order to restore force by building more muscle. Likewise, a mutation that decreases the calcium sensitivity of activation and results in less cross-bridge recruitment, could also reduce force production, and in turn lead to compensatory hypertrophy. Hypertrophy may also be a direct result of the mutational defect. For example, a mutation that impairs the structural integrity of the sarcomere may lead to a direct remodeling of cardiac fibers, or a mutation that increases the calcium sensitivity of activation may lead to improper diastolic relaxation, and could result in hypertrophy from sustained activation. Since multiple contractile alterations ultimately result in the same end point of hypertrophy, one must understand the pathology of any given mutation so that treatments can be tailored for each individual.

Cardiomyopathy-linked Mutations of the RLC

There are currently 13 documented FHC mutations in the *MYL2* gene that encodes the ventricular myosin regulatory light chain: A13T, F18L, M20L, E22K, N47K, R58Q, P95A, L103E, E134A, I158L, G162R, D166A, D166V [5] and one linked to dilated cardiomyopathy, D94A [53]. I studied two of these mutations, N47K and R58Q, to discern their effect on myosin function at the molecular level. While both mutations are located in the RLC N-terminus in close proximity to each other, each displays a drastically different disease phenotype. The N47K mutation is associated with mid-ventricular and papillary muscle hypertrophy

resulting in diastolic filling abnormalities. The onset of hypertrophy occurred late in life when the affected patient was in their late 50s, and rapidly progressed in the following the years [6]. The R58Q mutation is associated with a classic FHC phenotype of left ventricular hypertrophy, and an early onset occurring during childhood. The R58Q mutation is associated with multiple cases of sudden cardiac death [34].

Based on the crystal structure of skeletal RLC (Figure 1.9), N47 and R58 are located near the phosphorylation site and cation site of the RLC, with N47 forming part of the cation binding site [106]. Bacterially expressed human ventricular RLC (hvRLC) bearing either mutation abolished calcium binding to the isolated RLC in solution [138, 139]. The ability to bind calcium was restored to R58Q RLC upon phosphorylation of S15, and was accompanied by an increase in helical content [139]. When bacterially expressed N47K mutant RLCs were exchanged onto porcine cardiac fibers to test their sensitivity to calcium activation, the fibers displayed a significantly increased calcium sensitivity to the myofibrillar ATPase, while R58Q fibers displayed a significantly increased calcium sensitivity to force [138].

To gain an understanding of how RLC modifications affect myosin contractility, I studied cardiac β -myosin bearing WT and mutant hvRLC in the dephosphorylated and phosphorylated states using *in vitro* motility assays. *In vitro* motility assays retain the strengths of solution biochemistry experiments while simultaneously permitting the measurement of actomyosin contractility.

Unlike fiber studies which characterize bulk properties of muscle ensembles, the motility assay allows for the characterization of individual protein components within the system. Thus, it provides the advantage of distinguishing molecular based changes to myosin contractility directly resulting from RLC modifications.

Previous studies have shown that N47K and R58Q mutations disrupt myosin's strain sensitivity, stemming from a more compliant lever arm [Greenberg Thesis]. In contrast, RLC phosphorylation was shown to impart stiffness to the lever arm in skeletal muscle studies [Greenberg, 2009]. We hypothesized that phosphorylation of the FHC-RLC may mitigate distinct mutation-induced structural and functional abnormalities of the myosin motor.

To study the disease-linked mutations in the specific protein isoform in which they are found, bacterially expressed human ventricular RLCs were utilized in our experiments, however, because heart tissue samples from healthy adults are extremely difficult to obtain and are not readily available, myosin heavy chains were isolated from an animal model. The human ventricular myocardium is predominantly comprised of the β -MHC isoform, expressing a 9:1 ratio of β -MHC to α -MHC, and undergoes a shift to 100% β -MHC expression during heart failure [82]. The porcine cardiac β -MHC is 98% identical to human β -MHC, a difference of 45 out of 1935 amino acids, 26 of which are conserved substitutions. It is important to study pathological and physiological phenomenon in the context of which they occur, and β -MHC from porcine hearts provides a relevant framework for our studies.

In the work presented here, *in vitro* motility assays were utilized to investigate the effects of RLC phosphorylation on the FHC-RLC mutant phenotype in the presence of an α -actinin frictional load. The methodology, results and a discussion of my findings are presented in the following chapters of this thesis.

CHAPTER 2 – METHODS AND MATERIALS

2.1 Purification of Proteins

2.1.1 Porcine Cardiac Myosin

The left ventricle was removed from porcine hearts, and minced while chilled on ice. The minced tissue was ground, and 50-100 g of tissue was homogenized in 100 to 200 ml of Extraction Buffer (0.3 M KCl, 15 mM potassium phosphate, 20 mM EDTA, 5 mM MgCl₂, 5 mM DTT, 3.3 mM ATP, pH 6.7). The homogenate was diluted 4-fold with cold (4° C) distilled deionized water (ddH₂O) and filtered through cheesecloth. The solution was then diluted 10-fold with cold ddH₂O and allowed to precipitate for 4 hours at 4° C. The precipitate was collected by centrifugation (10,000 x g for 20 minutes) and resuspended in 1 M KCl, 60 mM potassium phosphate, 20 mM EDTA, 5 mM DTT, pH 6.7. The solution was dialyzed overnight against 0.6 M KCl, 25 mM potassium phosphate, 5 mM DTT, pH 6.7 at 4° C. An equal volume of cold ddH₂O was then added to the solution, stirred for 30 min at 4° C, followed by centrifugation at 41,000 x g for 1 hour to remove filamentous actin. Following centrifugation there was a distinct actin-containing pellet, a clear middle-layer supernatant containing myosin, and a cloudy top-layer containing fat. The middle layer was removed using a transfer pipette; the pellet and top-layer were discarded. The supernatant was diluted 10-fold with cold H₂O and allowed to precipitate for 4 hours at 4° C. The precipitate was collected by centrifugation (10,000 x g for 20 min) and resuspended in 3 M

KCl, 50 mM potassium phosphate, 5 mM DTT, pH 6.7, then dialyzed overnight against 0.6 M KCl, 50 mM potassium phosphate, 5 mM DTT, pH 7.0 at 4° C. A 5 mL volume of this buffer was saved for later use in determining protein concentration. The protein solution was clarified by centrifugation at 41,000 x g for 1 hour, and the supernatant was collected. Protein concentration was determined by measurement of solution absorbance at 280 nm (and reference wavelength at 320 nm) for three dilutions (1:25, 1:50, 1:100). An equal volume of cold glycerol (4° C) was added to the remaining protein solution and the resulting PC myosin was stored in 50% glycerol for up to three months at -20° C, until needed for experiments.

2.1.2 Regulatory Light Chains

Bacterially expressed human ventricular regulatory light chains (hvRLC) were prepared by our collaborators (D. Szczesna-Cordary Lab, University of Miami – Miller School of Medicine) as previously described [139]. Briefly, the cDNA (GenBank™ Accession No. AF020768) for wild-type (WT) and mutant (N47K and R58Q) hvRLCs were constructed with an NcoI site at the N-terminal ATG and a BamHI site following the stop codon to facilitate ligation into the NcoI–BamHI cloning site of the pET-3d (Novagen) plasmid vector. The vector was transformed into DH5- α cloning host bacteria for amplification. The vectors were transformed into BL21 expression host cells and all proteins were expressed in large (16 liter) cultures. Expressed proteins were purified using a S-Sepharose

column followed by a Q-Sepharose column, both equilibrated with 2 M urea, 25 mM Tris-HCl, 0.1 mM phenylmethylsulfonyl fluoride (PMSF), 1 mM DTT, 0.001% NaN₃, pH 7.5. The proteins were eluted with a salt gradient of 0 to 450 mM NaCl. The final purity of the proteins was evaluated using 15% SDS-PAGE. The hvRLCs were dialyzed against 2 M urea and stored at -80° C.

2.1.3 Myosin Light Chain Kinase

Smooth muscle myosin light chain kinase (MLCK) was isolated from chicken gizzards based on the protocol of Ngai et al. [93]. For the extraction procedure all steps were carried out in the cold room, and buffers were kept at 4°C. Chicken gizzards were thawed on ice and minced after connective tissue removal. The muscle mince (50g) was homogenized for three five second pulses in 200 mL wash buffer containing 20 mM Tris-HCl, 40 mM NaCl, 1 mM MgCl₂, 1 mM EGTA, 1 mM DTT, pH 7.5 supplemented with 0.05% Triton-X-100, then centrifuged at 17,000 g for 15 min at 4° C. The pellet was homogenized in wash buffer and collected by centrifugation (17,000 x g for 15 min at 4°C). This step was repeated. The blender was rinsed with ddH₂O between each centrifugation cycle. The pellet was resuspended in 200 mL extraction buffer containing 40 mM Tris-HCl, 60 mM NaCl, 25 mM MgCl₂, 1 mM EGTA, 1 mM DTT, pH 7.5 and centrifuged at 17,000 x g for 15 min at 4°C. The supernatant was filtered through glass wool and clarified via centrifugation at 250,000g for 45 min at 4° C. The supernatant was collected and filtered through a low protein binding syringe filter.

DEAE resin was washed three times in DEAE loading buffer (40 mM Tris-HCl, 20 mM NaCl, 25 mM MgCl₂, 1 mM DTT, 1 mM EGTA, pH 7.5). A third of the resin (~20 mL) was set aside for batch binding. The rest of the resin was packed into a DEAE Sepharose column, and washed with DEAE elution buffer (40 mM Tris-HCl, 1 M NaCl, 25 mM MgCl₂, 1 mM DTT, 1 mM EGTA, pH 7.5), and then re-equilibrated in DEAE loading buffer. The resin set aside for batch binding was allowed to settle for 10 minutes and excess buffer was removed, resulting in a concentrated slurry. The clarified protein solution was added to the resin slurry and mixed on an orbital shaker overnight at 4°C.

Batch bound resin was loaded onto the DEAE sepharose column. The column was equilibrated by addition of DEAE loading buffer until absorbance readings at 280 nm of flow through fractions reached a steady state baseline. A linear salt gradient was accomplished by mixing equal volumes of DEAE loading and elution buffers in a gradient mixer that was gravity fed into the column. The enzyme was eluted with a gradient from 20 to 300 mM NaCl over 3 column volumes. Protein fractions containing the kinase were determined by SDS-PAGE, and then pooled. The pooled fractions were dialyzed overnight against Cibracon loading buffer (20 mM K₂HPO₄, 1 mM EGTA, 1 mM EDTA, 1 mM DTT, 0.02% NaN₃, pH 8.0). Following dialysis the kinase enriched fractions were centrifuged at 300,000 x g for 10 min at 4° C. The supernatant was loaded onto an Affi-Gel Blue (Bio-Rad Laboratories, Inc., Hercules, CA, cat #153-7301) column equilibrated in Cibracon loading buffer. The kinase was eluted with a gradient

from 0 to 1.5 M NaCl in the same buffer over 10 column volumes. Protein fractions containing the kinase were determined by SDS-PAGE, and then pooled. Pooled fractions were dialyzed overnight against a buffer containing 25 mM MOPS, 50 mM NaCl, pH7.5. Enzyme concentration was determined using a Bradford Assay (Bio-Rad Laboratories, Inc., Hercules, CA). MLCK was mixed 1:1 with glycerol and stored for up to one year at -20° C until needed for experiments.

2.2 Preparation of Proteins

2.2.1 RLC Phosphorylation

Human recombinant RLC (WT, N47K or R58Q) was dialyzed against 25 mM MOPS, 25 mM NaCl, 10 mM MgCl₂, 0.2 mM PMSF, pH 7.3, 5 mM DTT at 4°C. Calmodulin (CaM) purchased from AG Scientific, Inc. (San Diego, CA, cat #C-1431) was pre-incubated with MLCK in a buffer containing 25 mM MOPS, 25 mM NaCl, 10 mM MgCl₂, 0.2 mM CaCl₂, pH 7.3, 40% glycerol, 5 mM DTT. Equal volumes of RLC and MLCK/CaM solutions were mixed together at room temperature, and ATP was added at final concentration of 5 mM to initiate the phosphorylation reaction. The stock ATP solution was adjusted to pH 6 prior to being added to the reaction in order to prevent significant acidification and subsequent precipitation of proteins in the reaction. RLCs at a concentration of ~100 µM were phosphorylated with 0.25 µM MLCK and 1 µM CaM in a buffer containing 25 mM MOPS, 25 mM NaCl, 10 mM MgCl₂, 0.1 mM CaCl₂, 0.1 mM PMSF, pH7.3, 20% glycerol, 5 mM DTT, 5 mM ATP. The reaction was incubated

at room temperature for 1 hour and then placed on ice. Mock reactions were performed alongside phosphorylation reactions for experiments using dephosphorylated hvRLCs. In the mock reaction, the volume of MLCK was replaced by an equal volume of buffer solution. To determine the extent of RLC phosphorylation, RLCs were dissolved in 8 M urea gel sample buffer and run on a 10% polyacrylamide gel containing 8 M urea (see section 2.3.1). Phosphorylation reactions and mock reactions remained on ice for 1 to 3 hours until the RLCs could be reconstituted on RLC-depleted porcine cardiac (PC) myosin.

Phosphorylation of native RLC bound to PC myosin was carried out as described above for isolated recombinant hvRLCs with the following modifications: PC myosin was diluted in 10 volumes of cold ddH₂O and 10 mM DTT, placed on ice for 1 hour and allowed to precipitate. PC myosin was collected by centrifugation at 10,000g for 25 min in a tabletop centrifuge (Microfuge® 18, Beckman Coulter, Inc., Pasadena, CA), and resuspended in a buffer containing 25 mM MOPS, 300 mM NaCl, 10 mM MgCl₂, 0.2 mM PMSF, pH 7.3, 5 mM DTT. The rest of the procedure was carried out as described above except that the reaction was performed at 160 mM NaCl, and in the presence of 4 μM PC myosin in place of isolated RLCs. Following incubation at room temperature for 1 hour, the myosin was precipitated in 10 volumes of cold ddH₂O and 10 mM DTT for 1 hour and collected by centrifugation (10,000 x g for 25 min). Phosphorylated PC myosin was resuspended in myosin buffer (0.3 M KCl,

25 mM BES, 4 mM MgCl₂, 1 mM EGTA, pH 7.4, 1 mM DTT), mixed 1:1 in glycerol and stored for up to one month at -20° C until needed for experiments.

2.2.2 RLC Depletion and Exchange

PC myosin was depleted of its endogenous RLC and reconstitution of RLC-depleted myosin was accomplished with bacterially expressed hvRLCs. PC myosin (2 mg/mL) was treated with 0.8% Triton X-100 and 15 mM CDTA, in a buffer containing 0.5 M KCl, 10 mM potassium phosphate, pH 8.5, for 15 minutes at room temperature with slow stirring. Myosin in solution was precipitated with 10 volumes of cold ddH₂O containing 10 mM DTT and collected by centrifugation (10,000g for 25 min). Myosin depleted of endogenous RLC was then resuspended in a buffer composed of 0.4 M KCl, 50 mM MOPS, pH 7, 2 mM MgCl₂, and 1 mM DTT and mixed in a 1:3 molar ratio (depleted myosin: RLC) with recombinant hvRLC (WT, N47K, or R58Q) and incubated at 4° C for 2 hours with slow stirring. RLC-reconstituted myosin was dialyzed in 10 mM MOPS, pH 7, 5 mM DTT at 4° C and collected by centrifugation (10,000 x g for 25 min). Myosin pellets were resuspended in myosin buffer, then mixed 1:1 with glycerol and stored at -20° C until needed for experiments. PC myosin, RLC depleted myosin and RLC exchanged myosins were analyzed for levels of RLC exchange via 12% SDS-PAGE.

2.2.3 TRITC Phalloidin Actin

Actin filaments were labeled with tetramethylrhodamine isothiocyanate (TRITC) and visualized using epifluorescence in *in vitro* motility assays. The TRITC fluorophore emits bright orange light (575 nm peak) when excited with yellow-green light (557 nm peak). TRITC conjugated to phalloidin was purchased from Invitrogen (Life Technologies, Carlsbad, CA, cat #R415) for the labeling reaction. TRITC-phalloidin was resuspended in methanol to a concentration of 100 μ M. Actin was labeled with the TRITC fluorophore by incubating 2 μ M TRITC-phalloidin with 1 μ M unlabeled actin in actin buffer composed of 55 mM KCl, 25 mM BES, 5 mM EGTA, 4 mM MgCl₂, and 1 mM DTT. The mixture was incubated for 2 hours at room temperature, and then 4° C overnight. TRITC-phalloidin actin was stored at 4° C in actin buffer, and protected from light.

2.3 Polyacrylamide Gel Electrophoresis (PAGE)

2.3.1 SDS-PAGE

Protein samples were frequently analyzed using SDS-PAGE. Gels were formed by pouring an acrylamide solution between two gel plates spaced 1 mm apart. Protein samples loaded onto the gel are separated by an applied electric field which causes the proteins to migrate through the gel based on their associated charge. For SDS-PAGE, the gel solution is composed of 375 mM Tris-base, pH 8.8, with a specified percentage of Acrylamide/Bis-Acrylamide (typically 10-12%). Gels were poured immediately following addition of 0.05%

TEMED and 0.05% ammonium persulfate, which initiate polymerization of the acrylamide. Protein samples were denatured in 8 M urea, and one part sample buffer was added to 4 parts protein sample. Sample buffer was composed of 300 mM Tris-HCl, pH 6.8, 8 M urea, 500 mg/ml sucrose, 0.05% Bromophenol Blue, 5% β -mercaptoethanol, and 5% SDS. Protein samples were loaded onto the gel and the experiment was carried out in a running buffer composed of 25 mM Tris-base, 192 mM glycine, pH 8.3, and 0.1% SDS.

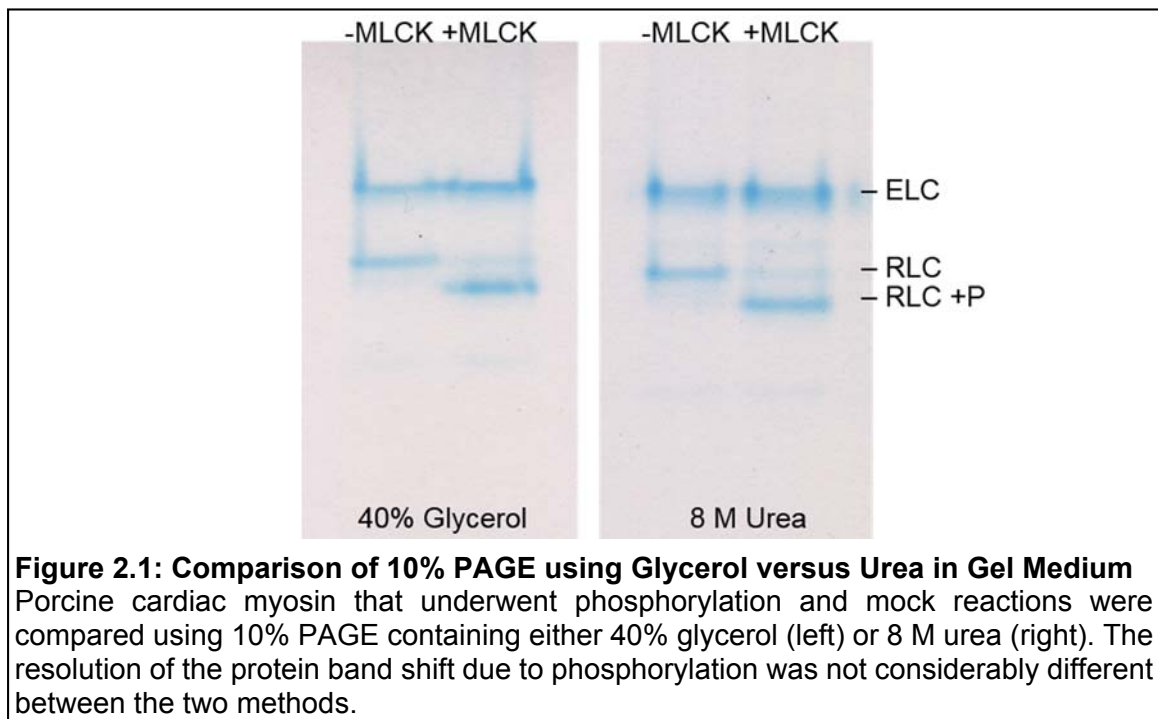
In SDS-PAGE, denatured proteins are coated in SDS, an anionic detergent that applies a negative charge to each protein in proportion to the protein's mass. The mobility of a protein through the gel matrix therefore depends on the size of the protein, due to a relatively equal charge-to-mass ratio of the protein samples, with smaller proteins migrating at a faster rate towards the anode.

2.3.2 Native-PAGE

Native-PAGE is one method that can be used to determine the charge state of a protein of interest. Using this method, denatured proteins retain their native charge, and separation of protein samples in the gel matrix depends on the protein's charge-to-mass ratio. Charge differences between proteins of similar size are resolved using native-PAGE, with more negatively charged proteins migrating at a faster rate toward the anode and further through the gel matrix. Urea-PAGE and glycerol-PAGE are two types of native-PAGE that are

used to determine protein phosphorylation states of myosin light chains [103, 125].

For native-PAGE experiments, the same protocol was used as for SDS-PAGE except no SDS was added to the sample buffer or running buffer. In addition the gel solution was supplemented with either 8 M urea or 40% glycerol. The only difference between the urea-PAGE and glycerol-PAGE preparation was the composition of the gel matrix. The two methods were compared to determine which gel medium provided a better resolution of charge separation between dephosphorylated and phosphorylated RLC. Differences in the resolution of



protein separation between urea-PAGE and glycerol-PAGE were negligible (Figure 2.1). However the glycerol based gel required an additional 2 hours to

polymerize compared to the urea-based gel, and therefore urea-PAGE was chosen as the method to analyze levels of RLC phosphorylation.

2.4 Actin-Activated ATPase

In the absence of actin, myosin undergoes ATP hydrolysis at a rate that is up to 200 times slower than that in the presence of actin [73]. The binding of myosin to actin induces conformational changes in the myosin motor domain that facilitate the release of phosphate at a much faster rate, and therefore significantly increases the myosin ATPase rate [126]. This actin-activation of myosin ATPase activity increases until the actin binding sites on myosin become fully saturated and myosin ATPase reaches a maximal rate. To determine myosin ATPase activity the rate of phosphate production was measured by monitoring solution absorbance at 360 nm. Using the Enzyme Linked Inorganic Phosphate Assay (ELIPA) kit purchased from Cytoskeleton, Inc. (Denver, CO, cat #BK051), myosin enzymatic activity is coupled to the catalytic conversion of 2-amino-6-mercapto-7-methylpurine ribonucleoside (MESG) to 2-amino-6-mercapto-7-methylpurine by purine nucleoside phosphorylase (PNP), resulting in an absorbance shift from 330-360 nm. When myosin releases one molecule of phosphate, it reacts with MESG to produce one molecule of 2-amino-6-mercapto-7-methylpurine in an essentially irreversible reaction. Myosin at 0.1 μM was mixed with 1 μM actin in the reaction buffer containing 100 mM KCl, 5 mM MgCl_2 , 15 mM PIPES, pH7.1, 0.5 mM DTT, and 0.17 mM MESG and 0.54 units PNP.

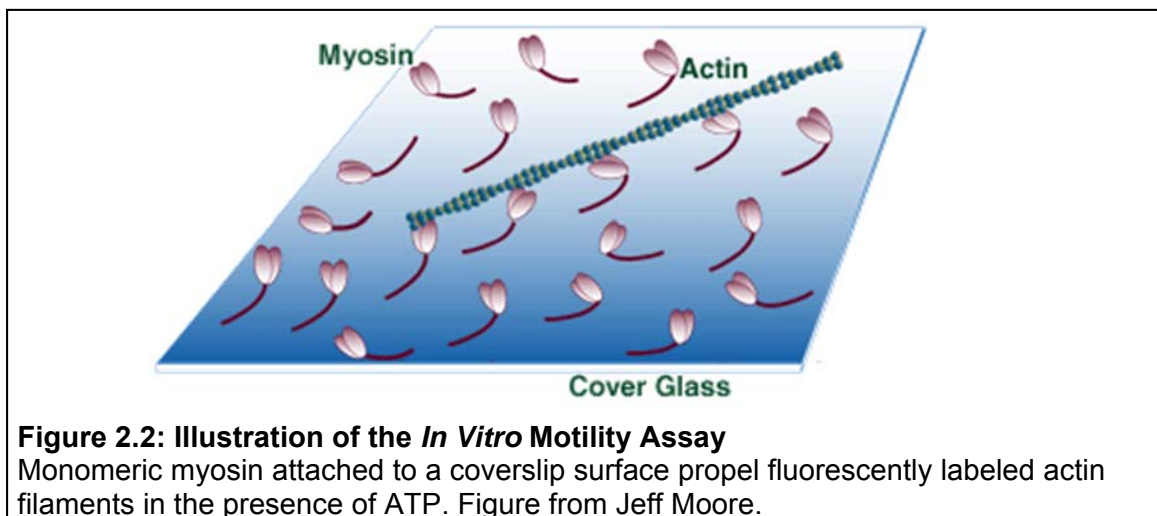
The reaction was initiated by the addition of 1 mM ATP. Solution absorbance was measured at 360 nm, with readings taken every 30 sec for 20 minutes. The change in absorbance over time was fit to a linear regression, and the myosin ATPase rate was determined from the slope of the trendline. A phosphate standard curve was used to convert solution absorbance to nmol phosphate. The same reaction buffer was used for generation of the standard curve, with myosin, actin and ATP replaced by 0 to 50 nmol phosphate. For each phosphate concentration, the solution absorbance was measured at 360 nm after a five minute incubation period.

For comparisons between two groups (i.e. dephosphorylated and phosphorylated, WT and mutant), a two-tailed t-test was used to determine the significance of differences in myosin ATPase rates. The p value was calculated from the Student's t-test distribution, and differences were considered significant for $p < 0.05$. For comparisons between multiple groups (i.e. dephosphorylated myosins, phosphorylated myosins, all myosins), significance of mean ATPase values was determined using a one-way ANOVA. The p value was calculated using the F distribution, and differences were considered significant for $p < 0.05$.

2.5 *In Vitro* Motility Assays

The *in vitro* motility assay was developed by Kron and Spudich in 1986 [67] and provides a method for characterizing the motile behavior of individual myosin molecules. In this assay, randomly oriented myosin molecules that are

adhered to a glass coverslip translocate fluorescently labeled actin filaments in the presence of ATP (Figure 2.2). Labeled actin filaments are observed using a fluorescence microscope. The measurement of actin sliding velocity under various biochemical conditions allows for the characterization of the bed of myosins. The *in vitro* motility assay probes the parameters of the actomyosin biochemical cycle by eliminating some of the elements that tend to complicate the interpretation of muscle fiber studies, such as myofilament lattice spacing, cross-bridge recruitment and structural sarcomeric protein components.



2.5.1 Epifluorescence Microscopy

Fluorescence is a property attributed to organic and inorganic specimens that are able to absorb light radiation at a specific wavelength, and subsequently re-emit the light at a longer wavelength. Fluorophores are fluorescent chemical compounds that can be used as probes to label an element of interest.

Fluorescence microscopy utilizes a specific set of chromatic filters to manipulate the wavelengths of light used for illumination and detection of the specimen. It is crucial to separate the light that travels through the illumination pathway (incident on the specimen) from the light that travels through the detection pathway (incident on the camera). This is accomplished using a filter cube which houses the chromatic filter set (Figure 2.3). The filter cube contains an excitation filter and an emission filter that are placed orthogonal to each other, and a dichroic beam-splitter that is placed between the two filters. The excitation and emission filters allow a narrow range of light to pass through that corresponds to the fluorophore's absorption and emission spectra, respectively. A dichroic beamsplitter is a filter that reflects light below a certain cutoff wavelength and transmits all light above that wavelength. The cutoff wavelength of the dichroic beamsplitter should be between the wavelengths of the excitation and emission filters.

Unfiltered light from the illumination source passes through the excitation filter to the dichroic mirror, where it is reflected upwards through the objective and focused on the specimen. Light emitted from the specimen passes through the objective and is transmitted through the dichroic and emission filters on to a detector. This type of fluorescence microscopy is known as epifluorescence, because the excitatory light passes through the objective before reaching the specimen, and therefore irradiates the specimen from the viewing side. A much greater percentage of excitatory light is transmitted through the specimen than is

reflected by the specimen. Therefore epifluorescence has the advantage that only reflected excitatory light from the specimen needs to be filtered out of the detection pathway, as opposed to the transmitted excitatory light which would be of a much higher intensity and result in a reduced signal to noise ratio [127].

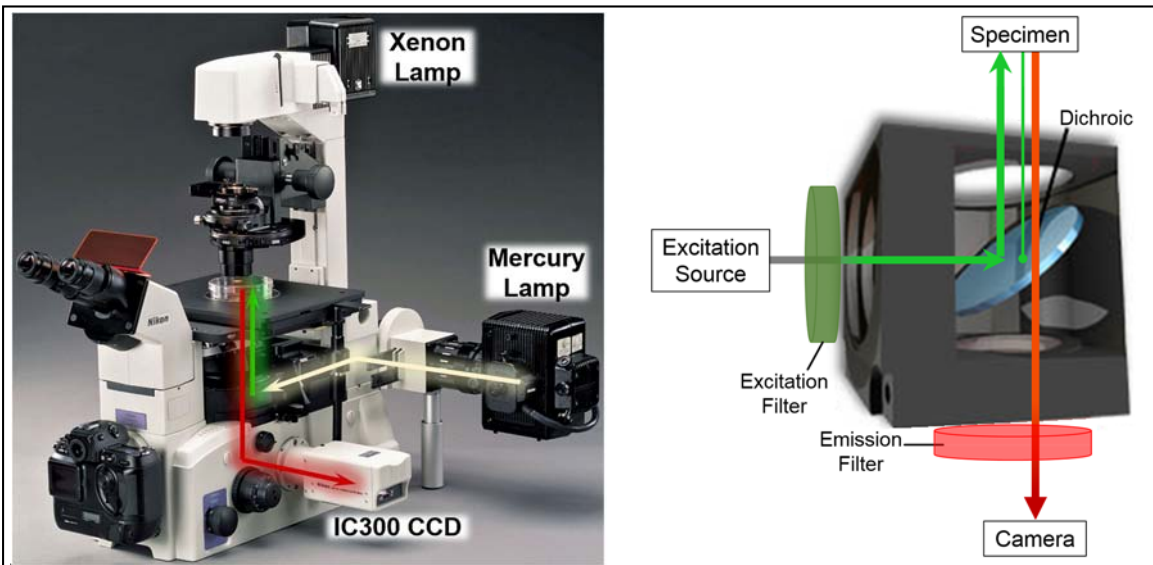


Figure 2.3: Fluorescence Microscope and Filter Cube Schematic

Left: An inverted Nikon Eclipse TE2000 microscope utilizes a mercury lamp for epifluorescence imaging, and a xenon lamp for bright-field imaging. An IC300 CCD and iXon EMCCD (not shown) detect light at either side port of the microscope. A turret that houses filter cubes lies in the detection pathway, and in the excitation pathway of the mercury lamp. *Right:* The filter cube houses a set of chromatic filters that manipulates the light traveling through the excitation and emission pathways. Adapted from <http://media-2.web.britannica.com/eb-media/70/136570-004-F313D891.jpg> and <http://www.olympusmicro.com/primer/techniques/fluorescence/images/fluorescencecube2.jpg>

Our microscope setup consists of a Nikon Eclipse TE2000 inverted microscope with a mercury lamp as the epifluorescence illuminator, and a xenon lamp as the brightfield transilluminator (Figure 2.3). Light is detected with one of two cameras located at the left (IC300 CCD, PTI, Birmingham, NJ) and right (iXon3 897 EMCCD, Andor Technology USA, Concord, MA) sideports of the

microscope. The set of chromatic filters used for motility assay experiments aimed at visualizing TRITC fluorophores coupled to actin are a 545/30 nm excitation filter, a 565 nm long pass dichroic, and a 600/45 nm emission filter.

2.5.2 Standard Motility Assay Protocol

Coverslips were coated with 1% nitrocellulose to permit the attachment of myosin molecules to the coverslip surface. Glass coverslips were plasma cleaned, then dipped in a solution of 1% nitrocellulose in isoamyl acetate and allowed to dry. A flow chamber was constructed by attaching two opposite sides of the coverslip to a glass microscope slide with double stick tape. The depth of the flow cell is equal to the thickness of the double stick tape (100 μm). The volume of the constructed flow chambers was approximately 15 μL . Assay conditions are determined by the experimental solutions added to the flow cell.

Damaged myosin heads that are unable to bind and release from actin were removed during the sample preparation by centrifugation prior to light microscopy. Then, myosin suspended in myosin buffer was mixed with 1.1 μM actin and 1 mM ATP and centrifuged in an Airfuge for 25 min at 100,000 \times g. The concentration of myosin in the supernatant was determined using the Bradford Assay, and myosin was diluted to a concentration of 100 $\mu\text{g/ml}$ in myosin buffer.

Solutions were added to the flow chamber in 30 μl volumes. One volume of myosin solution was added to the flow chamber and incubated for 2 min, during which time myosin is adsorbed to the coverslip surface. The chamber was

then washed with one volume of 1 mg/ml BSA in myosin buffer to fill any remaining gaps on the coverslip surface and thus prevent non-specific binding to the coverslip surface. After 1 minute BSA incubation, the chamber was washed with two volumes of actin buffer (55 mM KCl, 25 mM BES, 5 mM EGTA, 4 mM MgCl₂, and 1 mM DTT). To block any inactive myosin present on the coverslip surface, 1 μM unlabeled actin in actin buffer was added to the flow cell and allowed to bind to the myosin for 2 minutes. The chamber was washed with two volumes of actin buffer containing 1 mM ATP, followed by four volumes of actin buffer with no ATP. TRITC-labeled actin filaments (~ 10 nM) in actin buffer were then added and allowed to bind to the myosin in the absence of ATP for 1 min. The movement of actin was initiated by the addition of 1 mM ATP in actin buffer with 4 mg/mL glucose, oxygen scavengers (17 units/ml glucose oxidase and 125 units/ml catalase) and 0.5% methylcellulose. Actin filament movement was observed at 30°C with an intensified charge-coupled device camera (IC300; PTI, Birmingham, NJ, USA). Video images were captured using a PIXCI® EL1 frame grabber and XCAP software (Epix, Inc., Buffalo Grove, IL, USA), and two or more movies per flow cell were analyzed.

Modifications to the *in vitro* motility assay allow for the characterization of different myosin properties. In the following sections, experimental variations of the *in vitro* motility assay are discussed, and corresponding protocol modifications and data analysis are presented.

2.5.3 Unloaded Motility Assays

Introduction

For unloaded motility assays standard motility buffers were used and no modifications were introduced to the standard protocol. Actin sliding velocity was measured to assess and compare myosin activity. The unloaded actin sliding velocity measured in this assay is referred to as the observed maximal sliding velocity (V_{\max}) and provides a reference for assessing myosin activity.

Data Analysis

For each experimental preparation (one flow cell), at least two video segments were recorded, and actin sliding velocity was determined by averaging the velocities of at least 25 actin filaments. Actin filament velocities were measured using MTrackJ, a plugin supported by the public domain image processing program, ImageJ (U. S. National Institutes of Health, Bethesda, Maryland, USA). MTrackJ allows for the manual tracking of moving objects within an image sequence. Actin filament velocity was determined by tracking the distance the filament traveled between 10 to 30 consecutive video frames taken at one second intervals.

The maximal sliding velocity (V_{\max}) produced by each myosin type was determined by the averaging the actin sliding velocities measured from 4-8 experimental preparations. A two-tailed t-test based on the mean and standard deviation of sliding velocities was used to determine significance between V_{\max} values. The p value was calculated from the Student's t distribution, and

differences were considered significant for $p < 0.05$. Differences between maximal sliding velocities of multiple groups was determined from the F statistic of a one-way ANOVA. The p value was calculated using the F distribution, and differences were considered significant for $p < 0.05$.

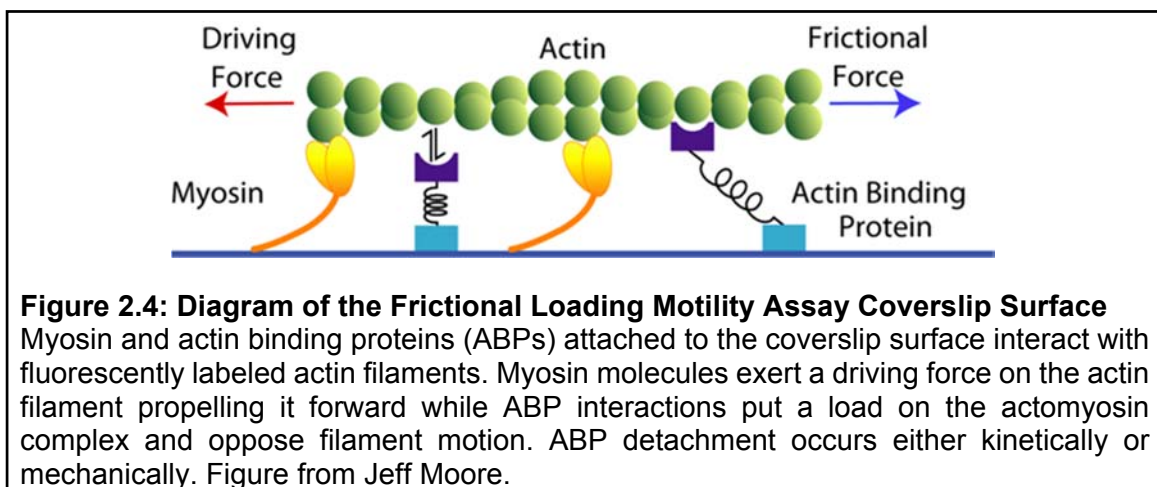
2.5.4 Frictional Loading Motility Assays

Introduction

A major factor that affects heart performance is the load experienced by the heart. In the previous sections, unloaded assays that measure velocity and ATPase were described. When there is no load imposed on the muscle, it does not produce any force and will contract at maximal velocity. Unloaded conditions are not physiological but provide a reference level of contractility for our experiments. Loaded *in vitro* motility assays mimic more physiologically relevant conditions and were performed for myosins containing various RLC.

When the load imposed on a muscle is equal to or greater than the maximal force generating capabilities of the muscle, the muscle is unable to shorten as it contracts. Since the afterload experienced by the heart is less than the maximal force output of the myocardium, the ventricular muscle can produce force equal to the afterload while shortening in order to eject blood. Using loaded *in vitro* motility assays, myosin load-dependent behavior mimicking that *in situ* was characterized where myosin generates both force and motion, and consequently power.

To determine mutant and WT myosin maximal force generation with and without phosphorylation we employed a frictional loading assay where α -actinin, a non-motor actin-binding protein, was used as a mechanical load in the standard *in vitro* motility assay (Figure 2.4) [57, 155]. Actin filament motility is reduced in the presence of α -actinin, a protein that weakly and transiently binds to actin [38, 68]. As α -actinin surface concentration increases, actin filaments experience a greater opposing force to the myosin driving force, and actin sliding velocity decreases. The myosin driving force can be estimated by modeling the relationship between the α -actinin concentration and actin sliding velocity [43].



Protocol Modifications for Frictional Loading

The procedure for frictional loading motility assays was identical to the standard *in vitro* motility assay except with one modification. The initial incubation of 100 $\mu\text{g}/\text{mL}$ myosin in myosin buffer was mixed with varying amounts of α -actinin before being added to the flow chamber. After incubation for one minute,

myosin and α -actinin were bound to the coverslip surface. BSA was added next and the procedure was completed as described in section 2.5.2.

Data Analysis

For each flow cell, at least two video segments were recorded, and actin filaments were tracked for 10 to 30 consecutive video frames taken at one to five second intervals. The actin sliding velocity was determined from 25 to 30 actin filaments for each flow cell. This average velocity and its associated α -actinin concentration represents one data point in a single experiment. RLC depletion and reconstitution was performed on at least three different PC myosin preparations, and an experimental data set incorporating a range of α -actinin concentrations was obtained for each preparation. A weighted average (based on the number of filaments analyzed) of the velocities from all data sets was calculated and are plotted in Figure 3.6. All parameters determined from model fitting were determined from the average data set.

In the absence of an exogenously added load, the myosin driving force (F_d) propels actin at maximal velocity (V_{max}). In the frictional loading motility assay, α -actinin provides an exogenous load (F_{load}) to the actin filament that opposes the myosin driving force. Actin sliding velocity (V) is determined by the balance of the forces acting on the actin filament:

$$V = \frac{V_{max} \times (F_d - F_{load})}{F_d} \quad (\text{Eq. 1})$$

The frictional load exerted by α -actinin, α in Eq. 2, in the motility assay is given by:

$$F_{load} = \frac{V \times \kappa \times \zeta \times L \times r \times k_A \times \chi \times [\alpha]^{5/2}}{k_D \times (k_A \times \chi \times [\alpha]^{3/2} + k_D)} \quad (\text{Eq. 2})$$

where κ is the system compliance associated with the α -actinin and the α -actinin–actin linkages, L is the length of a typical actin filament, r is the reach of an α -actinin protein to bind to an actin filament, k_A is the second-order rate constant for α -actinin attachment to actin, k_D is the α -actinin detachment rate, and ζ and χ are constants that define the surface geometry of α -actinin on the surface [43].

A model describing actin sliding velocity (V) dependence on α -actinin concentration ($[\alpha]$) is derived by substituting Eq. 2 into Eq. 1. This model was fit to the data obtained from frictional loading motility assays according to Eq. 3:

$$V = \frac{V_{max} \times F_d}{F_d + \left(\frac{V_{max} \times \kappa \times \zeta \times L \times r \times k_A \times \chi \times [\alpha]^{5/2}}{k_D \times (k_A \times \chi \times [\alpha]^{3/2} + k_D)} \right)} \quad (\text{Eq. 3})$$

The derivations of Eq. 2 and 3, values used for model fitting, and an explanation of model limitations are provided in Greenberg and Moore, 2010 [43].

The program SigmaPlot (Systat Software Inc., San Jose, CA) was used to fit data sets to Eq. 3 with a nonlinear least squares fitting algorithm. Errors in the least squares fit were used to determine coefficient parameters and standard errors for maximal sliding velocity (V_{max}) and isometric force (F_d) of the randomly oriented myosin ensemble. Significance between F_d values was examined using

a one-tailed t-test. First, F tests were performed to verify that two groups had equal variances. The t value was determined by calculating the pooled estimate of the variance using the standard errors of the coefficients from the least squares fit. The pooled variance is given by:

$$S_{P12} = \frac{SE_1^2(n_1 - 2) \times n_1 + SE_2^2(n_2 - 2) \times n_2}{n_1 + n_2 - 4}$$

where SE_x and n_x represent the standard error of the coefficient and number of data points defining the curve, respectively. The t value is then given by:

$$t = \frac{x_1 - x_2}{\sqrt{\left(\frac{S_{P12}}{n_1} - \frac{S_{P12}}{n_2}\right)}}$$

The degrees of freedom is equal to $n_1 + n_2 - 4$ [37]. A p value was obtained using the Student's t distribution, and differences in F_d values were considered significant for $p < 0.05$.

Comparison of Loaded In Vitro Motility Assay Models

In the loaded motility assay, an actin binding protein (ABP) bound to the coverslip surface is utilized as a load bearing molecule. When the ABP binds to actin, it provides an exogenous load to the actin filament and actomyosin complex. The α -actinin protein has been one of the most widely used ABP employed in the loaded *in vitro* motility assay [11, 41, 57, 75]. The properties of α -actinin and the α -actinin–actin bond are well characterized which allowed for the derivation of the frictional loading model described above. In a recent publication by Aksel et al., a new version of the loaded motility assay is described

that utilizes a utrophin-based ABP to provide an opposing load to the actomyosin [2]. The authors use this assay to characterize the behavior of myosin S1 constructs on the coverslip surface (as opposed to full length myosin). Below is a comparison of the two different loaded motility assays using either α -actinin or utrophin as the load bearing ABP.

In the utrophin-based assay, the authors express a short construct of the human cardiac β -myosin S1 (sS1). Characterizing human isoforms of myosin is a major advantage for studying disease-linked mutations; however, the sS1 construct lacks the RLC binding region and therefore cannot be used to study mutations and phosphorylation of the RLC. The expressed myosin sS1 and utrophin constructs are engineered with a short C-terminal peptide which binds to an anchoring protein that is attached to the motility assay surface [2]. This reduces variability in the linkage of myosin and utrophin to the coverslip surface. The utrophin construct used in the assay contains an actin binding domain and a single spectrin repeat; it was designed to be similar in size to the myosin sS1. In contrast, an α -actinin monomer contains an actin binding domain, four spectrin repeats, and an EF hand domain [27]; it is closer in size to full length myosin. The choice of ABP used in loaded motility assays must have a similar reach as the myosin on the surface in order for both myosin and ABP to be accessible to the actin filaments. Based on the mechanical differences between the two proteins and their bond to actin, it is expected that the nature of the load produced by α -actinin and utrophin will differ.

In a loaded motility assay, when an ABP binds to an actin filament it becomes stretched as the myosin driving force pulls the actin filament away. Strain accumulates in the ABP while it is attached to the actin filament, and it produces a load opposing the myosin driving force. The load imposed by a single ABP will depend on the elasticity of the ABP and the ABP–actin bond, as well as the duration of the ABP–actin bond.

For the loaded motility assays presented in this work, the load exerted by α -actinin is modeled as being velocity dependent due to the elastic nature of the α -actinin protein. An α -actinin molecule will exert a greater force on an actin filament the more it is stretched, and a faster moving actin filament will stretch the α -actinin molecule further during the kinetic lifetime of the α -actinin–actin bond. Therefore the load exerted by α -actinin is dependent on actin sliding velocity. The load produced by a certain concentration of α -actinin is defined in Eq. 2 which uses parameters for α -actinin stiffness and the duration of the α -actinin–actin bond that have been characterized in the literature. The model uses a first order approximation for α -actinin–actin detachment rate; this makes the simplifying assumption that the detachment rate of α -actinin is independent of strain. Characterization of the strain dependence of the α -actinin–actin bond would allow for a better approximation of the kinetic lifetime of the bond as it changes with load. Incorporation of this data (if it becomes available) would provide higher order corrections to the model described in Eq. 2 and 3.

Aksel et al. show that the actin filaments in the utrophin-based loaded motility assay are either moving at maximal velocity or are stopped. This implies that utrophin stops an actin filament immediately upon binding, which makes the assumption that utrophin (and the utrophin–actin bond) is not elastic or that elasticity is immediately pulled out of the protein and bond upon binding to actin. This is a valid assumption given the small size of the utrophin construct. For each utrophin concentration analyzed, Aksel and colleagues take into account the amount of time each filament spends moving versus stopped, as well as the average filament velocity as a result of this behavior. From this relationship, the authors are able to define a dissociation constant for the utrophin–actin interaction in the presence of myosin sS1 [2]. The data can be interpreted as a binding equilibrium between utrophin and actin that will change based on the force exerted on actin by myosin sS1 on the surface. Myosin that produces a higher force on an actin filament will increase the detachment rate of utrophin, and therefore yield a larger dissociation constant (i.e. the concentration of utrophin that corresponds to an equilibrium between motile and stopped actin filaments). Therefore the load exerted by the utrophin construct on an actin filament is interpreted as being dependent on the strain dependence of the detachment rate.

Both versions of the loaded *in vitro* motility assay make assumptions about the nature of the ABP used. For α -actinin, it is assumed that the strain dependence of the detachment rate is negligible compared to the effects from

protein's elastic properties. For utrophin, it is assumed that elasticity of the protein and bond to actin is negligible compared to the strain dependence of the detachment rate. Both assumptions are well suited to the nature of the ABP and interpretation of the data. An advantage of using the α -actinin loading model is that α -actinin surface concentration can be converted to a loading force based on physiological parameters of α -actinin and the α -actinin–actin bond that have been characterized in the literature. This allows for the characterization of myosin's load dependent behavior and the construction of myosin power output curves.

2.5.5 Power Transformation

Introduction

Cardiac power output represents the rate at which the heart can perform work (i.e. eject blood) and is a critical indicator of heart's ability to maintain cardiac output as heart rate changes. Power output can be determined from the force-velocity relationship of muscle. This relationship is a fundamental aspect of muscle contraction which demonstrates that force production increases as filament velocity decreases because myosin cross-bridges have more time to attach to the filament (and more time before detachment) leading to a greater population of bound myosin heads and increased force production of the muscle. The transformation of frictional loading motility assay data to myosin power output is described in the next section.

Data Analysis

Data from frictional loading motility assays was transformed to represent myosin power output as a function of frictional load. First, [α -actinin] for each data point was converted to a frictional loading force, F_{load} , using Eq. 2. Force-Velocity data (F_{load} , V) was obtained from the transform. At a frictional load equivalent to the myosin isometric force ($F_{load}=F_d$), velocity is equal to zero (see Eq. 1). Isometric force values obtained from frictional loading assays were included in the transformed data set (F_d , 0).

Power is the product of force and velocity. Force-velocity data were transformed to force-power data by taking the product of force and velocity, and then plotting the power versus force. Power curves were constructed by fitting the force-power data (F_{load} , P) to the empirically derived Hill equation for power given by [50]:

$$P = b \times F_{load} \times \left(\frac{F_o+a}{F_{load}+a} - 1 \right) \quad (\text{Eq. 4})$$

where F_o is the isometric force and a and b are constants. The equation was fit with a least squares fitting algorithm. The load at which maximal power output occurs was calculated by setting the derivative of the Hill power equation equal to zero and solving for F_{load} . This value was substituted into Eq. 4 to determine maximal power output. Errors in these parameters were determined from the errors in the least squares fit of Eq. 4.

2.5.6 Inhibition of Loaded Motility by ADP

Introduction

Load can only affect the transitions of the actomyosin biochemical cycle that occur while myosin is strongly bound to actin. The cross-bridge attachment time is set by the rates of ADP release and ATP binding, since they are the slowest steps in the attached state. The rate limiting step of the cycle is the release of ADP from the active site [124], and it has been established that the kinetics of the ADP release step are sensitive to load [95]. When a load is applied to muscle, the ADP release rate slows and actomyosin detachment is prolonged. ADP is a competitive inhibitor of ATP for the binding pocket in the rigor state when there is no nucleotide bound. In the following experiments, exogenous ADP was added to loaded *in vitro* motility assays to probe the rate limiting step of biochemical cycle, and study the effects of RLC modifications on the exchange of ADP for ATP in the myosin binding pocket under load.

Protocol Modifications for ADP Binding Studies

The following modifications were made to the standard *in vitro* motility assay protocol: For the initial incubation step, 1.5 $\mu\text{g/mL}$ α -actinin was mixed with 100 $\mu\text{g/mL}$ myosin and then added to the flow chamber. For the final incubation step, the motility buffer was supplemented with 2 mM ADP. Experiments were also performed in the absence of ADP. The concentration of 2 mM ADP is higher than physiological levels of ADP that accumulate in cardiac muscle, which is typically 20-50 μM [55]. This high concentration was chosen to provide an excess

of ADP in relation to ATP, which is present at a concentration of 1 mM, to ensure that ADP could effectively compete with ATP and that the effects of exogenous ADP on loaded motility could be resolved.

Data Analysis

For these experiments, an automated analysis was used to track the position of actin filaments in motility assay movies, as opposed to the previously employed manual tracking method. Automated data analysis was carried out using the ImageJ plug-in wrMTrck (written by J.S. Pedersen, <http://www.phage.dk/plugins/wrmtrck.html>). The wrMTrck plug-in utilizes centroid-tracking algorithms to automatically locate and track objects in an image sequence, and reports object velocities as well as other statistics. Filters were put in place to exclude actin filaments that displayed certain behaviors from the analysis. For example, actin filaments were excluded from analysis if the filament exceeded thresholds pertaining to actin filament length and impaired filament mobility, such as stalling, circling, or non-directional fluctuations. Video segments were recorded at a rate of three frames per second and a minimum of two movies were analyzed per flow cell. Actin filament sliding velocity was then determined by the automated analysis for each flow cell.

For each myosin studied, two experiments were performed, both originating from the same PC myosin preparation and RLC exchange procedure. Average actin sliding velocities were determined from two experiments and a minimum of 50 actin filaments tested. A two-tailed t-test based on the mean and

standard deviation of sliding velocities was used to determine significance between average velocities. The p value was calculated from the Student's t distribution, and differences were considered significant for $p < 0.05$.

CHAPTER 3 – RESULTS:

Effects of Physiological and Pathological RLC Modifications

Introduction

The regulatory light chain (RLC) of myosin provides structural support to the myosin neck region which acts as a lever arm during the myosin powerstroke. During the cyclical interaction of myosin with actin filaments, small conformational changes in the myosin catalytic domain are amplified by the lever arm to produce force and motion [106, 145]. In addition to serving a mechanical role in the transmission of contractile force, the RLC can also fine tune the kinetics of the actomyosin. Phosphorylation is a naturally occurring post-translational modification of the RLC that plays a role in modulating myosin cycling kinetics [42]. It has been established that RLC phosphorylation can increase muscle fiber activation at submaximal Ca^{2+} levels and the rate of force development [23], however a growing body of evidence suggests that RLC phosphorylation has a major influential role in cardiac muscle function, torsion, and disease [122]. Studies of muscle at the fiber and tissue level have begun to elucidate the range and complexity of actions exhibited by RLC phosphorylation, however the molecular based changes induced by RLC phosphorylation on the single myosin motor remains to be determined.

Several genetic mutations identified in the RLC lead to familial hypertrophic cardiomyopathy (FHC) [5]. FHC is characterized by left ventricular

hypertrophy, however the pattern of cardiac remodeling and symptoms that accompany disease vary widely. The phenotype is determined by the specific causal mutation, and may include chest pain, shortness of breath, diastolic filling abnormalities, arrhythmias, but often results in sudden cardiac death in the absence of any other symptoms [21]. Given that the clinical presentation and prognosis of the disease depends on the specific mutation, a detailed understanding of the pathogenesis of each mutation is crucial to the development of therapeutic agents. Two genetic mutations located in the N-terminal lobe of the RLC, N47K and R58Q, display drastically different clinical FHC phenotypes. N47K is associated with late onset, rapidly progressing mid-ventricular hypertrophy [6], while R58Q is associated with early onset hypertrophy and sudden cardiac death [34]. However both mutations result in loss of Ca^{2+} binding to the cationic binding site of the isolated RLC, and a reduction of myosin motility under load [41]. Phosphorylation was shown to restore Ca^{2+} binding ability to the R58Q RLC [139].

The studies presented in this chapter explore the effects of physiological and pathological RLC modifications on the cardiac β -myosin motor protein. We hypothesized that phosphorylation of the RLC could compensate for mutation-induced decreases in myosin contractility. *In vitro* motility assays were employed to test this hypothesis and characterize alterations in actomyosin interactions that occur at the most fundamental level of muscle contraction.

3.1 RLC Phosphorylation

Bacterially expressed WT, N47K and R58Q hvRLCs were phosphorylated by smooth muscle MLCK in order to study the naturally occurring post-translational modification and mutational variants of the RLC.

Phosphorylation of hvRLCs was performed alongside mock reactions under identical conditions except without the presence of CaM-MLCK. After 1 hour incubation at room temperature, hvRLC samples were run on 8 M urea 10% PAGE to determine the extent phosphorylation (Figure 3.1). Addition of a phosphate group to the RLC adds a negative charge to the protein, resulting in a more acidic isoelectric point. Therefore phosphorylated RLC migrates further towards the cathode than its dephosphorylated counterpart in urea-PAGE. As can be seen in Figure 3.1, there was no evidence of phosphorylation in mock reactions.

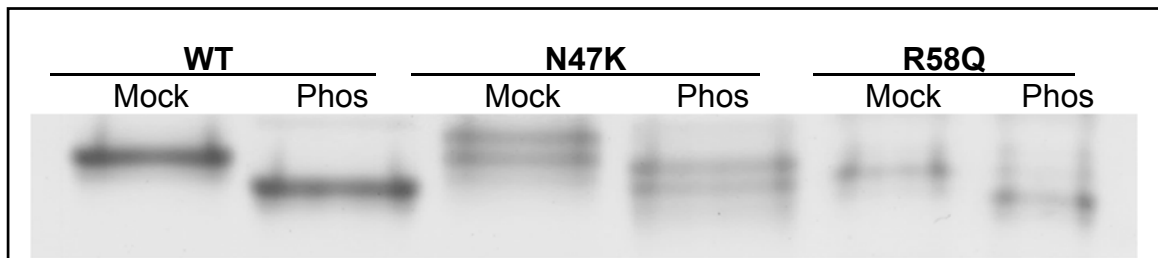


Figure 3.1: Phosphorylation of hvRLCs by MLCK

Charge separation of dephosphorylated and phosphorylated bacterially expressed human ventricular RLCs is shown on an 8 M urea 10% polyacrylamide gel. Due to a more acidic isoelectric point phosphorylated RLCs migrate further than their respective dephosphorylated counterparts. Charge differences introduced by the mutations can also be resolved.

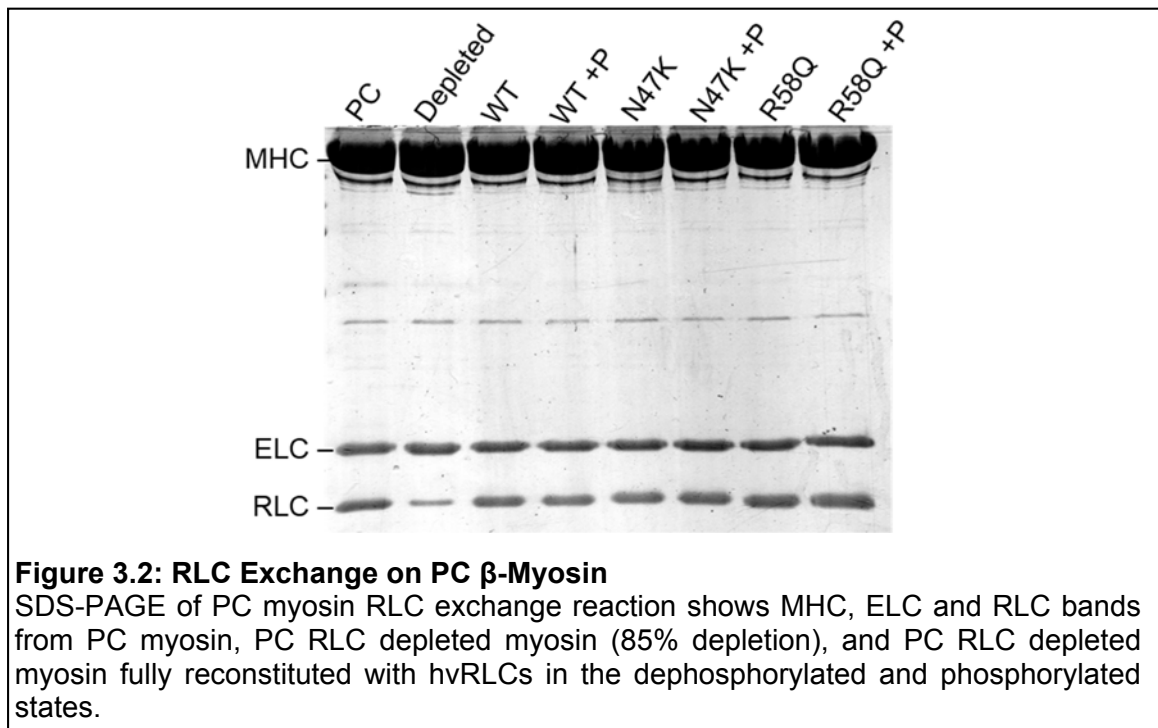
Regulatory light chains were readily phosphorylated as indicated by increased mobility in urea-PAGE. Densitometry analysis showed phosphorylation levels of $95.7 \pm 3.6\%$ for WT RLC, for $98.4 \pm 1.6\%$ N47K RLC, and $87.4 \pm 0.8\%$ for R58Q RLC (given as the mean \pm SE from 4-5 preparations). Phosphorylation of the R58Q light chain was consistently slower when compared to WT and N47K light chains. Therefore, the reaction incubation time was chosen based on the slower kinetics of the enzymatic reaction for the R58Q RLC substrate, which assures complete phosphorylation of each light chain. In addition, the R58Q light chain was more susceptible to proteolytic digestion, as evidenced by the existence of smaller molecular weight fragments appearing with storage times greater than two months. It is possible that increased proteolytic susceptibility and the decreased rate of phosphorylation were caused by structural alterations induced by the R58Q mutation, which could potentially alter the affinity of MLCK and/or proteases for the mutant RLC.

The N47K RLC migrated as a double band in urea-PAGE, but as a single band in SDS-PAGE (see Figures 3.1 and 3.2), indicating the existence of charge variants of the N47K RLC. Both charge variants were consistently phosphorylated. The charge variants may arise from acetylation of the lysine residue introduced by the mutation, or from deamidation of asparagine residues that flank the phosphorylation site at serine15 [119]. Both processes are known to occur in bacterial expression systems. Following mock or phosphorylation

reactions, hvRLCs were kept on ice for 1 to 3 hours and then reconstituted onto porcine cardiac myosin.

3.2 RLC Depletion and Reconstitution

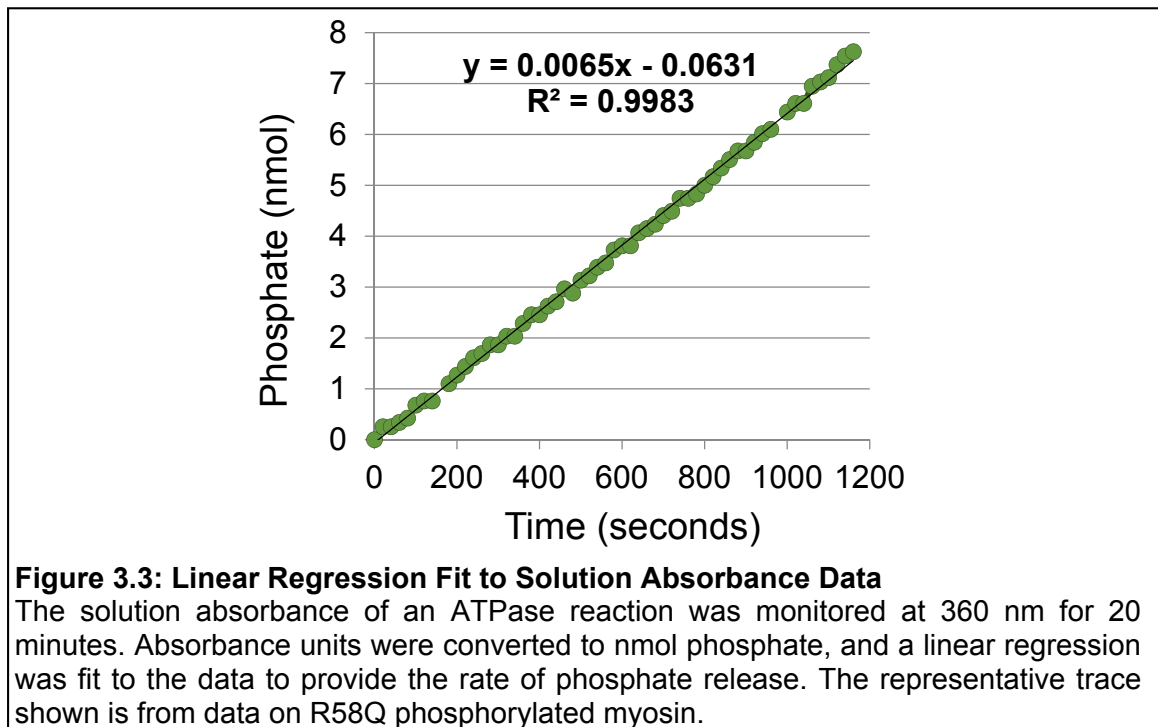
Porcine cardiac (PC) myosin was chosen to study the effect of RLC modifications on β -MHC performance. PC myosin depleted of its native RLC following treatment with triton X-100 and CDTA (Figure 3.2; lane 2) was recombined with dephosphorylated or phosphorylated hvRLCs at a 1:3 molar ratio. Myosin samples were analyzed using 12% SDS-PAGE (Figure 3.2). The level of RLC depletion was determined to be $84.8 \pm 5.8\%$ based on 4 preparations of PC myosin. MHCs were fully reconstituted with hvRLCs.



3.3 Actin-Activated ATPase

Actin-activated ATPase rates were measured under conditions similar to those of the motility assay to assess potential differences in the enzymatic activity between WT and mutant myosins in the phosphorylated or dephosphorylated state. Actin activated ATPase measurements provide valuable information about alterations in actin filament velocity as the rate of actin sliding velocity in the motility assay is directly proportional to the myosin ATPase rate. The actin-activated ATPase assay was performed as described in section 2.3.2.

Myosin at 0.1 μM and actin at 1 μM were mixed in solution with 1 mM ATP. The coupled reaction measuring the amount of phosphate generated by ATP hydrolysis was linear with time and standardized to convert absorbance units to nmol phosphate (Figure 3.3).



The slope of a regression line gives the rate of phosphate release from myosin in nmol/s. The actin-activated myosin ATPase rate is derived from the phosphate release rate by accounting for the amount of myosin present in solution. Table 1 shows the average myosin ATPase rate from three experiments in units of nmol phosphate per nmol myosin per minute. The actin-activated myosin ATPase was not significantly altered by mutations or phosphorylation of RLC.

Table 1: Actin-Activated Myosin ATPase Rates						
	WT	WT Phos	N47K	N47K Phos	R58Q	R58Q Phos
ATPase (min⁻¹) ± Std Error	7.067 ± 1.241	6.500 ± 0.836	6.375 ± 0.897	8.667 ± 1.304	5.700 ± 0.634	6.775 ± 0.844

Shown are mean ATPase rates ± SE from three experiments. There are no significant differences in myosin ATPase rates for any myosin.

3.4 *In Vitro* Motility Assays

Motility assays provide a method for investigating the molecular mechanisms of muscle contraction, and like any technique has a set of limitations. Actin filament sliding is unidirectional due to the polarity of the actin filament, but will follow a winding path rather than a straight line. This is due to the randomly oriented myosins on the coverslip surface that the actin filament encounters, and is a major source of scatter in the sliding velocities of individual filaments. For this reason it is necessary to use an average value from a minimum of 10 filaments [132]. Another source of heterogeneity stems from the

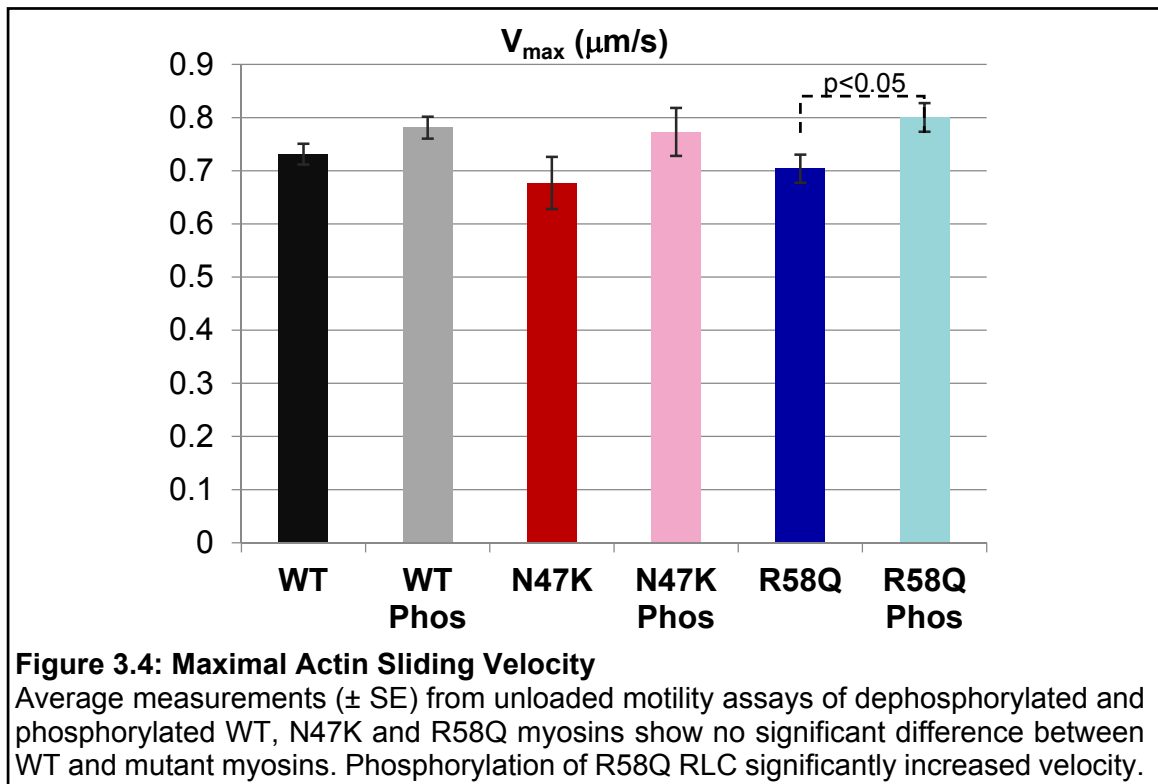
nature of the linkage between the coverslip surface and the myosin molecules. In experiments utilizing myosin S1-S2 fragments where the S2 portion was truncated in various positions, actin sliding velocity decreased as S2 was shortened [96]. Furthermore, damaged myosin heads that form rigor-like bonds may introduce a resistance to the filament sliding velocity, although care is taken to reduce the number of damaged myosins during preparation. These factors cause variation in the measurement of actin sliding velocity and give rise to the inherently noisy nature of the motility assay. Despite these limitations the motility assay is effective in characterizing various fragments, chemical modifications and mutations of myosin and actin as well as other regulatory proteins.

3.4.1 Unloaded Sliding Velocity

The maximal actin sliding velocities of myosin bearing WT, N47K or R58Q RLC in the dephosphorylated and phosphorylated states were measured in the unloaded *in vitro* motility assay (Figure 3.4). Observed values at 100 $\mu\text{g/mL}$ myosin were $V_{\text{max}}(\text{WT})=0.73 \pm 0.02 \mu\text{m/s}$, $V_{\text{max}}(\text{WT Phos})=0.78 \pm 0.02 \mu\text{m/s}$, $V_{\text{max}}(\text{N47K})=0.68 \pm 0.05 \mu\text{m/s}$, $V_{\text{max}}(\text{N47K Phos})=0.77 \pm 0.05 \mu\text{m/s}$, $V_{\text{max}}(\text{R58Q})=0.70 \pm 0.03 \mu\text{m/s}$, and $V_{\text{max}}(\text{R58Q Phos})=.80 \pm 0.03 \mu\text{m/s}$. There was no significant difference in V_{max} values between myosins bearing dephosphorylated RLCs ($p>0.45$), or between myosins bearing phosphorylated RLCs ($p>0.84$), as determined by one-way ANOVA. Additionally, differences in V_{max} values for myosin with dephosphorylated and phosphorylated RLC was not

significantly different for the WT RLC ($p>0.10$) or for the N47K RLC ($p>0.18$).

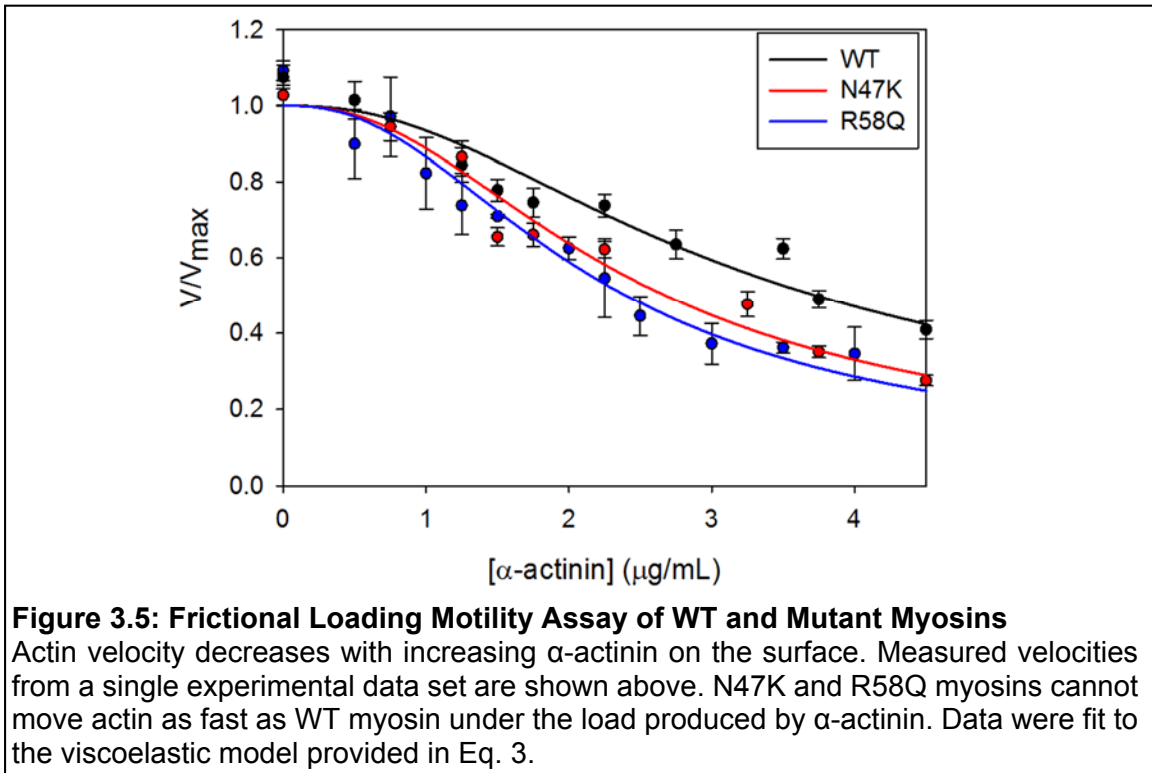
However, there was a significant difference in the V_{\max} values for myosin bearing R58Q RLC in the dephosphorylated and phosphorylated states ($p<0.05$) as determined by a two-tailed Student's t-test assuming equal variances.



3.4.2 Myosin Isometric Force

The frictional loading motility assay was used to study myosin force generation. In this variation of the *in vitro* motility assay, a low affinity actin binding protein, α -actinin, was added to the coverslip surface along with myosin. Binding of α -actinin to actin imposes a viscoelastic drag on the actomyosin. This means the drag force imposed is time dependent, and will depend on the kinetic

lifetime of the α -actinin – actin bond as well as actin filament velocity. Frictional loading motility assays were employed to compare the force producing capabilities of myosin bearing dephosphorylated and phosphorylated hvRLCs. Data from frictional loading motility assays were fit to the viscoelastic model provided in Eq. 3, which models the relationship between actin sliding velocity and the load imposed by α -actinin.



The isometric force of myosin (F_d) was determined from this relationship. In the absence of load, the N47K and R58Q myosins propelled actin at a similar velocity as WT myosin. However, in the presence of an α -actinin-induced frictional load, N47K and R58Q mutant myosins moved actin at slower velocities

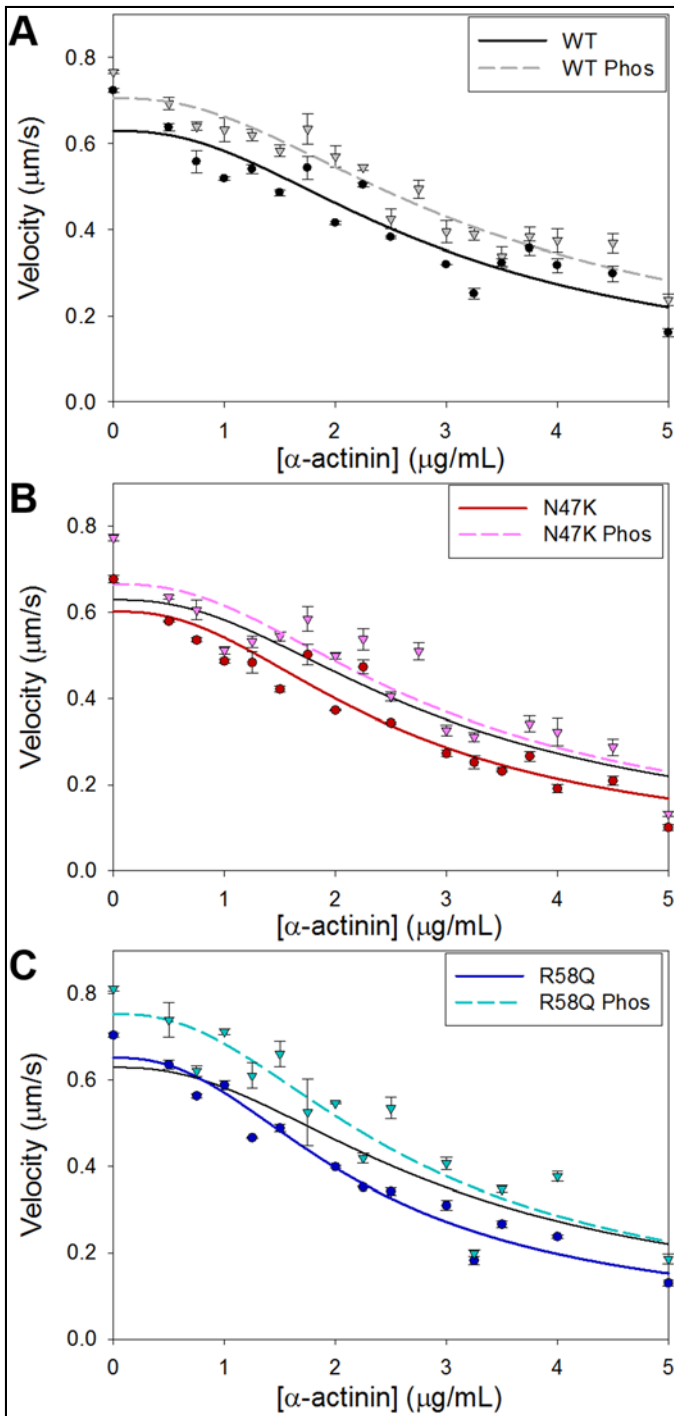


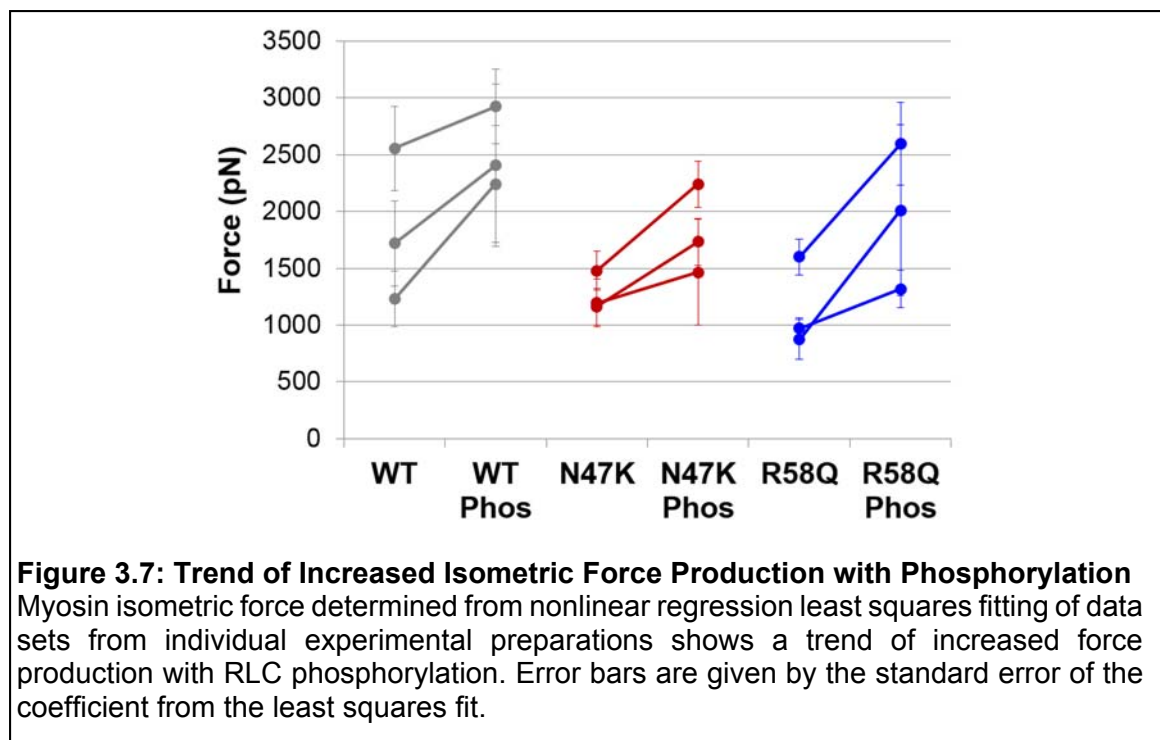
Figure 3.6: Frictional Loading Assays Comparing RLC Phosphorylation States

Average actin sliding velocities and SEs are plotted as a function of α -actinin added to the motility assay surface. Average velocity is determined from 3-4 experiments. Panels show myosin bearing RLCs in the dephosphorylated (circles, solid line) and phosphorylated (triangles, dashed line) states for **A)** WT, **B)** N47K, and **C)** R58Q RLCs. The fit of WT data to Eq. 3 (solid black line) is shown in panels **B** and **C** to aid in visual comparison.

than WT myosin. This trend was seen for the individual experimental data sets (Figure 3.5) as well as for the averaged data sets (Figure 3.6). This resulted in significantly decreased force production for both mutations compared to WT ($p < 0.05$), consistent with previous results [41].

Upon MLCK-induced phosphorylation of the RLC, we see increased actin sliding velocity for WT and mutant myosins at all loads measured (Figure 3.6A-C), resulting in increased force production for myosins containing phosphorylated RLC.

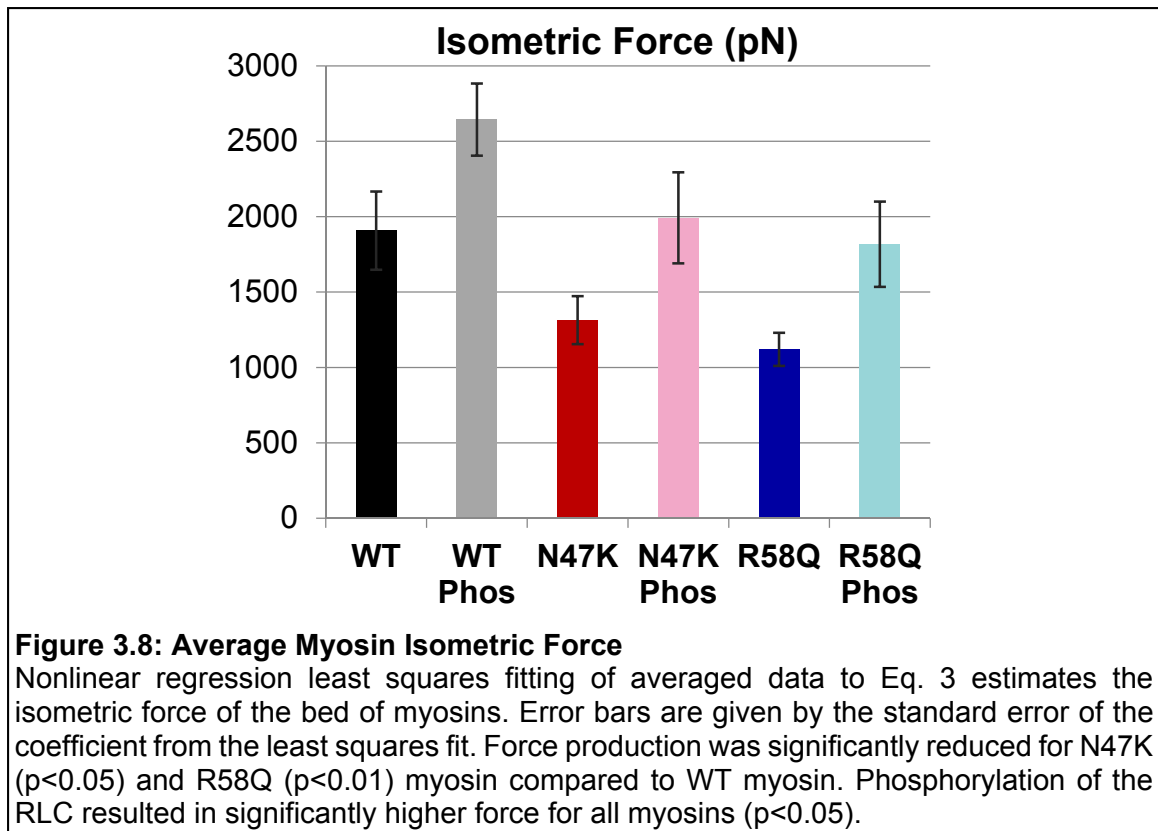
Isometric force values calculated from the model fit were $F_d(WT) = 1908 \pm 259$ pN, $F_d(WT\ Phos) = 2644 \pm 239$ pN, $F_d(N47K) = 1314 \pm 159$ pN, $F_d(N47K\ Phos) = 1992 \pm 302$ pN, $F_d(R58Q) = 1129 \pm 110$ pN, and $F_d(R58Q\ Phos) = 1817 \pm 283$ pN. Phosphorylation-based increases in force were observed for each individual experimental preparation as well as for the averaged data (Figure 3.7 and 3.8).



The data from the motility assays presented above display a fair amount of scatter. This is in part due to the inherent noise associated with the motility assay, and in part due to the averaged data set stemming from three different myosin preparations (each originating from a different pig heart, and undergoing subsequent RLC exchange procedures). In addition, the slow nature of β -myosin, especially when working against a load imposed by high α -actinin surface concentrations, results in actin sliding velocities that approach zero, which limits

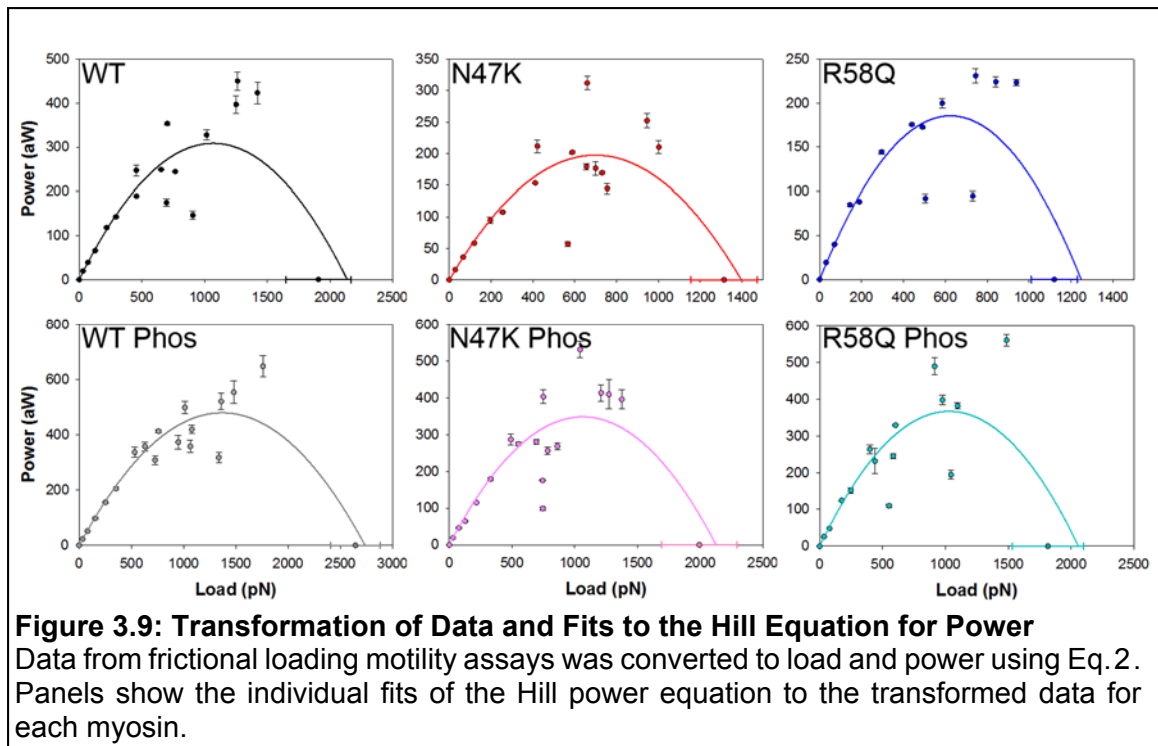
resolving power. To overcome the variance in the data and maintain confidence in parameter estimates, three individual experimental curves were defined for each myosin, each with a high number of data points defining the curve. The trends of the individual experiments are the same for the average data sets (Figure 3.7 and 3.8). Most importantly, the statistical analysis used was suitable for the comparison of coefficient parameters determined from nonlinear regression models. In addition, when the chosen statistical analysis method (see section 2.5.4) was compared to two other methods for determining significance of parameters in nonlinear regression models, the method of choice returned less significant values indicating it is a more stringent statistical analysis method [16].

Myosin isometric force values are presented in Figure 3.8. N47K and R58Q mutations reduced β -myosin force production to 69% and 59% of WT myosin force, respectively. Phosphorylation of the RLC resulted in a 39% increase in force production for WT myosin, as well as a 52% and 62% increase in force for N47K and R58Q myosins, respectively. Differences between the isometric force of myosin bearing dephosphorylated or phosphorylated RLC were significant ($p < 0.05$) for WT, N47K and R58Q light chains. The phosphorylation induced increase in force production for myosin bearing N47K and R58Q light chains restored both mutations to WT dephosphorylated force levels. Figure 3.8 demonstrates that RLC phosphorylation enhances force output of the cardiac β -myosin motor in health and disease.



3.4.3 Myosin Power Output

The heart must generate power during systole in order to efficiently pump blood against the load imposed by aortic blood pressure. Cardiac power output can be modulated by altering the intrinsic power of the myosin molecule. To gain insight into how myosin power output is affected by modifications of the RLC at the molecular level, data from frictional loading motility assays were transformed to reflect load and power using Eq. 2. Power curves were generated by fitting the data to the Hill equation for power (Eq. 4), and are plotted in Figure 3.9.



Values of maximal power output and the load at which maximal power output occurs were determined from the power curves shown in Figure 3.9, and the errors in these parameters were determined from the least squares fit of the data. Parameters from the fit are summarized in Table 2. To compare power output between different myosins, all model fits are plotted on the same graph in Figure 3.10 and data points were removed for better visualization of the power trends.

N47K and R58Q FHC-linked mutations of the cardiac RLC caused a reduction in the maximal power output of myosin and the load at which maximal power occurs. Phosphorylation of the mutant RLCs restored power values to near WT myosin levels in the dephosphorylated state (Table 2). Phosphorylation

of WT RLC resulted in a greater myosin power output, and a shift to slightly higher loads for peak power.

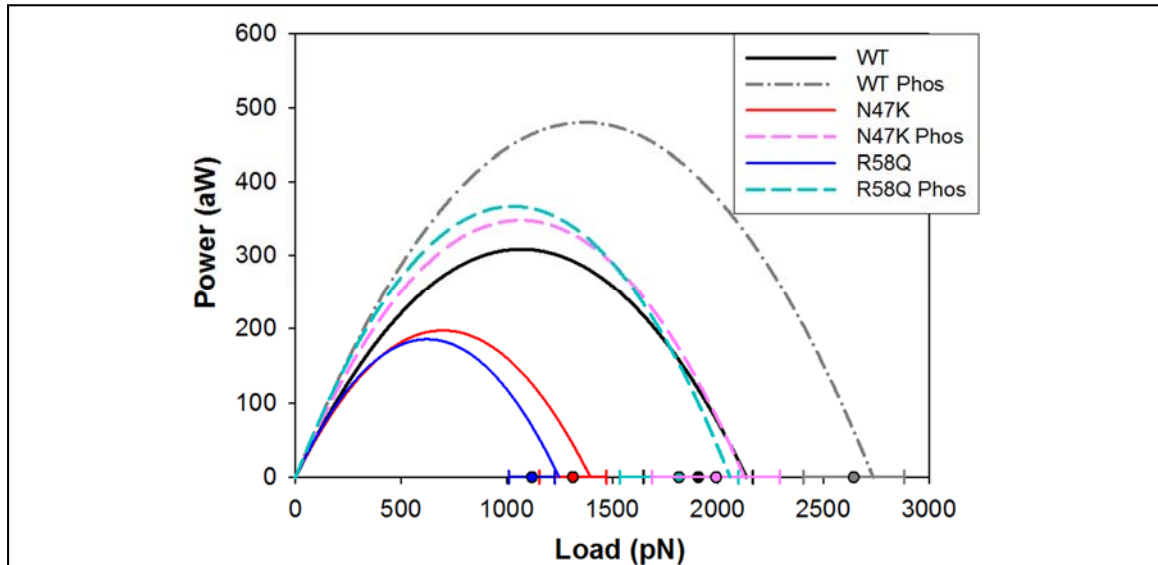


Figure 3.10: Comparison of Myosin Power Output

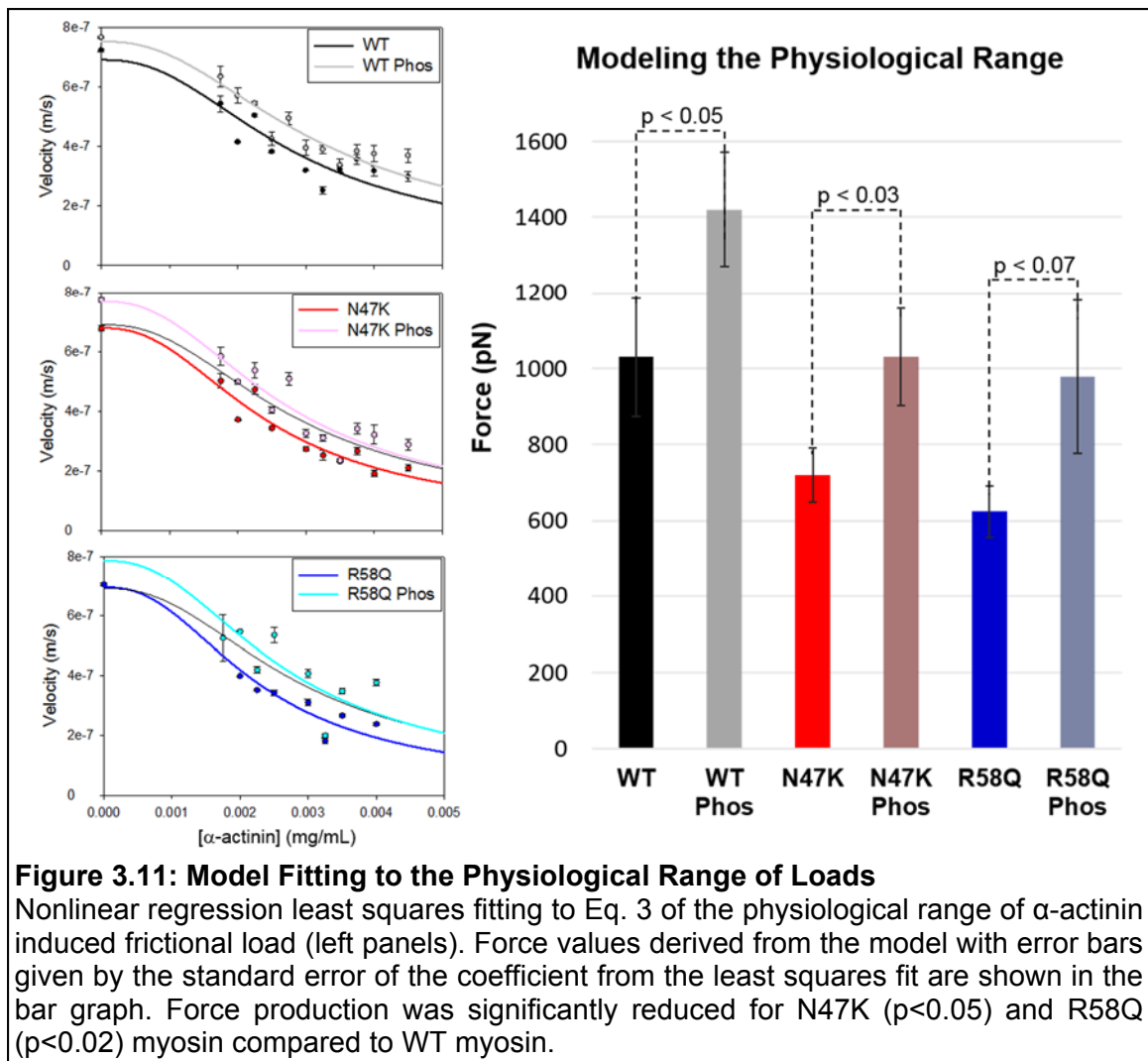
Fits of the power model are shown in the absence of transformed data, and isometric force values (\pm SE) estimated from frictional loading motility assays are shown on the x-axis. RLC mutations and RLC phosphorylation exhibit contrasting effects on maximal power output and the load at which maximal power output occurs.

Table 2: Loaded Parameters of Cardiac β -Myosin Predicted from Model Fitting

	WT	WT Phos	N47K	N47K Phos	R58Q	R58Q Phos
Max Power (aW)	309 \pm 93	480 \pm 81	198 \pm 57	348 \pm 95	186 \pm 53	367 \pm 117
Load _{M.Power} (pN)	1069 \pm 112	1368 \pm 72	698 \pm 63	1063 \pm 122	624 \pm 51	1029 \pm 134
F_o (pN)	2137 \pm 224	2736 \pm 143	1396 \pm 126	2126 \pm 244	1248 \pm 102	2058 \pm 268
F_d (pN)	1908 \pm 259	2644 \pm 239	1314 \pm 159	1992 \pm 302	1120 \pm 110	1817 \pm 283

Parameters \pm SE from least squares fitting of loaded motility assay data. Maximal power, load at maximal power and F_o were determined from the model fits of Eq. 4. F_d was determined from the model fits of Eq. 3. Note: F_d values were included in the data sets that were fit to Eq. 4.

The physiological range of loads experienced by the heart are assumed to be those spanning the region of maximum power output. Based WT myosin power curves in Figure 3.10, this range of loads corresponds to data points with α -actinin concentrations between 1.75-4.5 $\mu\text{g/mL}$ (the range is determined for power values greater than or equal to 70% maximum power). These data points were plotted and fit to Eq. 3 to compare myosin behavior in the physiological range of loads that it experiences (Figure 3.11).



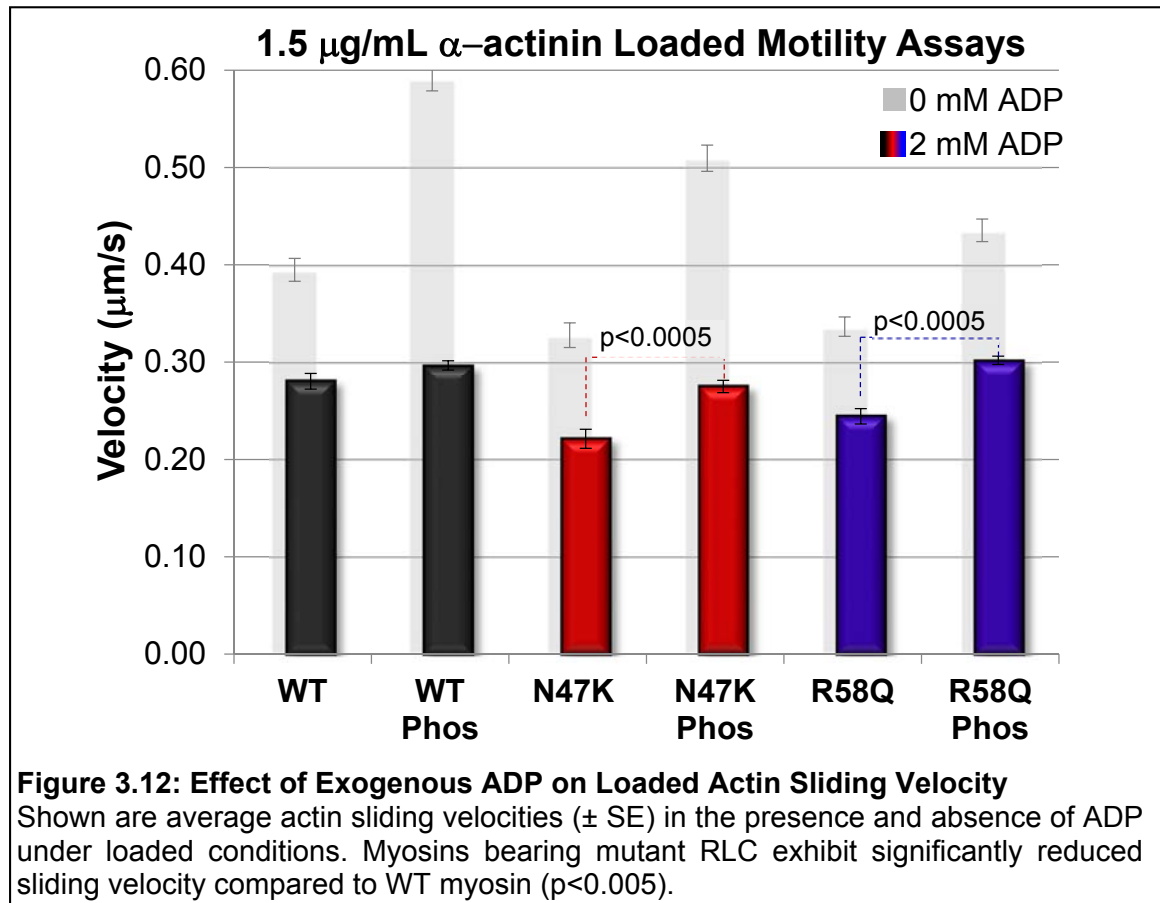
Curve fitting of the frictional loading model (Eq. 3) showed the same trend when comparing only the physiologically relevant loads as when comparing the entire data sets (Figure 3.6 and 3.10); however, R58Q dephosphorylated and phosphorylated myosin no longer exhibited a significant difference between isometric force values.

3.4.4 Effect of Exogenous ADP on Loaded Velocity

Actin sliding velocity was measured under loaded conditions in the presence of ADP for myosin bearing WT and mutant RLC in the dephosphorylated and phosphorylated states. Average velocities were first determined in the absence of ADP with 1.5 $\mu\text{g/mL}$ α -actinin load using an automated analysis. The same trends in velocities were observed for the automated data analysis as for the manual analysis of loaded motility assays. Actin sliding velocity was decreased for all myosins upon addition of 2 mM ADP to the motility buffer (Figure 3.12).

In the presence of ADP and α -actinin frictional load, N47K and R58Q myosin exhibited decreased sliding velocity compared to WT myosin ($p < 0.005$), and phosphorylation of the mutant light chains restored velocity to WT levels. Interestingly, the motility of WT myosin was not altered by RLC phosphorylation in the presence of ADP. This is in contrast to the effect of RLC phosphorylation on loaded velocity in the absence of exogenously added ADP which acts to increase WT myosin velocity. This suggests that the presence of high levels of

ADP minimizes the effect of RLC phosphorylation under load for WT myosin but not mutant myosins.



CHAPTER 4 – DISCUSSION AND PERSPECTIVES

Introduction

In this work, *in vitro* motility assays were performed to study the effects of myosin regulatory light chain (RLC) phosphorylation and familial hypertrophic cardiomyopathy (FHC)-linked mutations on myosin contractility at the molecular level. Application of a frictional load in the assay allowed for the characterization of the load dependent behavior of porcine cardiac β -myosin bearing various RLCs. I found that RLC-FHC mutations, N47K and R58Q, reduced the isometric force and power output of β -myosin. On the other hand, phosphorylation of the RLC increased force production and power output for wild-type and mutant myosin. Phosphorylation of the mutant RLCs restored mutant-induced decreases in force and power to WT dephosphorylated levels. Myosin motors are the molecular machinery responsible for powering muscle contraction, therefore, it is expected that the changes in myosin properties described in this thesis, such as sliding velocity and force generation, ultimately lead to significant changes in cardiac muscle contraction.

Although amino acid point mutations in many of the various sarcomeric proteins result in FHC [35], the end stage disease is a product of several factors. It has been shown that each mutation displays a unique pathophysiology, and the prognosis of the disease depends on the specific causal mutation [156]. Furthermore, in addition to the direct mutational effects on the single protein, the

disease phenotype could also stem from the culmination of altered protein interactions of associated proteins and/or compensatory mechanisms resulting from the original mutational defect. Often, physiological compensations that improve function eventually lead to effects that can ultimately be more detrimental than the initial effect of the mutation. RLC phosphorylation, a post-translational modification, also exerts effects at the tissue level where it plays a role in fine tuning physiological processes such as the generation of cardiac torsion [123, 154]. Thus, small structural variations of the contractile proteins of the sarcomere appear to result in complex cascades of pathological or physiological effects that should be studied and understood at several levels of muscle organization in order to understand their molecular mechanisms and develop successful therapies.

Contractile properties of muscle can be studied using single molecule, muscle fiber, and tissue/organ techniques. Each technique has advantages and limitations that can be compensated for by the other experimental methods. For example, experiments using intact fibers permit the study of cellular based changes and probe the contractile properties of the myofibrillar lattice. However, causal and compensatory effects are harder to distinguish when studying higher order structures of muscle due to the complexity of the system. It is also hard to resolve which protein components specifically contribute to the observed effects. While it is more difficult to understand the molecular details and causation of

observed effects, higher order studies can better relate the consequences of mutations and post-translational modifications to global heart function.

The *in vitro* motility assay can be used to study the individual protein components involved in the contractile processes of muscle at the molecular level. The motility assay has the advantage of assessing the fundamental process that drives muscle contraction (i.e. the cyclical interaction of myosin motors that results in the sliding of an actin filament) while allowing the freedom to control solution concentrations in a precisely defined way. This approach is superior to solution biochemistry of actomyosin ATPase because it allows for the characterization of biochemical properties, as well as mechanical properties of the myosin motor as an individual force generator. For example, experiments presented in chapter 3 allowed for direct observation of the changes induced by RLC modifications on the properties of myosin. This bottom-up approach is valuable for understanding the molecular mechanisms by which FHC mutations and RLC phosphorylation exert their effect on myosin function. In addition, it aids the interpretation of the effects seen at higher order levels of muscle (e.g., transgenic mice studies) where compensations may cloud the original molecular defects, or contributions from various protein components may complicate the data interpretation.

In this section I will suggest and discuss potential molecular mechanisms by which FHC mutations and RLC phosphorylation alter myosin properties

(section 4.1), and then relate my findings to data from cellular and whole heart function studies performed by collaborators and others in the field (section 4.2).

4.1 Molecular Effects of RLC modifications on Myosin Mechanochemistry

Data from motility assays are interpreted with velocity as a detachment-limited process, first proposed by A.F. Huxley in 1957 [54]. This model assumes that each myosin acts as an independent force generator to move actin, and that myosin moves actin at a maximal velocity when there is at least one myosin head interacting with the actin filament at any given time. Actin sliding velocity, V , is limited by the detachment of myosin from actin, and given by:

$$V = \frac{d}{t_{on}} = \frac{d \times k_{ATPase}}{f} \quad (\text{Eq. 5})$$

where d is the myosin step size, t_{on} is the amount of time that myosin spends attached to actin, f is the myosin duty cycle (t_{on}/t_{cycle}), and k_{ATPase} is the actin-activated ATPase rate ($1/t_{cycle}$). Observed changes in actin sliding velocity can therefore be attributed to a change in one or more of these parameters.

Myosin containing mutant RLCs (N47K or R58Q) or phosphorylated RLC showed no difference in maximal unloaded sliding velocity compared to WT myosin (Figure 3.4). Unloaded measurements of the actin-activated ATPase activity also yielded no difference between myosins bearing various RLCs (Table 3.1). This finding was expected based on other documented studies in the literature which show that removal of the RLC from cardiac myosin [100] and

skeletal muscle myosin [72] have no effect on the actin-activated ATPase rate of the myosin in solution. Although unlikely, it is conceivable that a lack of effect on velocity could result from compensating effects on myosin step size and duty cycle. A former graduate student in the Moore laboratory, Michael Greenberg, found no differences in duty cycle of WT, N47K, and R58Q myosins when measuring actin sliding velocity as a function of myosin concentration [40], indicating that myosin step size is also unchanged by the mutations in unloaded conditions (Eq. 5). The lack of effect on unloaded activity *in vitro* is surprising given that the mutations lead to disease. However, since the heart operates under loaded conditions, observations of contractility *in vitro* working against an external load were required to reveal the mutant phenotype.

We introduced a load into the motility assay by the addition of surface bound α -actinin which transiently interacts with actin filaments gliding along the surface of a motility assay (see section 2.5.4). As described in sections 3.5.2 and 3.5.3 and figures 3.7-11, both RLC mutations and phosphorylation affected the actin sliding velocities measured from frictional loading motility assays, and ultimately myosin force and power output. Velocity, force and power are determined by the inherent kinetic and mechanical properties of the myosin motor. The force produced by a single myosin molecule is given by:

$$F_{uni} = k \times d \quad (\text{Eq. 6})$$

where k is the stiffness of the myosin cross-bridge and d is myosin step size. For ensembles of myosin, the force exerted depends on the number of myosin heads

bound to actin at any given time. Therefore the isometric force produced by an ensemble of myosins is given by:

$$F = F_{uni} \times f \times n \quad (\text{Eq. 7})$$

where f is myosin duty cycle (fraction of the ATPase cycle that myosin spends strongly bound to actin) and n is the total number of myosin heads available to interact. In all experiments performed, n is held constant since the concentration of myosin on the surface remains the same. Therefore the changes induced by modifications to the RLC are due to an alteration in one or a combination of k , d , or f . Although myosin duty cycle and step size were unchanged by the RLC mutations for unloaded conditions, they may be altered in the presence of load since it is well established that exogenous load (or strain) can alter myosin kinetics [50].

Reduction in mutant motility was observed when a load was applied to the actomyosin in the *in vitro* motility assay. N47K and R58Q mutant myosins were unable to move actin as fast as WT myosin in the presence of an α -actinin frictional load, with decreases in actin sliding velocity being more prominent at higher loads. Model fits to the data using Eq. 3 demonstrated that the RLC mutations caused significant reductions in myosin isometric force.

One explanation for the lower force production of the mutant myosins could be decreased unitary force as a result of a reduction in stiffness of the myosin lever arm (Eq. 6). The RLC molecule sits at the base of the myosin lever arm, binding directly to the α -helical neck region of the myosin heavy chain at the

S1-S2 junction. This interaction mechanically stabilizes the lever arm and allows for the transmission of force from the myosin active site down the lever arm. It follows that increased compliance in this region as a result of the RLC mutations would reduce the ability of myosin to transmit contractile force, consistent with our findings. In addition, solution studies using isolated RLCs showed that both mutations abolish calcium binding to the RLC [138, 139], indicating some degree of structural defects for the mutant RLCs, which could impact the lever arm mechanics where the RLC binds. In addition, previous studies from our laboratory have implicated a decrease in cross-bridge stiffness leading to reduced strain sensing ability for myosin bearing these mutations [41].

The reduction in loaded velocity seen for these mutations cannot be accounted for by an increase in compliance alone since actin sliding velocity is not directly dependent on cross-bridge compliance. Therefore, reduced velocity may stem from a decrease in step size or an increase in duty cycle. A change in myosin duty cycle would have competing effects on force and velocity, however it is plausible that increased compliance could result in dragging of the bound head and delayed detachment of myosin until all elasticity is pulled out of the cross-bridge. This drag and prolonged t_{on} would act to reduce velocity. The resulting increase in duty cycle would then require a large reduction in stiffness to significantly reduce the force generating capability of the mutant myosins. In addition, ATP is readily available to bind myosin in our assays and it is likely that ATP dependent detachment would limit the ability of dragging heads to prolong

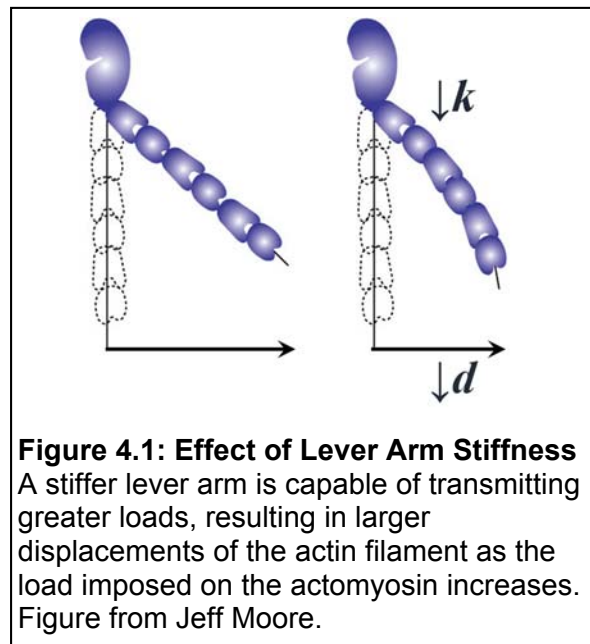
attachment, especially at higher loads when actin sliding velocity is reduced and there is more time for ATP to bind before the elasticity is pulled out of the cross-bridge.

A more likely scenario is that the observed decreases in loaded velocity result from a decrease in step size under load that accompanies the decrease in stiffness. A more compliant lever arm would be less effective at transmitting contractile force through the molecule leading to a smaller displacement of the actin filament (Figure 4.1). Accordingly, if binding of the N-terminal lobe of mutant RLC to the MHC neck α -helix is

severely disrupted such that the neck α -helix becomes exposed to solvent, this could lead to a collapse of the helix thus shortening of the length of the lever arm, and decreasing myosin step size. Although less likely, it is also conceivable that the lever arm swing angle set by conformational changes in the converter domain

could be affected by altered RLC interactions that propagate up the lever arm.

Lever arm swing angle has been shown to vary depending on the myosin family member studied [65, 66], although these differences were associated with isoform specific differences in the converter rather than the light chain binding



domain. A decrease in step size is more likely to stem from a lack of force transmission down the lever arm resulting from increased compliance of the hinge region. Thus, the effects seen here for N47K and R58Q RLC mutations are most likely accounted for by a decrease in k and d .

The effect of RLC phosphorylation on myosin motility under load observed here was opposite to the effect of FHC mutations on motility. Unlike the decrease in actin sliding velocity observed for the FHC mutations, velocity was increased across all loads for myosin with phosphorylated RLC, which reflects the corresponding increased force production. Whereas the FHC mutations may disrupt RLC interactions with the lever arm, reducing myosin stiffness, phosphorylation seems to do the opposite, possibly enhancing RLC binding and mechanically stabilizing the lever arm, ultimately leading to increased cross-bridge stiffness and myosin step size. This interpretation is consistent with data from both unloaded and loaded motility assays when comparing dephosphorylated and phosphorylated RLC. In the unloaded case, RLC phosphorylation did not produce significantly different maximal velocity values from its dephosphorylated counterpart (with the exception of the R58Q RLC); however, it is evident that there appears to be a slight increase in unloaded velocity upon RLC phosphorylation (Figure 3.4). An increase in myosin step size is a likely cause of this subtle unloaded effect. The difference in unloaded velocity values approaches the resolving limits of the motility assay which makes it difficult to discern significance. Computational modelling of data obtained from

control and gene-targeted knock in mice with a nonphosphorylatable ventricular RLC found that *in vivo* data suggested the lever arm stiffness was increased via RLC phosphorylation [123]. In a separate study, the comparison between actin filament motility at low ATP concentrations to simulated step size data distributions found that RLC phosphorylation shifted porcine cardiac β -myosin to slightly higher step sizes [151]. It follows that phosphorylation of RLC is likely to have the inverse effect on lever arm stiffness and myosin step size when compared to the FHC-RLC mutations.

Phosphorylation of the mutant RLCs restored mutation-induced decreases in myosin contractility to WT dephosphorylated levels. It is possible that RLC phosphorylation restores altered RLC-MHC interactions induced by the mutations. Isolated RLC studies on the R58Q RLC showed that phosphorylation restored its calcium binding ability and increased helical content of the mutant RLC [139]. This increase in helical content could explain the more resolved increase in unloaded velocity seen for the R58Q RLC upon phosphorylation.

The effects of RLC phosphorylation on force and velocity can be explained by an increase in stiffness and step size of myosin; however, in experiments where exogenous ADP was added to the buffer there was no observed increase in loaded velocity after phosphorylation of WT myosin as would be expected with an increased step size (Figure 3.12). The lack of an effect for RLC phosphorylation under these conditions might result from both load and exogenous ADP tending to increase the time that myosin remains strongly bound

to actin (t_{on}). It may be that a subtle increase in step size is undiscernible under conditions where t_{on} is greatly increased.

A second possibility for the lack of an effect of WT RLC phosphorylation under conditions of high ADP levels is that RLC phosphorylation affects the kinetics of the strongly bound states under load, and the presence of exogenous ADP attenuates this effect. ADP release is a load sensitive transition that is associated with an additional swing of the lever arm which results in a more open nucleotide binding pocket in the rigor state. RLC phosphorylation may shift the equilibrium towards the rigor state by accelerating the load sensitive ADP release, and stabilizing the rigor state. When exogenous ADP is added to the motility buffer it acts as a competitive inhibitor of ATP for the nucleotide binding pocket and slows velocity (Figure 3.12). The lack of an effect of RLC phosphorylation on WT myosin in the presence of high levels of exogenous ADP could be due to higher levels of ADP exchange with the nucleotide pocket due to a phosphorylation induced stabilization of the open binding pocket in the rigor state. This could explain the larger inhibitory effect of exogenous ADP on WT phosphorylated myosin compared to WT dephosphorylated myosin.

Results from our motility assays show that RLC phosphorylation mechanically alters the myosin molecule to make a more robust motor capable of transmitting greater loads at faster rates. This is functionally significant since the heart typically operates against a load imposed by diastolic blood pressure. Subtle changes to myosin velocity in the loaded *in vitro* motility assay and to the

force-velocity relationship lead to pronounced alterations in myosin power output. RLC phosphorylation increases myosin peak power and the load at which peak power is achieved. Phosphorylation of N47K and R58Q myosin restores mutation-induced decreases in force and power to near WT dephosphorylated levels. Changes in myosin power output are functionally significant because it affects the power output of the heart, which determines the rate of energy the heart can provide to meet its performance needs.

Summary

The integrity of the lever arm is dependent on RLC binding [100]. While the RLC binds at a hinge region of the lever arm approximately 10 nm away from the myosin catalytic domain and actin binding site [106], RLC modifications alter myosin force production and velocity under load. The data is consistent with an interpretation where RLC modifications alter the stiffness of the lever arm. For FHC mutations this is most likely accompanied by a decrease in step size under load. For RLC phosphorylation this could result in increased step size and/or duty cycle. Without the use of single molecule techniques, it is difficult to dissect the precise molecular mechanism exerted by FHC mutations and RLC phosphorylation on myosin function. This topic will be discussed further in the next chapter. Nonetheless, it is intriguing to consider RLC phosphorylation as a therapeutic target for treatment of FHC resulting from N47K and R58Q RLC mutations given its restorative effects on RLC cation binding [139] and myosin force and power generation (Figures 3.7 and 3.10).

By omitting the complexity that arises from the cellular environment, the *in vitro* motility assay permits observation of the direct effect RLC mutations and phosphorylation exert on myosin function. In combination with data from higher order muscle ensembles, one can begin to elucidate the pathogenesis and physiological consequences that result from small alterations at the molecular level. In the following sections I will discuss my findings in relation to data from muscle fiber experiments and *in vivo* studies.

4.2 Higher Order Muscle Function

4.2.1 Correlating RLC Phosphorylation Effects to Cellular and *In Vivo* Function

By applying a frictional load induced by α -actinin in the *in vitro* motility assay, we provided information about the load-velocity relationship for the interaction of myosin with actin. When comparing myosin containing dephosphorylated RLC (0% phosphorylation) and phosphorylated RLC (~85% phosphorylation), we found that phosphorylated myosin subtly increased actin sliding velocity at all loads measured, and significantly increased the isometric force production of myosin by 39%. This resulted in greater power output for myosin, with maximal power increased by 55% upon RLC phosphorylation. These experiments demonstrated that in the absence of thick filament assembly and calcium regulatory mechanisms, RLC phosphorylation affected isolated actomyosin mechanochemistry.

The mechanical performance of muscle fibers is similarly altered via RLC phosphorylation. Skinned fibers from mouse trabeculae treated with MLCK exhibited increased steady-state force at rest and during maximal Ca^{2+} activation, indicating that the phosphorylation-induced increases in force were independent of calcium-activating mechanisms [23]. This is in agreement with our findings (Figure 3.8) which were performed in the absence of calcium and thin filament regulatory proteins. Recent studies on permeabilized trabeculae that were reconstituted with variably phosphorylated recombinant RLC showed a trend of increased force production with increasing levels of phosphorylation at saturating calcium [6]. This resulted in an upward shift of the force-velocity relationship and subsequent increase in power output, consistent with results of our work. In addition, increased phosphorylation of fibers resulted in significantly increased maximal shortening velocity as determined from slack tests [142]. While the same trends are observed in our work, the RLC phosphorylation in the fiber work was not as broad (~20-70%) yet the effects due to phosphorylation were much more pronounced, with a 3.7-fold increase in isometric force and a 7.5-fold increase in maximal power [142]. This indicates that the phosphorylation induced changes in fiber mechanics are influenced by other cellular factors in addition to the contributions from the individual myosin molecule. For example, phosphorylation has been shown to alter thick filament structure such that myosin heads move away from the thick filament backbone, which in turn increases recruitment of myosin heads to the thin filament [23]. This thick

filament dependent process may increase the number of myosins bound and collectively increase force generation.

Increased maximal force generation and power output of muscle increases the total amount of work the muscle can perform. This property is crucial to phosphorylation dependent processes in the heart that require stronger contractions, or faster contractions under load. The effects of phosphorylation are not uniform in the heart because phosphorylation levels are present in a gradient pattern with higher levels in the epicardium [25, 48]. It follows that RLC phosphorylation is responsible, at least in part, for the enhanced performance of epicardial fibers needed to maintain cardiac torsion under basal conditions. In addition, an increase in work capacity conferred by phosphorylation would enhance the hearts ability to adapt to conditions of increased afterload.

4.2.2 Familial Hypertrophic Cardiomyopathy-linked Mutations

FHC is characterized by a thickening of the left ventricular muscle or intraventricular septum, as well as myocyte disarray, and fibrosis. The pattern of cardiac remodeling varies with the genetic mutation. The RLC N-terminal mutations studied here, N47K and R58Q, are close to each other structurally but lead to different clinical phenotypes. *In vitro* motility assays, using porcine cardiac (PC) myosin, where the native RLC was exchanged with human ventricular RLC containing the N47K and R58Q mutations, showed reduced force production (Figure 3.8) and power output (Figure 3.10) of the myosin motor.

Relating In Vitro Motility Data to Fiber Studies and Clinical Phenotypes

We propose that N47K and R58Q mutations disrupt the sensitivity of myosin to load by changing the structure and mechanical properties of the α -helical neck region of myosin. Indeed, N47K and R58Q mutations disrupt the cation binding site leading to a loss of calcium binding to the RLC [138, 139]. Consistent with the decrease in force production observed in the motility assays in this work, measurements of skinned papillary muscle fibers from R58Q transgenic mice demonstrated a significant decrease in maximal force production [12, 152], while N47K transgenic mouse fibers demonstrated a minor decrease in force [152].

Reduction of actomyosin power is expected to impair the ability of the heart to eject blood. A mismatch in the power output of the FHC heart and the power needed to overcome afterload would reduce the ability of the heart to contract against the arterial blood pressure and would ultimately reduce cardiac output. Similar to the results observed here for isolated mutant actomyosin (Figure 3.10), measurements on isolated perfused working hearts from transgenic mice containing the N47K and R58Q mutations resulted in decreased cardiac power and cardiac output [1]. These mice showed hypertrophy with age and diastolic dysfunction, and while both mice had significantly impaired cardiac function the consequences of the R58Q mutation were much more profound. In addition, the R58Q mutation led to decreased levels of RLC phosphorylation before the onset of hypertrophy. [1].

The R58Q mutation also presents with a more severe phenotype at the clinical level [60]. The N47K RLC mutation is associated with rapidly progressing mid-ventricular hypertrophy and diastolic filling abnormalities occurring late into adulthood, while the R58Q mutation is associated with left ventricular hypertrophy occurring during childhood leading to ventricular fibrillation and sudden cardiac death [6, 34, 60]. It is likely that the malignant phenotype associated with the R58Q mutation stems from decreases in the levels of RLC phosphorylation associated with the R58Q mutation [1]. Consistent with this idea, MLCK treatment of the R58Q RLC performed in this work resulted in less effective phosphorylation of the light chain compared with WT and N47K RLC, potentially due to altered substrate affinity for MLCK. Chemical modification of lysine and arginine residues within the regulatory light chain severely inhibited phosphorylation by MLCK [102], while chimeric light chains which altered the N-terminal subdomains resulted in reduced reaction kinetics demonstrating that regions distal to the phosphorylation consensus sequence are important to MLCK activity [158]. It is conceivable that the loss of a positive arginine residue in the RLC N-terminal lobe could impair the ability of serine15 to be phosphorylated.

RLC Phosphorylation as a Therapeutic Target

Here we show that phosphorylation of WT or mutant RLC increases force, suggesting an enhancement of myosin neck domain stiffness. Furthermore, it has been shown that phosphorylation of the mutant light chains can restore

calcium binding to the R58Q recombinant RLC [139]. Thus phosphorylation-induced structural changes of the RLC likely affect its interactions with the myosin neck region and underlie the ability of phosphorylation to enhance myosin force and velocity under load, and restore these parameters of the mutant myosins to near WT levels. A shift toward higher power and higher loads for peak power may be accomplished via RLC phosphorylation. It is intriguing to consider phosphorylation as a drug target for alleviating symptoms in patients with RLC FHC mutations that exhibit reduced force generation.

Studies performed on another RLC FHC mutation, D166V, have also targeted RLC phosphorylation as a rescue mechanism for the mutation induced detrimental phenotype [90, 91]. In the tertiary structure of myosin RLC, the D166V mutation is predicted to be in close proximity to the RLC phosphorylation site [106]. Similar to R58Q, the D166V mutation resulted in decreased levels of RLC phosphorylation which likely contributed to decreased force production in skinned papillary muscle fibers from transgenic D166V mice [63, 91] and the malignant phenotype in humans [62, 110]. In the studies carried out by Muthu et al., a phospho-mimetic S15D was incorporated into the RLC [91]. This pseudo-phosphorylation restored force production of the D166V myosin in the *in vitro* motility assay, similar to the rescue by RLC phosphorylation seen in this work. Similar results with phosphomimetic and MLCK-induced phosphorylation of the RLC suggests that it is the addition of a negatively charged residue that is responsible for the reversal of mutation induced effects.

In addition to the reversal of mutation-induced effects at the molecular and cellular level, upregulation of RLC phosphorylation has also shown promising effects *in vivo*. Increasing the level of RLC phosphorylation in rodent hearts has been shown to improve cardiac performance during cardiac dysfunction. Overexpression of cMLCK resulting in increased phosphorylation levels was able to compensate for pressure overload and attenuate hypertrophy in mouse hearts [154] as well as improve cardiac performance post myocardial infarction in rat hearts [44]. These results are encouraging and suggest that regulation of RLC phosphorylation should be explored further as a mechanism to improve cardiac function.

Therapeutic strategies targeting RLC phosphorylation could be accomplished through upregulation of cMLCK, downregulation of myosin phosphatase, or the use of small molecule effectors that mimic phosphorylation. One possible way to upregulate cMLCK would be to inhibit ubiquitin protease which degrades cMLCK [154]. This would act to increase levels of cMLCK and has the added advantage of maintaining the native distribution of cMLCK in the heart. Successful downregulation of myosin phosphatase might target MYPT2, the protein subunit that binds type 1 phosphatase, PP1c- δ , to form the holoenzyme specific for myosin regulatory light chain [83, 97]. This would preserve the activity of the phosphatase for its other targets while specifically decreasing RLC dephosphorylation. Therapeutic interventions seeking to increase RLC phosphorylation may pursue a number of avenues; however the

best route will be one that preserves the gradient of RLC phosphorylation [25] and does not interfere with other processes in the heart.

The results from our motility assays show that RLC FHC mutations and phosphorylation have opposite effects on isolated cardiac myosin load-dependent behavior. While N-terminal mutations disrupt myosin's ability to produce force and power, phosphorylation of the RLC enhances myosin force and power production and is a mechanism that may be explored further as a potential therapeutic target. Follow up studies to the *in vitro* motility assays presented here may pursue two different directions, one which proceeds with single molecule techniques to dissect the precise molecular mechanism exerted by RLC N-terminal modifications on a single myosin motor, or one which proceeds with *in vitro* studies of higher order myosin ensembles to bridge the gap between the properties of isolated cardiac muscle proteins and cardiac muscle cells. In the next chapter I will discuss experiments that may be utilized in pursuit of both of these avenues.

CHAPTER 5 – FUTURE DIRECTIONS

Introduction

The work presented in this thesis shows that cardiac myosin force production is altered by modifications of the RLC N-terminus. Continuation of this work might focus on dissecting the precise mechanism responsible for altered force production by directly measuring myosin stiffness (k), step size (d), and strongly bound time (t_{on}). This can be accomplished using optical trapping techniques which can probe a single myosin interacting with an actin filament and provide high resolution measurements of the system. Another route might aim to bridge the gap between the contractile properties of isolated monomeric myosin and muscle fibers. *In vitro* assays that probe myosin assembled into thick filaments could explore the contributions of the thick filament backbone to myosin function and muscle fiber properties. In this chapter I will discuss potential experiments using optical trapping techniques and thick filament assays which aim to characterize a single myosin protein and the cooperative thick filament unit, respectively.

5.1 Optical Trapping

5.1.1 Basic Principles

Optical trapping is a technique that utilizes a tightly focused laser beam to hold microscopic particles stable in three dimensions. This phenomenon was first

described by Arthur Ashkin at Bell Laboratories whose group was able to trap an object with an index of refraction greater than the surrounding medium using a focused laser beam [8]. A light beam that passes through a particle with an index of refraction different from the surrounding medium is deflected according to Snell's law. This results in a change of momentum of the light as it is refracted, which exerts a force on the particle due to the law of conservation of momentum. Light radiation from a laser imparts piconewton level forces to refractile objects by transferring momentum to the object when light is scattered or refracted by the object. Light with higher intensity will exert a greater force on the object as the light vector changes direction. A particle with an index of refraction greater than the surrounding medium is pulled toward the area of highest intensity (Figure 5.1).

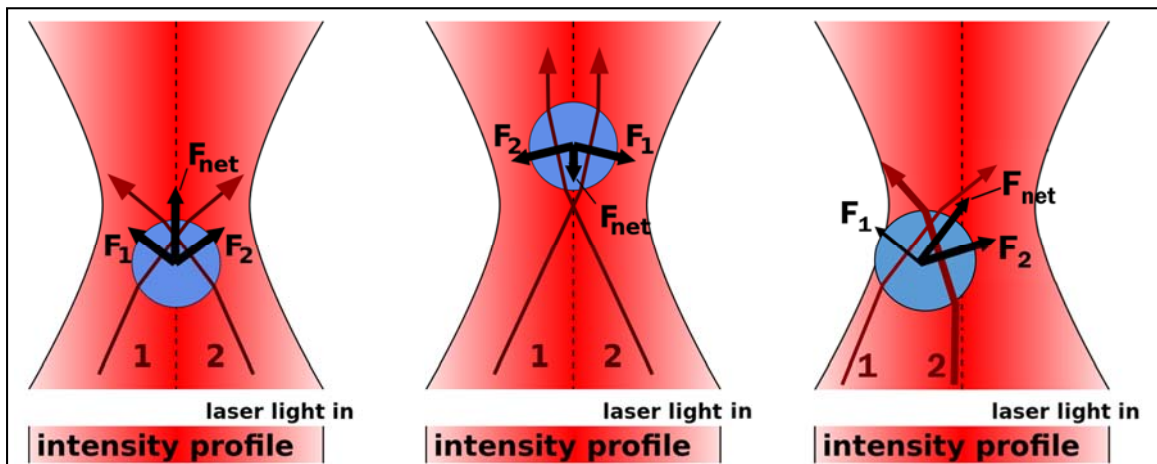


Figure 5.1: Optical Trapping Force Diagram

Light vectors are shown in dark red and the force exerted on the bead due to refracted light is shown with black arrows. The net force of the optical trap pulls the bead toward the beam waist. Forces from scattered light (not shown) apply an upward force on the bead in the direction the laser beam.

Figure from https://en.wikipedia.org/wiki/Optical_tweezers

A Gaussian beam exhibits a radial gradient of light intensity in the X-Y plane of the beam's cross section with the most intense light at the center of the beam. Focusing the laser beam through a microscope objective creates a gradient of intensity along the Z-axis with the highest intensity at the beam waist. This allows a refractile particle to become trapped in three dimensions at the beam's focal point.

Some of the light that is incident on the particle will be scattered rather than refracted. Scattered light rays exert a force on the particle in the direction of the light beam. In order to stably trap the particle, the forces exerted by the intensity gradient must be greater than the forces exerted by the scattered light. Therefore a microscope objective with a high numerical aperture is more desirable for optical trapping because it allows for a steeper gradient of light. When a particle is trapped it occupies a space just below the beam waist due to the force exerted by scattered light. The net gradient force exerted on the particle is linearly proportional to the particle's displacement from the beam focus. The optical trap effectively acts as a Hookean spring with a characteristic stiffness that is proportional to laser power. The restoring force exerted by the trap on the bead is equal to $k_{trap} * x$, where k_{trap} is the characteristic trap stiffness and x is the displacement of the bead from the center of the trap.

The stiffness of the optical trap can be calibrated by three methods: the equipartition theorem, Stokes law, or the power spectrum method. All three methods depend on a statistical analysis of the motion of a trapped bead.

Sensitive photodiodes are utilized to measure the deflection of light from an object in the beam path which provides high resolution data of the object's position. The equipartition theorem states that an object in thermal equilibrium has the same kinetic energy associated with each translational degree of freedom, which is equivalent to $\frac{1}{2}k_B T$ for one-dimensional diffusion. This kinetic energy is equivalent to the potential energy of the trap, which acts as a linear spring, and is given by $\frac{1}{2}k_{trap}\langle x^2 \rangle$, where $\langle x^2 \rangle$ is the variance of bead position. Therefore the trap stiffness can be determined by measuring the variance of a trapped bead. The second method to determine trap stiffness uses Stokes law, which describes the drag force exerted on a small sphere that is moving through a viscous fluid. By moving a trapped bead at a known constant velocity through a medium of known viscosity, the Stokes drag force can be calculated and equated to the trap force. The effective spring constant (k_{trap}) can be solved by measuring the displacement of the bead from the center of the trap as it moves at constant velocity through the viscous medium. The final method for determining trap stiffness is the power spectrum method. The variance of bead position over time can be broken down into frequency components, and the power spectrum describes how the variance in position is distributed over frequency. When a force is acting on the bead this will give rise to a power spectrum with a characteristic corner frequency. Trap stiffness can be determined from the corner frequency. For a review of optical trapping principles and stiffness calibrations, see [116].

Laser based optical traps have made a significant impact in the study of biological systems by providing a method to apply and measure piconewton forces and nanometer displacements of microscopic particles. In most applications the optical trap is used to manipulate micron-sized polystyrene beads which are coupled to various biological membranes, organelles, polymers, proteins, DNA or whole cells. Optical trapping has been extensively used in the study of single molecules, most notably motor proteins [28, 100, 129, 141, 143, 149].

5.1.2. Optical Layout

An optical trap was designed around a Nikon Eclipse TE2000 inverted microscope in the Moore Laboratory. The excitation pathway consists of a solid state, 1064 nm Nd:YVO₄ laser, five mirrors which guide the beam into the back aperture of the microscope, 12 lenses which expand the beam diameter, and a pair of acousto-optical deflectors (AOD) which steer the laser beam in the X-Y plane of detection with nanometer precision (Figure 5.2). The laser beam is collimated as it enters the back aperture of the microscope and becomes focused by passing through a microscope objective with a 1.3 NA. The diode laser that pumps the Nd:YO₄ crystal is computer controlled. The user sets the current running through the diode laser which determines laser power; the laser has a maximum power of 4 watts. An AOD consists of a TeO₂ crystal and a

piezoelectric device that generates sound waves within the crystal. The index of refraction of the crystal can be changed as a function of the sound wave frequency. The laser beam is deflected as it passes through the crystal generating a first order diffraction spot which can be moved in one dimension by altering the driving frequency. To steer the beam in two dimensions a second AOD is placed at a 90° angle to the first AOD, and the first order diffraction spot is deflected in a direction perpendicular to the first deflection. This creates a second order diffraction spot which can be manipulated in the X-Y plane and allows for precise control over the optical trap position. The radio frequency that drives the AODs and manipulates the laser beam position is computer controlled. By rapidly switching between two different frequencies the laser beam can be time-shared to create an additional second order diffraction spot, effectively creating two separate optical traps.

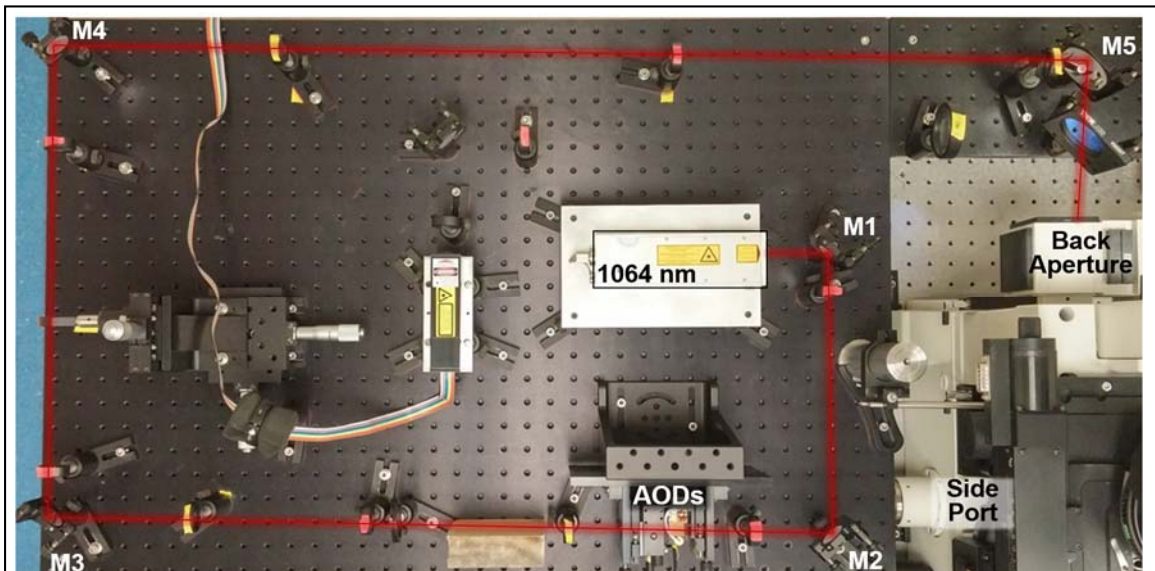
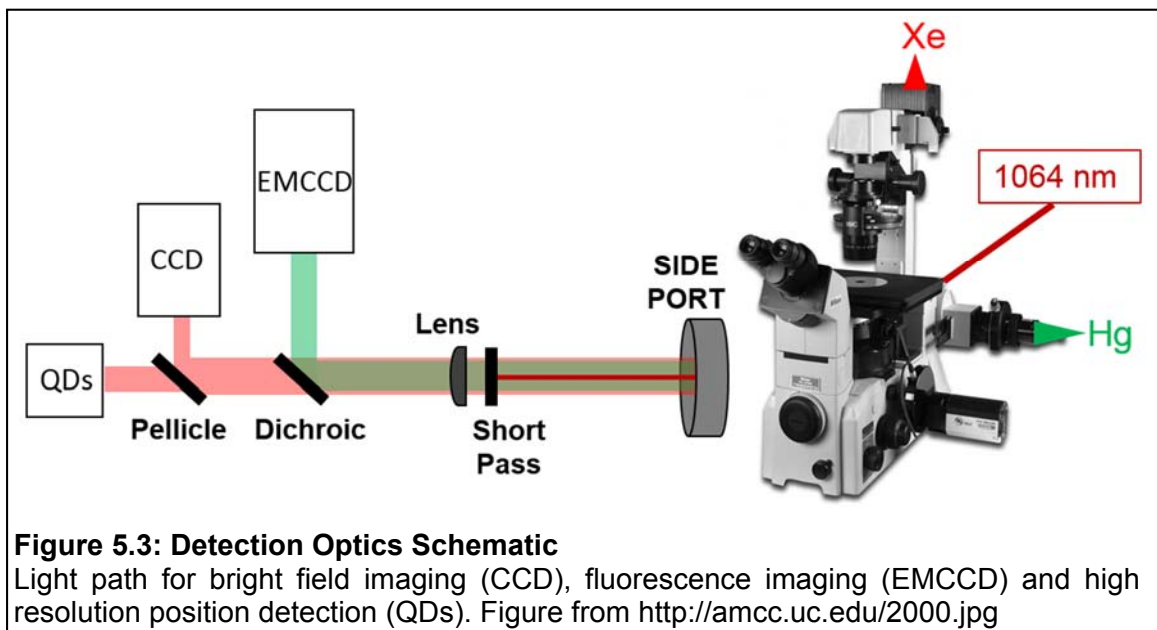


Figure 5.2: Optical Trapping Design

A picture of the optical layout used for laser-based trapping in the Moore Laboratory.

The design of the detection optics permits simultaneous bright field and fluorescence imaging while monitoring bead position with high precision. The detection optics lie below the breadboard housing the trapping optics and collect light coming out of the side port of the microscope; it consists of a charge coupled device (CCD) for bright field imaging, an electron multiplying CCD for fluorescence imaging, and two quadrant detectors (QD) for high resolution measurements of bead position (Figure 5.3). The light coming out of the side port of the microscope is converging, therefore care had to be taken to ensure that each optical detector was aligned parfocal to each other, as well as to the focal plane at the side port of the microscope. This was accomplished by inserting a lens in the detection pathway, determining the distance from the lens that created a parfocal image plane with the side port image, and mounting each detector at this same distance from the lens.



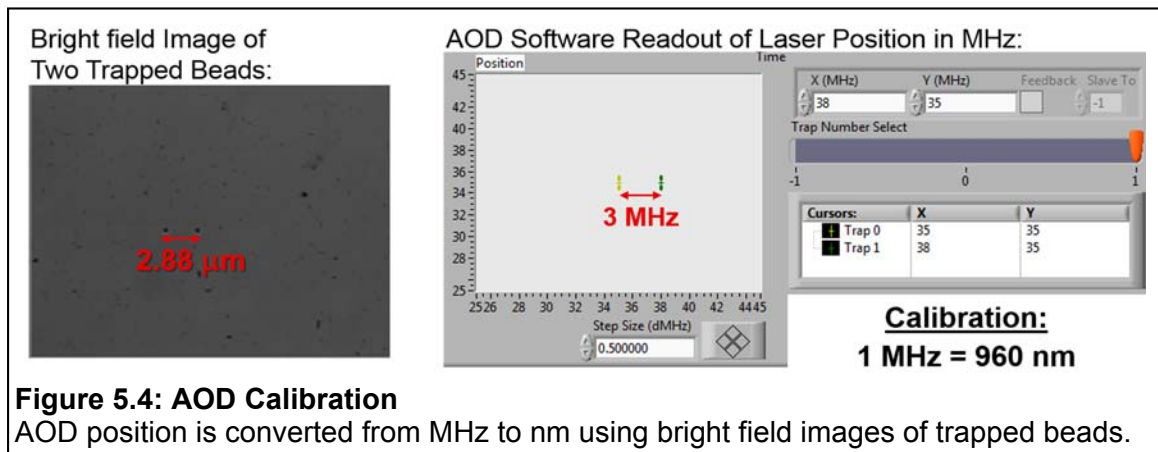
A 1000nm short pass filter was placed in the detection pathway to block infrared laser light from interfering with the detection optics. A dichroic is used to reflect light below 650 nm to the EMCCD for fluorescence viewing. Finally, a pellicle beam splitter reflects 8% of the remaining light to the CCD to produce a bright field image of the trapped beads, and the remaining 92% of the light falls on the QDs (Figure 5.3).

A quadrant detector (QD) is a camera with four pixels, and the voltage output of each pixel is proportional to the amount of light that is incident on the pixel. An object in the light path of the quadrant detector will block light from reaching the quadrant detector and as the object moves the amount of light hitting each of the four pixels will change. The voltage output in the X and Y directions can be calculated by taking the sum and difference of pixels from the left and right sides, or top and bottom, to measure movement of the object with high precision.

5.1.3 System Calibrations

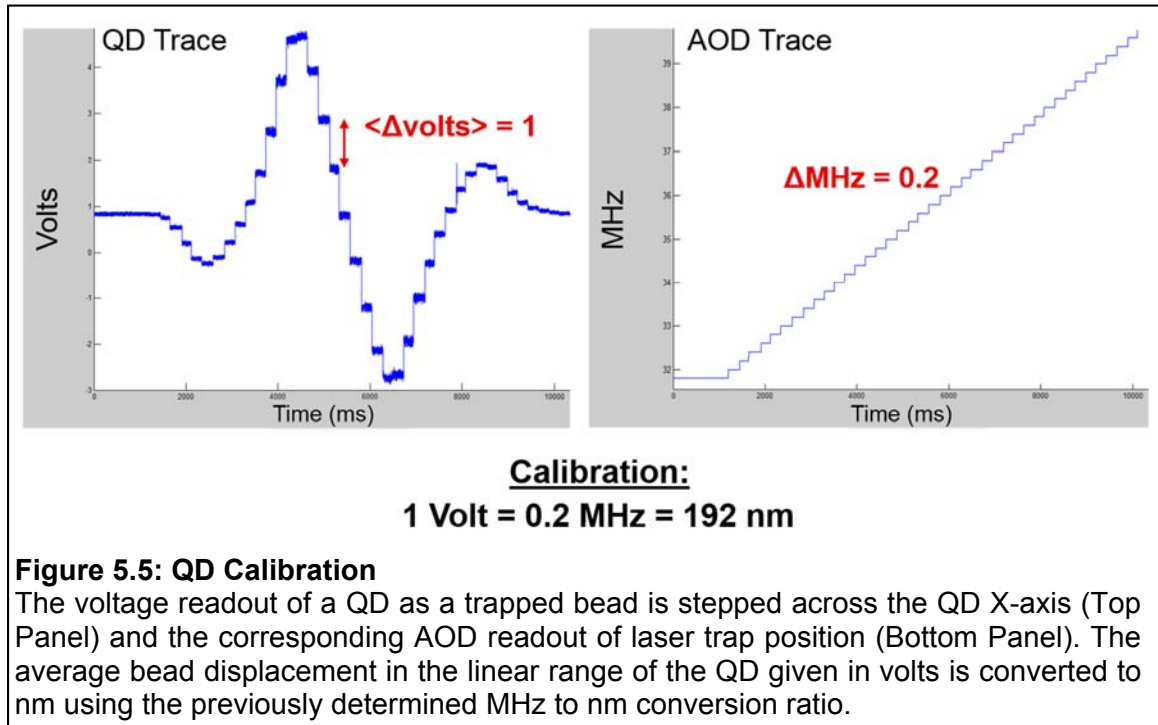
Prior to performing experiments using the optical trap, three calibrations must be performed in order to analyze the raw data. Laser beam movements, trapped bead movements, and the stiffness of the optical trap must be calibrated. The beam position is controlled by a pair of AODs with the output given in units of MHz, and the position of a bead trapped in the beam is measured by the QD

with output given in units of volts. Therefore the software output for the AODs and QDs must be converted from MHz and volts to distance. This is accomplished using bright field images with a known pixel to nanometer conversion ratio.

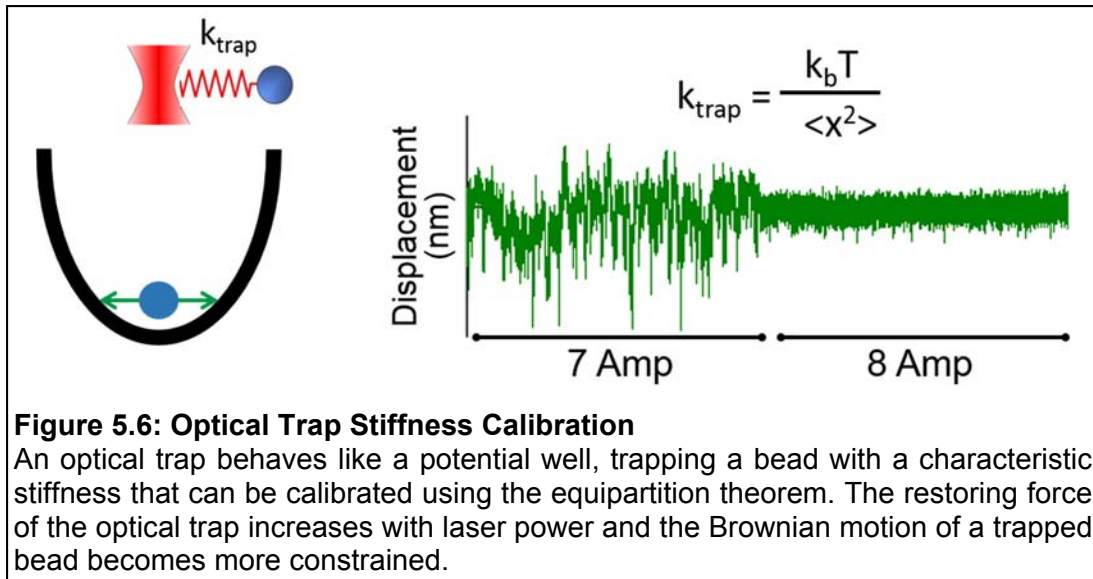


To calibrate the AOD, the distance between two tightly trapped beads is determined from a bright field image and equated to the distance between the two trap positions given in MHz (Figure 5.4). The voltage output of the QDs must be calibrated in both the X and Y dimensions. To calibrate the QD, a trapped bead is moved across the QD in one dimension by stepping the AOD by a known amount. The QD has a narrow range where the voltage output is proportional to the change in MHz of the AOD position; experimental measurements must be taken within this range of the QD which corresponds to bead positions that lie completely within the boundaries of the four pixel detector. The average voltage change as the bead is stepped across the linear range of the QD is measured

and equated to the AOD step size to determine the volts to nm calibration (Figure 5.5).



The calibration of laser trap stiffness using the equipartition theorem is shown in Figure 5.6. The Brownian motion of a trapped bead is monitored, and the root mean squared displacement of the bead is used to calculate trap stiffness. The stiffness of the trap increases with laser power. It is important to measure the stiffness of the optical trap at the laser power that is used during experimental measurements. After performing all three calibration measurements experimental procedures may begin.



5.1.4 Three Bead Assay

The three bead assay was originally developed in the Spudich Laboratory [32]. In this experiment an actin filament is attached to trapped beads and pulled taut to form a bead-actin-bead dumbbell. Nitrocellulose coated beads are firmly attached to the coverslip surface and act as a pedestal to raise myosin off the surface. The actin dumbbell is lowered over a bead pedestal which is sparsely coated with myosin, and a single myosin can interact with the suspended actin filament (Figure 5.7).

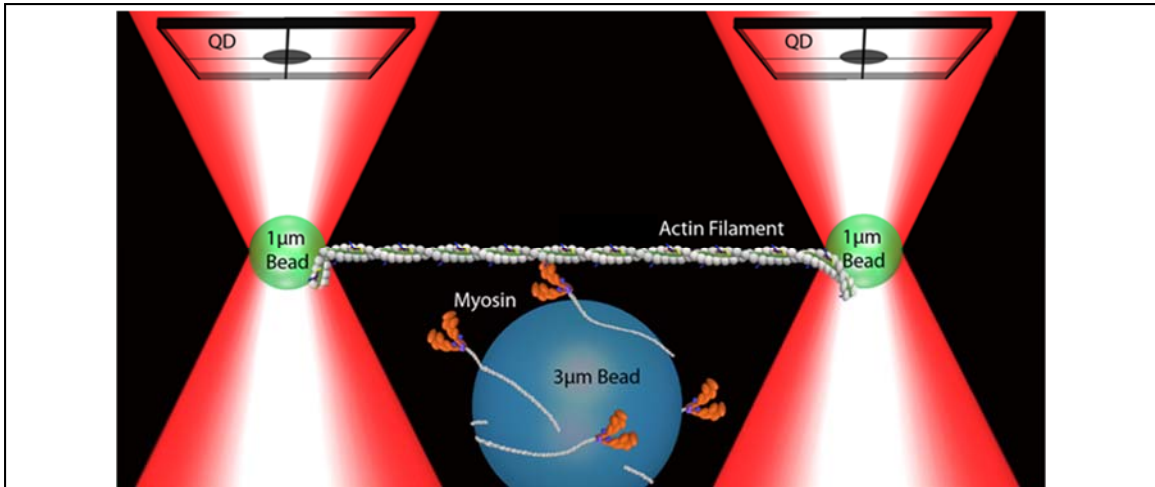
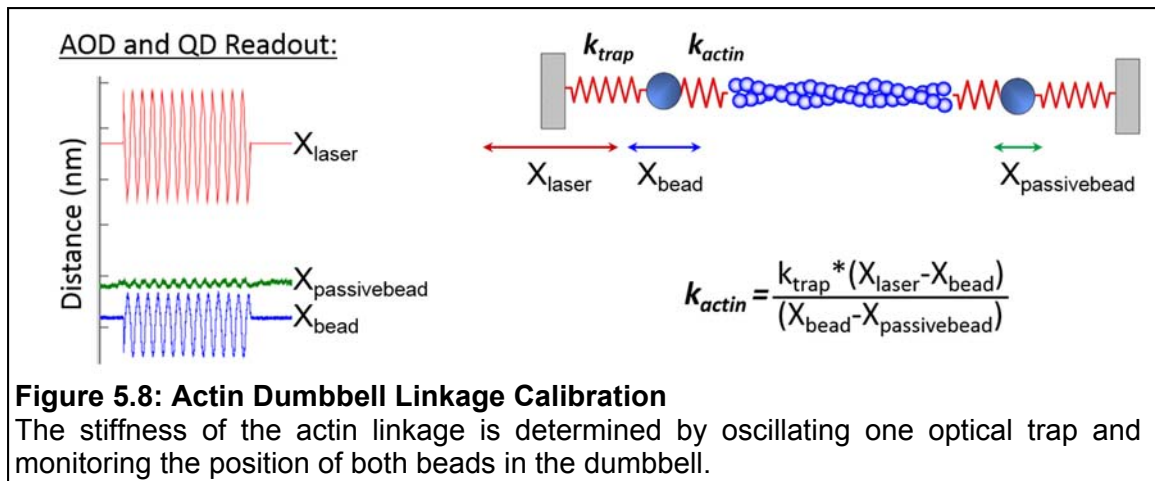


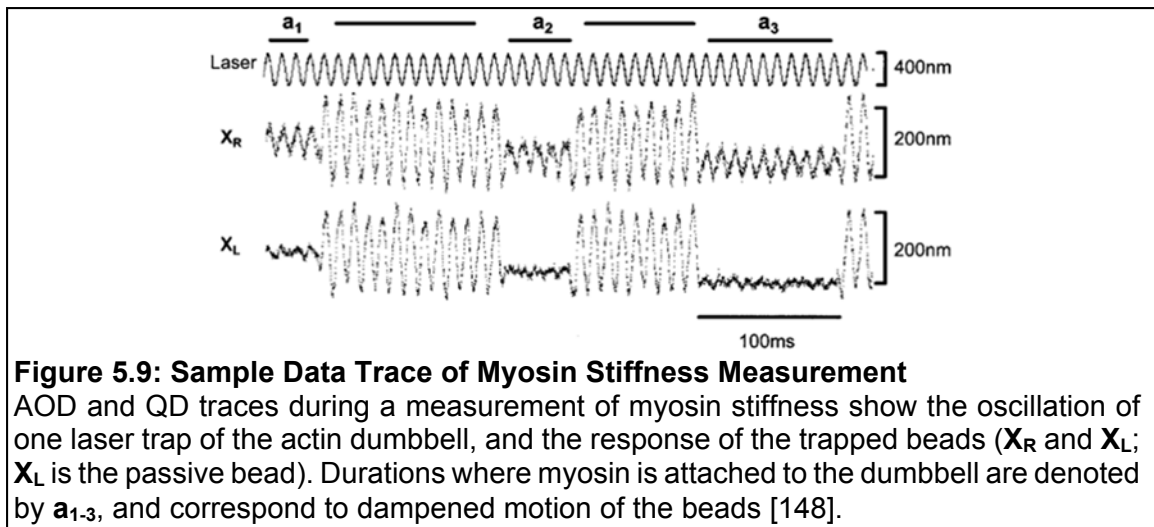
Figure 5.7: Illustration of the Three Bead Assay

A diagram of the flow cell shows myosin sparsely coating bead pedestals attached to the coverslip surface, two laser-based optical traps, and a suspended bead-actin-bead dumbbell held in a position where a single myosin can interact with the actin filament. Figure from <http://www.umass.edu/musclebiophy/techniques%20-20laser%20trap.html>

The position of the actin dumbbell is monitored and the variance of the beads in the laser trap are calculated. When a myosin molecule binds to the actin filament the variance of the beads is reduced because the myosin molecule acts as an elastic linkage that dampens the Brownian motion of the dumbbell. Myosin binding events can be distinguished from Brownian motion due to the drop in variance. At low trap stiffness values, myosin can displace the actin filament as it binds and performs its powerstroke, which will displace the beads out of the center of the optical trap. This displacement is equal to the myosin step size, d . In addition, the drop in bead variance when myosin is bound can be measured over time to give the strongly bound time, t_{on} .



Myosin cross-bridge stiffness, k , can also be measured using the three bead assay. First the stiffness of actin linkage to the bead must be calibrated. This is done by oscillating one laser trap position and monitoring the displacements of both beads. The passive bead will have a smaller oscillation amplitude due to the series elasticity. The differences in amplitude of laser position, its trapped bead, and the passive bead, along with trap stiffness give a measurement of the dumbbell stiffness (k_{actin}). Myosin stiffness is measured using these same parameters. When myosin binds to the actin filament it acts as an elastic element and shunts the oscillation of the dumbbell (Figure 5.9). The compliance of the myosin spring element can be calculated from the change in amplitudes observed upon myosin binding. The three bead assay allows for the measurement of single molecule properties using optical trapping techniques and is a valuable tool for studying molecular motors.



Myosin can be tested using the three bead assay to determine the mechanism by which RLC FHC mutations and phosphorylation alter myosin force production. RLC N-terminal modifications are likely to affect myosin crossbridge stiffness, therefore myosin should be tested using the experiment described in Figure 5.9. I would expect to see opposing effects of FHC mutations and RLC phosphorylation on measurements myosin stiffness. I predict that dumbbell bead oscillations would exhibit a greater amplitude during myosin attachment states for myosin bearing RLC FHC mutations which corresponds to a more compliant myosin crossbridge. Upon RLC phosphorylation I would expect the bead oscillations to have a smaller amplitude during myosin attachment which corresponds to a stiffer crossbridge linkage.

Myosin step size and strongly bound time can also be measured in the three bead experiment as mentioned above. For these measurements the actin dumbbell is positioned over a myosin coated bead and there is no oscillation or movement applied to the optical trap position (and dumbbell). The dumbbell will

have an associated bead position and variance in solution, and these parameters will change when a myosin molecule binds to the dumbbell. A drop in bead variance indicates a myosin binding event, and myosin strong binding time can be determined by measuring the duration of the binding event. This should be done in conditions of high ATP concentration such that the availability of ATP to bind myosin is not limiting myosin detachment. The change in dumbbell bead position in the absence and presence of myosin binding will give a measurement of myosin's step size. I predict that myosin with RLC FHC mutations would lead to smaller displacements of the actin dumbbell, and that phosphorylation of the RLC would lead to larger displacements of the actin dumbbell. However, it is likely that changes in myosin step size would be difficult to resolve because the muscle myosin step size is less than 15 nm [67, 151] and alterations in step size would be on the order of a few nanometers which approaches the resolving power of our optical trapping system. The resolution of single molecule measurements is reduced by the random nature of myosin's attachment to the bead surface. In addition, certain parameters such as the strongly bound time, t_{on} , are expected to be greatly affected by myosin's interactions with the thick filament backbone. These two variables can be better controlled by attaching myosin to a thick filament rod surface, which is discussed in the following section.

5.2 Towards Thick Filaments

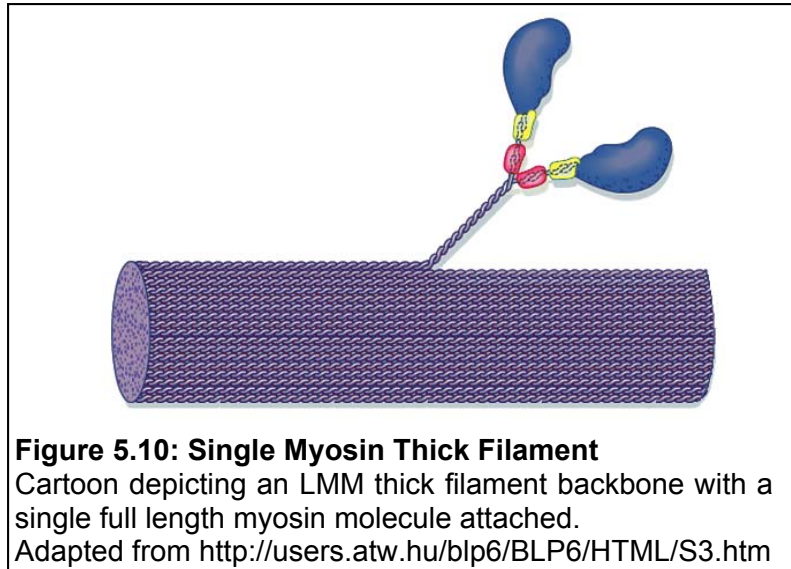
Myosin is arranged in bipolar thick filaments *in vivo*. The RLC binds to the head-rod junction in a position where it is able to affect the ensemble state of myosin through interactions with the thick filament backbone as well as the mechanochemical properties of the individual myosin motor. *In vitro* thick filament assays provide an opportunity to distinguish between the effects exerted by RLC modifications on monomeric myosin versus thick filament ensembles of myosin. By adding complexity to our *in vitro* assays one step at a time, the system is well defined and myosin function from the single molecule to ordered ensembles can be characterized without complications that arise from other cellular components.

First I will describe potential experiments that explore how RLC modifications affect the function of a single myosin in a setting where the thick filament backbone is intact. Second I will describe experiments that characterize the emergent properties of myosin thick filaments.

5.2.1 Contribution of Thick Filament Backbone to *In Vitro* Measurements

The contribution of the thick filament backbone to myosin function can be studied in the context of a single myosin which allows for the characterization of the myosin molecule in its native setting without characterizing the cooperative myosin thick filament ensemble. This can be accomplished through purification of the LMM fragment of myosin which forms the rod portion of myosin and is responsible for the oligomerization of myosin molecules in the thick filament.

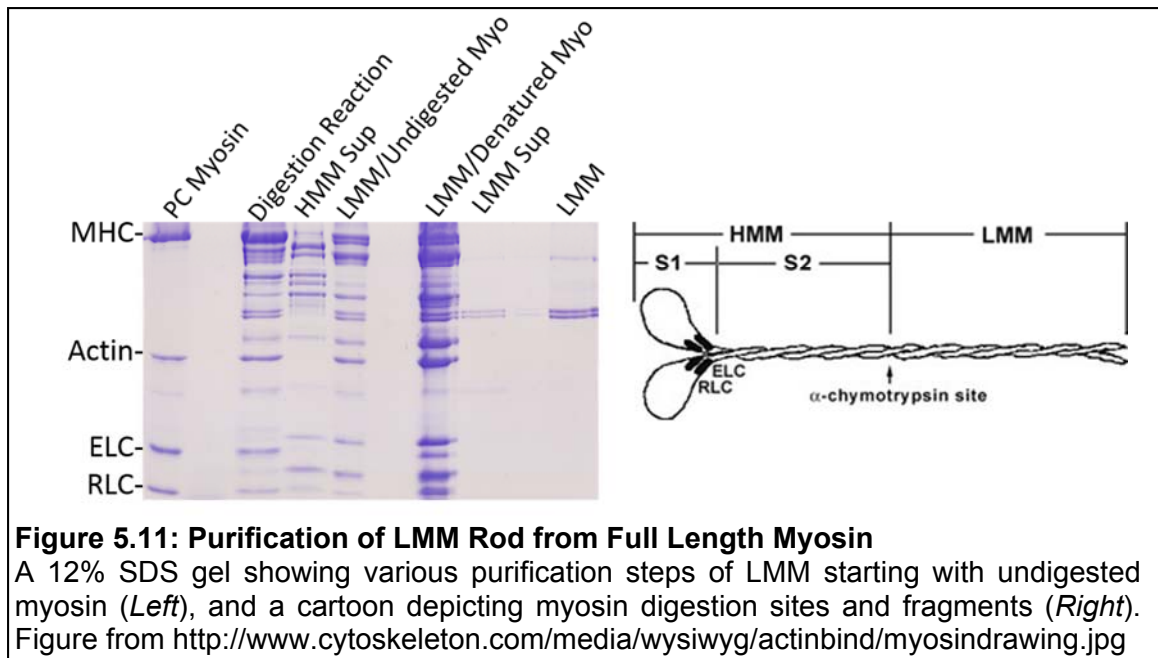
Under favorable conditions the LMM protein fragments will assemble into thick filaments creating the thick filament backbone void of myosin cross-bridges. Mixing a dilute



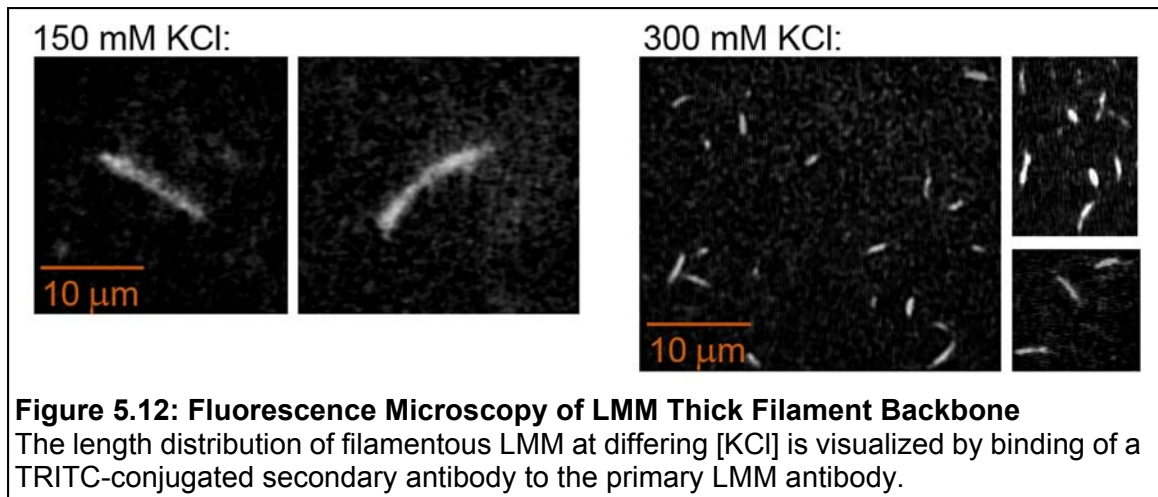
amount of full length monomeric myosin with the LMM backbone results in the formation of a single myosin thick filament (Figure 5.10). Single myosin thick filaments can be used in place of full length monomeric myosin in the three bead assay described in the previous section. This would allow for a comparison of single myosin properties when myosin is randomly attached to a nitrocellulose coated surface versus when it is assembled in a thick filament backbone. Data from optical trapping assays where the filamentous backbone is preserved would provide valuable information about the contribution of myosin head-rod interactions to the inherent properties and function of myosin. Toward this aim, LMM was purified and assembled into thick filament rods as described below.

Soluble myosin is digested by chymotrypsin to purify LMM, based on the protocol of Lowey and Cohen [71]. Briefly, 10 mg/mL myosin suspended in high-salt buffer (0.6 M KCl, 50 mM potassium phosphate, pH7.0) was mixed with α -chymotrypsin diluted in 0.001 N HCl to a final concentration of 0.05 mg/mL. The

solution was stirred for 7 minutes and the reaction was stopped by addition of 0.5 mM PMSF and dialyzed overnight against low-salt buffer (25 mM KCl, 20 mM potassium phosphate, pH7.0, 1 mM DTT). Following centrifugation at 111,000g for 1 hour the pellet containing undigested myosin and LMM was resuspended in high-salt buffer (Figure 5.11; lane 5). Three volumes of cold ethanol were added to the solution and stirred for 3 hours at 4°C to denature the undigested myosin. The precipitate was collected by centrifugation at 18,000g for 30 minutes and resuspended in high-salt buffer (Figure 5.11; lane 7). The solution was dialyzed against high-salt buffer with frequent changes to ensure the complete removal of ethanol. Following centrifugation at 111,000g for 1 hour the supernatant containing LMM was collected (Figure 5.11; lane 8) and dialyzed against low salt buffer. The precipitate was collected by centrifugation at 18,000g for 30 minutes, and the pellet containing purified LMM was resuspended in salt buffer, mixed 1:1 with glycerol and stored at -20°C.



Trial and error was used to determine favorable conditions for the formation of the filament backbone with LMM. The main determinant in this process is the salt concentration. Purified LMM at 0.1 mg/mL was dialyzed against myosin buffer, pH7.5 with varying KCl concentrations and then visualized via fluorescence microscopy (Figure 5.12). A monoclonal primary antibody to the ventricular β -myosin heavy chain that recognizes the LMM fragment was purchased from EMD Millipore (Billerica, MA, cat #MAB1552) and a polyclonal secondary antibody conjugated to TRITC was purchased from Abcam PLC (Cambridge, MA, cat #ab6725) for visualization of the LMM filaments.



At 300 mM KCl concentration, the LMM filaments have a fluorescence profile that is approximately 2-4 microns long (Figure 5.12). This is an appropriate size to use in the three bead assay. The only change to the three bead assay is that the nitrocellulose coated bead pedestals on the coverslip surface would first be incubated with filamentous LMM, followed by incubation with BSA in the same buffer to block the surface. Incubation with full length myosin would follow and also use the same buffer to ensure that LMM filaments do not disperse during the loading of the flow cell. Myosin is soluble when loaded into the flow cell and will bind to LMM filaments. After the formation of single myosin thick filaments on the flow cell surface the remaining buffer solutions can be composed at any salt concentration lower than the LMM buffer.

The use of single myosin thick filaments in the three bead assay described in section 5.1.4 would result in more consistent and accurate measurements of single myosin properties because the variability of myosin attachment to the surface would be eliminated and the myosin molecule would be probed in a more

physiologically relevant environment. In addition, the actin dumbbell may be aligned parallel to the LMM filament by fluorescently labeling the LMM rod which would allow the myosin molecule to interact with the actin filament in an optimal orientation. This would further reduce variability between single molecule measurements.

5.2.2 Thick Filament Motility Assays

The work presented in this thesis focused on the characterization of monomeric myosin with various RLC modifications. Myosin is assembled into bipolar filaments *in vivo* and myosin molecules may cooperatively interact with each other to tune the function of the ensemble unit. In addition the RLC of myosin sits at the head-rod junction where it has the ability to influence the thick filament ensemble. Using myosin thick filaments in the *in vitro* motility assay may provide insight into the cooperative mechanisms employed by multiple myosins working in concert, and offers an opportunity to study how RLC modifications modulate myosin contractility in higher order structures.

Thick filaments can be reconstituted from monomeric myosin simply by lowering the salt concentration of the solution. Myosin will form thick filaments between salt concentrations of 100-200 mM, and in the pH range 6.5-8.0, however formation of a bare zone requires higher pH values closer to pH 8.0. Thick filaments are usually reconstituted either by directly diluting a sample of myosin, or by dialyzing myosin against a linear decreasing salt gradient. Myosin

concentration must be kept at or above 0.1 mg/mL for thick filaments to form. Once thick filaments have been reconstituted they can be used in place of monomeric myosin in the *in vitro* motility assay. Care must be taken to keep solutions at a salt concentration at or below that of the thick filaments to ensure the myosin ensemble does not disperse in the flow cell. Actin filament movement along bipolar thick filaments will proceed in a straight line, and will demonstrate two distinct populations of the actin sliding velocities. Actin filaments sliding towards the bare zone (favorable) will move at a faster velocity than actin filaments sliding away from the bare zone (unfavorable). In the *in vitro* motility assay with monomeric myosin randomly oriented on the coverslip surface, the actin sliding velocity measured is an intermediate value since the actin filament encounters myosin in a number of different orientations. Data from thick filament assays may clarify discrepancies seen between *in vitro* motility assays and muscle fiber studies.

In the unloaded motility assay, I would not expect to see differences between WT and mutant myosin thick filament motility since there was no difference between the monomeric myosins for any parameter tested under unloaded conditions. However, it is possible that the interactions of the mutant RLC with the thick filament backbone could affect the recruitment of myosin to the actin filament which in turn could affect thick filament actin sliding velocity. For myosin thick filaments with phosphorylated RLC, I would expect to see an increase in actin sliding velocity compared to dephosphorylated thick filaments.

Monomeric myosin with phosphorylated RLC showed slight increases in actin sliding velocity for unloaded conditions as well as across all loads tested, giving rise to an upward shift in the myosin force-velocity relationship, although a significant difference of such a subtle change could not be shown for one condition alone. This was interpreted as a phosphorylation induced increase in lever arm stiffness and subsequent increase in myosin step size, leading to significantly increased myosin force production with only a small increase in actin sliding velocity. In the setting of a thick filament where multiple myosins are optimally aligned and working in concert, I would expect this subtle change in actin sliding velocity to become more resolved. In addition, both thick filament structural studies and fiber studies support the idea that RLC phosphorylation increases the recruitment of myosin to thin filament by lifting the myosin crossbridge off the thick filament backbone surface [23, 69, 81, 98]. In muscle fiber studies, maximal shortening velocity was significantly increased as phosphorylation levels were increased from ~20% to ~70% [142], while 0% to ~85% RLC phosphorylation of monomeric myosin only slightly increased actin sliding velocity in the experiments presented in this work. The effect of RLC phosphorylation on velocity was more than four times greater in muscle fiber experiments versus motility assays despite testing a smaller increase in the level of RLC phosphorylation. An increase in myosin recruitment or attachment rate with RLC phosphorylation could potentially explain the discrepancy in velocity values between these experiments. This effect of RLC phosphorylation is also

likely to be present in thick filament motility assays. I would expect the increase in actin sliding velocity between dephosphorylated and phosphorylated thick filaments to be greater than with monomeric myosin in the *in vitro* motility assay; however, this difference still may not be as great as in muscle fibers which have an intact filament lattice and multiple sarcomeres in series.

5.3 Summary

In this thesis I explored the role of RLC N-terminal FHC mutations and phosphorylation in modulating cardiac β -myosin contractility. I characterized the load dependent behavior of myosin using *in vitro* motility assays with an applied frictional load exerted by α -actinin. Myosin bearing FHC mutations N47K and R58Q exhibited reduced actin sliding velocity under load resulting in reduced isometric force production of myosin. This subsequently led to a decrease in the maximum power output of mutant myosins as well as the load at which peak power is achieved. Interpretation of these results point to decreased compliance of the myosin lever arm as the cause of reduced mutant motility, which may also be accompanied by a decrease in myosin step size. Phosphorylation of the RLC had a contrasting effect on myosin load dependence, enhancing actin sliding velocity across all loads for WT and mutant myosins. RLC phosphorylation increased myosin's isometric force production, maximum power output, and shifted myosin to higher loads for peak power. Phosphorylation of myosin bearing RLC FHC mutations restored the mutation induced defects back to WT

myosin levels. It is probable that RLC bearing FHC mutations have structural defects which may alter its interaction with the myosin heavy chain, and that phosphorylation may serve to restore these mechanical interactions. RLC phosphorylation shows promise as a therapeutic target for FHC-linked mutations of the RLC. The precise mechanism by which RLC phosphorylation and FHC mutations work may be further dissected using single molecule optical trapping techniques, which could yield results that may aid the search for potential therapeutic interventions.

Results from our motility assays show that RLC phosphorylation mechanically alters the myosin molecule to make a more robust motor capable of transmitting greater loads at faster rates. RLC phosphorylation most likely exerts its effect by increasing myosin lever arm stiffness and myosin step size. In addition, studies where high levels of exogenous ADP were present suggest that RLC phosphorylation could potentially play a role in altering myosin's strongly bound states by stabilizing the rigor state, though it is unknown whether this has any effect on ADP release rates or whether this would alter the time that myosin spends strongly bound to actin. It is important to note that myosin duty cycle is highly influenced by thick filament interactions and the lattice spacing of the sarcomere. Therefore the effect exerted by RLC modifications on this parameter is hard to predict at the cellular level based on observations at the protein level from motility assays where the contribution from these factors are not present. Thick filament assays could provide insight into the cooperative higher order

ensemble properties of myosin, and the contribution of RLC interactions with the thick filament backbone. Therefore, thick filament assays may be able to distinguish which effects of RLC modifications are more dominant in the native setting.

CHAPTER 6 - REFERENCES

1. **Abraham, T.P., M. Jones, K. Kazmierczak, H.Y. Liang, A.C. Pinheiro, C.S. Wagg, G.D. Lopaschuk, and D. Szczesna-Cordary**, Diastolic dysfunction in familial hypertrophic cardiomyopathy transgenic model mice. *Cardiovascular research*, 2009. **82**(1): p. 84-92.
2. **Aksel, T., E. Choe Yu, S. Sutton, K.M. Ruppel, and J.A. Spudich**, Ensemble force changes that result from human cardiac myosin mutations and a small-molecule effector. *Cell reports*, 2015. **11**(6): p. 910-20.
3. **Alcalai, R., J.G. Seidman, and C.E. Seidman**, Genetic basis of hypertrophic cardiomyopathy: from bench to the clinics. *Journal of cardiovascular electrophysiology*, 2008. **19**(1): p. 104-10.
4. **Alpert, N.R., C. Brosseau, A. Federico, M. Krenz, J. Robbins, and D.M. Warshaw**, Molecular mechanics of mouse cardiac myosin isoforms. *American journal of physiology. Heart and circulatory physiology*, 2002. **283**(4): p. H1446-54.
5. **Álvarez-Acosta, L., A. Mazzanti, X. Fernández, M. Ortiz, R. Barriales-Villa, D. García, E. Maneiro, P. Rebolo, E. Álvarez, and L. Monserrat**, Regulatory Light Chain (MYL2) Mutations in Familial Hypertrophic Cardiomyopathy. *Journal of Cardiovascular Disease*, 2014. **2**(2): p. 73-81.
6. **Andersen, P.S., O. Havndrup, H. Bundgaard, J.C. Moolman-Smook, L.A. Larsen, J. Mogensen, P.A. Brink, A.D. Borglum, V.A. Corfield, K. Kjeldsen, J. Vuust, and M. Christiansen**, Myosin light chain mutations in familial hypertrophic cardiomyopathy: phenotypic presentation and frequency in Danish and South African populations. *Journal of medical genetics*, 2001. **38**(12): p. E43.
7. **Ashikaga, H., T.I. van der Spoel, B.A. Coppola, and J.H. Omens**, Transmural myocardial mechanics during isovolumic contraction. *JACC. Cardiovascular imaging*, 2009. **2**(2): p. 202-11.
8. **Ashkin, A.**, Acceleration and Trapping of Particles by Radiation Pressure. *Physical Review Letters*, 1970. **24**(4): p. 156.
9. **Babu, Y.S., J.S. Sack, T.J. Greenhough, C.E. Bugg, A.R. Means, and W.J. Cook**, Three-dimensional structure of calmodulin. *Nature*, 1985. **315**(6014): p. 37-40.

10. **Batters, C., C.P. Arthur, A. Lin, J. Porter, M.A. Geeves, R.A. Milligan, J.E. Molloy, and L.M. Coluccio**, Myo1c is designed for the adaptation response in the inner ear. *The EMBO journal*, 2004. **23**(7): p. 1433-40.
11. **Bing, W., A. Knott, and S.B. Marston**, A simple method for measuring the relative force exerted by myosin on actin filaments in the in vitro motility assay: evidence that tropomyosin and troponin increase force in single thin filaments. *The Biochemical journal*, 2000. **350 Pt 3**: p. 693-9.
12. **Borejdo, J., D. Szczesna-Cordary, P. Muthu, and N. Calander**, Familial hypertrophic cardiomyopathy can be characterized by a specific pattern of orientation fluctuations of actin molecules. *Biochemistry*, 2010. **49**(25): p. 5269-77.
13. **Bos, J.M., J.A. Towbin, and M.J. Ackerman**, Diagnostic, prognostic, and therapeutic implications of genetic testing for hypertrophic cardiomyopathy. *Journal of the American College of Cardiology*, 2009. **54**(3): p. 201-11.
14. **Botcherby, E.J., A. Corbett, R.A. Burton, C.W. Smith, C. Bollensdorff, M.J. Booth, P. Kohl, T. Wilson, and G. Bub**, Fast measurement of sarcomere length and cell orientation in Langendorff-perfused hearts using remote focusing microscopy. *Circulation research*, 2013. **113**(7): p. 863-70.
15. **Carniel, E., M.R. Taylor, G. Sinagra, A. Di Lenarda, L. Ku, P.R. Fain, M.M. Boucek, J. Cavanaugh, S. Miodic, D. Slavov, S.L. Graw, J. Feiger, X.Z. Zhu, D. Dao, D.A. Ferguson, M.R. Bristow, and L. Mestroni**, Alpha-myosin heavy chain: a sarcomeric gene associated with dilated and hypertrophic phenotypes of cardiomyopathy. *Circulation*, 2005. **112**(1): p. 54-9.
16. **Carvalho, L.R.d., S.Z.d. Pinho, and M.M. Mischan**, Methods to verify parameter equality in nonlinear regression models. *Scientia Agricola*, 2010. **67**: p. 218-222.
17. **Chan, J.Y., M. Takeda, L.E. Briggs, M.L. Graham, J.T. Lu, N. Horikoshi, E.O. Weinberg, H. Aoki, N. Sato, K.R. Chien, and H. Kasahara**, Identification of cardiac-specific myosin light chain kinase. *Circulation research*, 2008. **102**(5): p. 571-80.
18. **Chang, A.N., P.K. Battiprolu, P.M. Cowley, G. Chen, R.D. Gerard, J.R. Pinto, J.A. Hill, A.J. Baker, K.E. Kamm, and J.T. Stull**, Constitutive phosphorylation of cardiac Myosin regulatory light chain in vivo. *The Journal of biological chemistry*, 2015. **290**(17): p. 10703-16.

19. **Cheney, R.E. and M.S. Mooseker**, Unconventional myosins. *Current opinion in cell biology*, 1992. **4**(1): p. 27-35.
20. **Chung, M.W., T. Tsoutsman, and C. Semsarian**, Hypertrophic cardiomyopathy: from gene defect to clinical disease. *Cell research*, 2003. **13**(1): p. 9-20.
21. **Cirino, A.L. and C. Ho**, Hypertrophic Cardiomyopathy Overview, in *GeneReviews(R)*, R.A. Pagon, et al., Editors. 1993: Seattle (WA).
22. **Clement, O., M. Puceat, M.P. Walsh, and G. Vassort**, Protein kinase C enhances myosin light-chain kinase effects on force development and ATPase activity in rat single skinned cardiac cells. *The Biochemical journal*, 1992. **285 (Pt 1)**: p. 311-7.
23. **Colson, B.A., M.R. Locher, T. Bekyarova, J.R. Patel, D.P. Fitzsimons, T.C. Irving, and R.L. Moss**, Differential roles of regulatory light chain and myosin binding protein-C phosphorylations in the modulation of cardiac force development. *The Journal of physiology*, 2010. **588**(Pt 6): p. 981-93.
24. **Craig, R. and W. Lehman**, Crossbridge and tropomyosin positions observed in native, interacting thick and thin filaments. *Journal of molecular biology*, 2001. **311**(5): p. 1027-36.
25. **Davis, J.S., S. Hassanzadeh, S. Winitsky, H. Lin, C. Satorius, R. Vemuri, A.H. Aletras, H. Wen, and N.D. Epstein**, The overall pattern of cardiac contraction depends on a spatial gradient of myosin regulatory light chain phosphorylation. *Cell*, 2001. **107**(5): p. 631-41.
26. **Davis, J.S., S. Hassanzadeh, S. Winitsky, H. Wen, A. Aletras, and N.D. Epstein**, A gradient of myosin regulatory light-chain phosphorylation across the ventricular wall supports cardiac torsion. *Cold Spring Harbor symposia on quantitative biology*, 2002. **67**: p. 345-52.
27. **Davison, M.D. and D.R. Critchley**, alpha-Actinins and the DMD protein contain spectrin-like repeats. *Cell*, 1988. **52**(2): p. 159-60.
28. **Debold, E.P., J.P. Schmitt, J.B. Patlak, S.E. Beck, J.R. Moore, J.G. Seidman, C. Seidman, and D.M. Warshaw**, Hypertrophic and dilated cardiomyopathy mutations differentially affect the molecular force generation of mouse alpha-cardiac myosin in the laser trap assay. *American journal of physiology. Heart and circulatory physiology*, 2007. **293**(1): p. H284-91.

29. **Ding, P., J. Huang, P.K. Battiprolu, J.A. Hill, K.E. Kamm, and J.T. Stull**, Cardiac myosin light chain kinase is necessary for myosin regulatory light chain phosphorylation and cardiac performance in vivo. *The Journal of biological chemistry*, 2010. **285**(52): p. 40819-29.
30. **Esch, B.T. and D.E. Warburton**, Left ventricular torsion and recoil: implications for exercise performance and cardiovascular disease. *Journal of applied physiology*, 2009. **106**(2): p. 362-9.
31. **Fenn, W.O.**, A quantitative comparison between the energy liberated and the work performed by the isolated sartorius muscle of the frog. *The Journal of physiology*, 1923. **58**(2-3): p. 175-203.
32. **Finer, J.T., R.M. Simmons, and J.A. Spudich**, Single myosin molecule mechanics: piconewton forces and nanometre steps. *Nature*, 1994. **368**(6467): p. 113-9.
33. **Fitts, R.H.**, The cross-bridge cycle and skeletal muscle fatigue. *Journal of applied physiology*, 2008. **104**(2): p. 551-8.
34. **Flavigny, J., P. Richard, R. Isnard, L. Carrier, P. Charron, G. Bonne, J.F. Forissier, M. Desnos, O. Dubourg, M. Komajda, K. Schwartz, and B. Hainque**, Identification of two novel mutations in the ventricular regulatory myosin light chain gene (MYL2) associated with familial and classical forms of hypertrophic cardiomyopathy. *Journal of molecular medicine (Berlin, Germany)*, 1998. **76**(3-4): p. 208-14.
35. **Frey, N., M. Luedde, and H.A. Katus**, Mechanisms of disease: hypertrophic cardiomyopathy. *Nature reviews. Cardiology*, 2012. **9**(2): p. 91-100.
36. **Geeves, M.A., C. Perreault-Micale, and L.M. Coluccio**, Kinetic analyses of a truncated mammalian myosin I suggest a novel isomerization event preceding nucleotide binding. *The Journal of biological chemistry*, 2000. **275**(28): p. 21624-30.
37. **Glantz, S.A.**, Primer of Biostatistics. 7th ed. 2012, New York, New York: The McGraw-Hill Companies, Inc.
38. **Goldmann, W.H. and G. Isenberg**, Analysis of filamin and alpha-actinin binding to actin by the stopped flow method. *FEBS letters*, 1993. **336**(3): p. 408-10.
39. **Gordon, A.M., E. Homsher, and M. Regnier**, Regulation of contraction in striated muscle. *Physiological reviews*, 2000. **80**(2): p. 853-924.

40. **Greenberg, M.**, Modulation of Myosin Mechanics and Kinetics by the Myosin Regulatory Light Chain, in *Department of Biophysics*. 2010, Boston University, School of Medicine.
41. **Greenberg, M.J., K. Kazmierczak, D. Szczesna-Cordary, and J.R. Moore**, Cardiomyopathy-linked myosin regulatory light chain mutations disrupt myosin strain-dependent biochemistry. *Proceedings of the National Academy of Sciences of the United States of America*, 2010. **107**(40): p. 17403-8.
42. **Greenberg, M.J., T.R. Mealy, J.D. Watt, M. Jones, D. Szczesna-Cordary, and J.R. Moore**, The molecular effects of skeletal muscle myosin regulatory light chain phosphorylation. *American journal of physiology. Regulatory, integrative and comparative physiology*, 2009. **297**(2): p. R265-74.
43. **Greenberg, M.J. and J.R. Moore**, The molecular basis of frictional loads in the in vitro motility assay with applications to the study of the loaded mechanochemistry of molecular motors. *Cytoskeleton (Hoboken, N.J)*, 2010. **67**(5): p. 273-85.
44. **Gu, X., X. Liu, D. Xu, X. Li, M. Yan, Y. Qi, W. Yan, W. Wang, J. Pan, Y. Xu, B. Xi, L. Cheng, J. Jia, K. Wang, J. Ge, and M. Zhou**, Cardiac functional improvement in rats with myocardial infarction by up-regulating cardiac myosin light chain kinase with neuregulin. *Cardiovascular research*, 2010. **88**(2): p. 334-43.
45. **Hall, J.E., and Arthur C. Guyton** Textbook of Medical Physiology. Philadelphia, PA: Saunders, 2011. Print.
46. **Harrington, K.B., F. Rodriguez, A. Cheng, F. Langer, H. Ashikaga, G.T. Daughters, J.C. Criscione, N.B. Ingels, and D.C. Miller**, Direct measurement of transmural laminar architecture in the anterolateral wall of the ovine left ventricle: new implications for wall thickening mechanics. *American journal of physiology. Heart and circulatory physiology*, 2005. **288**(3): p. H1324-30.
47. **Hasenfuss, G., L.A. Mulieri, E.M. Blanchard, C. Holubarsch, B.J. Leavitt, F. Ittleman, and N.R. Alpert**, Energetics of isometric force development in control and volume-overload human myocardium. Comparison with animal species. *Circulation research*, 1991. **68**(3): p. 836-46.
48. **Hidalgo, C., Y. Wu, J. Peng, W.F. Siems, K.B. Campbell, and H. Granzier**, Effect of diastolic pressure on MLC2v phosphorylation in the rat

- left ventricle. *Archives of biochemistry and biophysics*, 2006. **456**(2): p. 216-23.
49. **Hilber, K., Y.B. Sun, and M. Irving**, Effects of sarcomere length and temperature on the rate of ATP utilisation by rabbit psoas muscle fibres. *The Journal of physiology*, 2001. **531**(Pt 3): p. 771-80.
 50. **Hill, A.V.**, The Heat of Shortening and the Dynamic Constants of Muscle. *Proceedings of the Royal Society of London. Series B, Biological Sciences*, 1938. **126**(843): p. 136-195.
 51. **Houdusse, A. and C. Cohen**, Target sequence recognition by the calmodulin superfamily: implications from light chain binding to the regulatory domain of scallop myosin. *Proceedings of the National Academy of Sciences of the United States of America*, 1995. **92**(23): p. 10644-7.
 52. **Huang, J., J.M. Shelton, J.A. Richardson, K.E. Kamm, and J.T. Stull**, Myosin regulatory light chain phosphorylation attenuates cardiac hypertrophy. *The Journal of biological chemistry*, 2008. **283**(28): p. 19748-56.
 53. **Huang, W., J. Liang, C.C. Yuan, K. Kazmierczak, Z. Zhou, A. Morales, K.L. McBride, S.M. Fitzgerald-Butt, R.E. Hershberger, and D. Szczesna-Cordary**, Novel familial dilated cardiomyopathy mutation in MYL2 affects the structure and function of myosin regulatory light chain. *The FEBS journal*, 2015.
 54. **Huxley, A.F.**, Muscle structure and theories of contraction. *Progress in biophysics and biophysical chemistry*, 1957. **7**: p. 255-318.
 55. **Ingwall, J.S. and R.G. Weiss**, Is the failing heart energy starved? On using chemical energy to support cardiac function. *Circulation research*, 2004. **95**(2): p. 135-45.
 56. **Jacques, A.M., N. Briceno, A.E. Messer, C.E. Gallon, S. Jalilzadeh, E. Garcia, G. Kikonda-Kanda, J. Goddard, S.E. Harding, H. Watkins, M.T. Esteban, V.T. Tsang, W.J. McKenna, and S.B. Marston**, The molecular phenotype of human cardiac myosin associated with hypertrophic obstructive cardiomyopathy. *Cardiovascular research*, 2008. **79**(3): p. 481-91.
 57. **Janson, L.W., J.R. Sellers, and D.L. Taylor**, Actin-binding proteins regulate the work performed by myosin II motors on single actin filaments. *Cell Motil Cytoskeleton*, 1992. **22**(4): p. 274-80.

58. **Jayatileke, I., M. McGuire, V. Booth, D.R. Richmond, and C. Semsarian**, Sudden death prevented in hypertrophic cardiomyopathy. *Heart, lung & circulation*, 2003. **12**(3): p. 196-8.
59. **Jontes, J.D., E.M. Wilson-Kubalek, and R.A. Milligan**, A 32 degree tail swing in brush border myosin I on ADP release. *Nature*, 1995. **378**(6558): p. 751-3.
60. **Kabaeva, Z.T., A. Perrot, B. Wolter, R. Dietz, N. Cardim, J.M. Correia, H.D. Schulte, A.A. Aldashev, M.M. Mirrakhimov, and K.J. Osterziel**, Systematic analysis of the regulatory and essential myosin light chain genes: genetic variants and mutations in hypertrophic cardiomyopathy. *Eur J Hum Genet*, 2002. **10**(11): p. 741-8.
61. **Kampourakis, T., Y.B. Sun, and M. Irving**, Orientation of the N- and C-terminal lobes of the myosin regulatory light chain in cardiac muscle. *Biophysical journal*, 2015. **108**(2): p. 304-14.
62. **Keller, D.I., C. Coirault, T. Rau, T. Cheav, M. Weyand, K. Amann, Y. Lecarpentier, P. Richard, T. Eschenhagen, and L. Carrier**, Human homozygous R403W mutant cardiac myosin presents disproportionate enhancement of mechanical and enzymatic properties. *Journal of molecular and cellular cardiology*, 2004. **36**(3): p. 355-62.
63. **Kerrick, W.G., K. Kazmierczak, Y. Xu, Y. Wang, and D. Szczesna-Cordary**, Malignant familial hypertrophic cardiomyopathy D166V mutation in the ventricular myosin regulatory light chain causes profound effects in skinned and intact papillary muscle fibers from transgenic mice. *Faseb J*, 2009. **23**(3): p. 855-65.
64. **Khromov, A.S., A.V. Somlyo, and A.P. Somlyo**, Thiophosphorylation of myosin light chain increases rigor stiffness of rabbit smooth muscle. *The Journal of physiology*, 1998. **512** (Pt 2): p. 345-50.
65. **Kohler, D., C. Ruff, E. Meyhofer, and M. Bahler**, Different degrees of lever arm rotation control myosin step size. *The Journal of cell biology*, 2003. **161**(2): p. 237-41.
66. **Kollmar, M., U. Durrwang, W. Kliche, D.J. Manstein, and F.J. Kull**, Crystal structure of the motor domain of a class-I myosin. *The EMBO journal*, 2002. **21**(11): p. 2517-25.
67. **Kron, S.J. and J.A. Spudich**, Fluorescent actin filaments move on myosin fixed to a glass surface. *Proceedings of the National Academy of Sciences of the United States of America*, 1986. **83**(17): p. 6272-6.

68. **Kuhlman, P.A., J. Ellis, D.R. Critchley, and C.R. Bagshaw**, The kinetics of the interaction between the actin-binding domain of alpha-actinin and F-actin. *FEBS letters*, 1994. **339**(3): p. 297-301.
69. **Levine, R.J., R.W. Kensler, Z. Yang, J.T. Stull, and H.L. Sweeney**, Myosin light chain phosphorylation affects the structure of rabbit skeletal muscle thick filaments. *Biophysical journal*, 1996. **71**(2): p. 898-907.
70. **Locher, M.R., M.V. Razumova, J.E. Stelzer, H.S. Norman, J.R. Patel, and R.L. Moss**, Determination of rate constants for turnover of myosin isoforms in rat myocardium: implications for in vivo contractile kinetics. *American journal of physiology. Heart and circulatory physiology*, 2009. **297**(1): p. H247-56.
71. **Lowey, S. and C. Cohen**, Studies on the structure of myosin. *Journal of molecular biology*, 1962. **4**: p. 293-308.
72. **Lowey, S., G.S. Waller, and K.M. Trybus**, Skeletal muscle myosin light chains are essential for physiological speeds of shortening. *Nature*, 1993. **365**(6445): p. 454-6.
73. **Lymn, R.W. and E.W. Taylor**, Mechanism of adenosine triphosphate hydrolysis by actomyosin. *Biochemistry*, 1971. **10**(25): p. 4617-24.
74. **MacIntosh, B.R.**, Role of calcium sensitivity modulation in skeletal muscle performance. *News in physiological sciences : an international journal of physiology produced jointly by the International Union of Physiological Sciences and the American Physiological Society*, 2003. **18**: p. 222-5.
75. **Malmqvist, U.P., A. Aronshtam, and S. Lowey**, Cardiac myosin isoforms from different species have unique enzymatic and mechanical properties. *Biochemistry*, 2004. **43**(47): p. 15058-65.
76. **Marian, A.J.**, Contemporary treatment of hypertrophic cardiomyopathy. *Texas Heart Institute journal / from the Texas Heart Institute of St. Luke's Episcopal Hospital, Texas Children's Hospital*, 2009. **36**(3): p. 194-204.
77. **Martyn, D.A. and A.M. Gordon**, Length and myofilament spacing-dependent changes in calcium sensitivity of skeletal fibres: effects of pH and ionic strength. *Journal of muscle research and cell motility*, 1988. **9**(5): p. 428-45.
78. **McKillop, D.F. and M.A. Geeves**, Regulation of the interaction between actin and myosin subfragment 1: evidence for three states of the thin filament. *Biophysical journal*, 1993. **65**(2): p. 693-701.

79. **McNally, E.M., J.R. Golbus, and M.J. Puckelwartz**, Genetic mutations and mechanisms in dilated cardiomyopathy. *The Journal of clinical investigation*, 2013. **123**(1): p. 19-26.
80. **Mendoza, D.D., H.A. Cooper, and J.A. Panza**, Cardiac power output predicts mortality across a broad spectrum of patients with acute cardiac disease. *American heart journal*, 2007. **153**(3): p. 366-70.
81. **Metzger, J.M., M.L. Greaser, and R.L. Moss**, Variations in cross-bridge attachment rate and tension with phosphorylation of myosin in mammalian skinned skeletal muscle fibers. Implications for twitch potentiation in intact muscle. *The Journal of general physiology*, 1989. **93**(5): p. 855-83.
82. **Miyata, S., W. Minobe, M.R. Bristow, and L.A. Leinwand**, Myosin heavy chain isoform expression in the failing and nonfailing human heart. *Circulation research*, 2000. **86**(4): p. 386-90.
83. **Mizutani, H., R. Okamoto, N. Moriki, K. Konishi, M. Taniguchi, S. Fujita, K. Dohi, K. Onishi, N. Suzuki, S. Satoh, N. Makino, T. Itoh, D.J. Hartshorne, and M. Ito**, Overexpression of myosin phosphatase reduces Ca(2+) sensitivity of contraction and impairs cardiac function. *Circulation journal : official journal of the Japanese Circulation Society*, 2010. **74**(1): p. 120-8.
84. **Moore, J.R., E.B. Kremontsova, K.M. Trybus, and D.M. Warshaw**, Does the myosin V neck region act as a lever? *Journal of muscle research and cell motility*, 2004. **25**(1): p. 29-35.
85. **Moore, J.R., L. Leinwand, and D.M. Warshaw**, Understanding cardiomyopathy phenotypes based on the functional impact of mutations in the myosin motor. *Circulation research*, 2012. **111**(3): p. 375-85.
86. **Morano, I.**, Effects of different expression and posttranslational modifications of myosin light chains on contractility of skinned human cardiac fibers. *Basic research in cardiology*, 1992. **87 Suppl 1**: p. 129-41.
87. **Morano, I., H. Arndt, C. Bachle-Stolz, and J.C. Ruegg**, Further studies on the effects of myosin P-light chain phosphorylation on contractile properties of skinned cardiac fibres. *Basic research in cardiology*, 1986. **81**(6): p. 611-9.
88. **Morano, I., A. Osterman, and A. Arner**, Rate of active tension development from rigor in skinned atrial and ventricular cardiac fibres from swine following photolytic release of ATP from caged ATP. *Acta physiologica Scandinavica*, 1995. **154**(3): p. 343-53.

89. **Morimoto, S.**, Sarcomeric proteins and inherited cardiomyopathies. *Cardiovascular research*, 2008. **77**(4): p. 659-66.
90. **Muthu, P., K. Kazmierczak, M. Jones, and D. Szczesna-Cordary**, The effect of myosin RLC phosphorylation in normal and cardiomyopathic mouse hearts. *Journal of cellular and molecular medicine*, 2011.
91. **Muthu, P., J. Liang, W. Schmidt, J.R. Moore, and D. Szczesna-Cordary**, In vitro rescue study of a malignant familial hypertrophic cardiomyopathy phenotype by pseudo-phosphorylation of myosin regulatory light chain. *Archives of biochemistry and biophysics*, 2013.
92. **Nadal-Ginard, B. and V. Mahdavi**, Molecular basis of cardiac performance. Plasticity of the myocardium generated through protein isoform switches. *The Journal of clinical investigation*, 1989. **84**(6): p. 1693-700.
93. **Ngai, P.K., C.A. Carruthers, and M.P. Walsh**, Isolation of the native form of chicken gizzard myosin light-chain kinase. *The Biochemical journal*, 1984. **218**(3): p. 863-70.
94. **Niimura, H., K.K. Patton, W.J. McKenna, J. Soultis, B.J. Maron, J.G. Seidman, and C.E. Seidman**, Sarcomere protein gene mutations in hypertrophic cardiomyopathy of the elderly. *Circulation*, 2002. **105**(4): p. 446-51.
95. **Nyitrai, M. and M.A. Geeves**, Adenosine diphosphate and strain sensitivity in myosin motors. *Philosophical transactions of the Royal Society of London*, 2004. **359**(1452): p. 1867-77.
96. **Oishi, N., K. Sutoh, S. Suzuki, and H. Sugi**, Evidence for the functional role of myosin subfragment-2 in the in vitro actin-myosin sliding. *J. Muscle Res. Cell Motil*, 1996. **17**: p. 281.
97. **Okamoto, R., T. Kato, A. Mizoguchi, N. Takahashi, T. Nakakuki, H. Mizutani, N. Isaka, K. Imanaka-Yoshida, K. Kaibuchi, Z. Lu, K. Mabuchi, T. Tao, D.J. Hartshorne, T. Nakano, and M. Ito**, Characterization and function of MYPT2, a target subunit of myosin phosphatase in heart. *Cellular signalling*, 2006. **18**(9): p. 1408-16.
98. **Padron, R., N. Pante, H. Sosa, and J. Kendrick-Jones**, X-ray diffraction study of the structural changes accompanying phosphorylation of tarantula muscle. *Journal of muscle research and cell motility*, 1991. **12**(3): p. 235-41.

99. **Palmiter, K.A., M.J. Tyska, D.E. Dupuis, N.R. Alpert, and D.M. Warshaw**, Kinetic differences at the single molecule level account for the functional diversity of rabbit cardiac myosin isoforms. *The Journal of physiology*, 1999. **519 Pt 3**: p. 669-78.
100. **Pant, K., J. Watt, M. Greenberg, M. Jones, D. Szczesna-Cordary, and J.R. Moore**, Removal of the cardiac myosin regulatory light chain increases isometric force production. *Faseb J*, 2009.
101. **Parry, D.A. and J.M. Squire**, Structural role of tropomyosin in muscle regulation: analysis of the x-ray diffraction patterns from relaxed and contracting muscles. *Journal of molecular biology*, 1973. **75(1)**: p. 33-55.
102. **Pearson, R.B. and B.E. Kemp**, Chemical modification of lysine and arginine residues in the myosin regulatory light chain inhibits phosphorylation. *Biochimica et biophysica acta*, 1986. **870(2)**: p. 312-9.
103. **Perrie, W.T. and S.V. Perry**, An electrophoretic study of the low-molecular-weight components of myosin. *The Biochemical journal*, 1970. **119(1)**: p. 31-8.
104. **Persechini, A., J.T. Stull, and R. Cooke**, The effect of myosin phosphorylation on the contractile properties of skinned rabbit skeletal muscle fibers. *The Journal of biological chemistry*, 1985. **260(13)**: p. 7951-4.
105. **Phillips, G.N., Jr., J.P. Fillers, and C. Cohen**, Tropomyosin crystal structure and muscle regulation. *Journal of molecular biology*, 1986. **192(1)**: p. 111-31.
106. **Rayment, I., W.R. Rypniewski, K. Schmidt-Base, R. Smith, D.R. Tomchick, M.M. Benning, D.A. Winkelmann, G. Wesenberg, and H.M. Holden**, Three-dimensional structure of myosin subfragment-1: a molecular motor. *Science (New York, N.Y.)*, 1993. **261(5117)**: p. 50-8.
107. **Reedy, M.C.**, Visualizing myosin's power stroke in muscle contraction. *Journal of cell science*, 2000. **113 (Pt 20)**: p. 3551-62.
108. **Reinach, F.C., K. Nagai, and J. Kendrick-Jones**, Site-directed mutagenesis of the regulatory light-chain Ca²⁺/Mg²⁺ binding site and its role in hybrid myosins. *Nature*, 1986. **322(6074)**: p. 80-3.
109. **Reiser, P.J., M.A. Portman, X.H. Ning, and C. Schomisch Moravec**, Human cardiac myosin heavy chain isoforms in fetal and failing adult atria

and ventricles. *American journal of physiology. Heart and circulatory physiology*, 2001. **280**(4): p. H1814-20.

110. **Richard, P., P. Charron, L. Carrier, C. Ledeuil, T. Cheav, C. Pichereau, A. Benaiche, R. Isnard, O. Dubourg, M. Burban, J.P. Gueffet, A. Millaire, M. Desnos, K. Schwartz, B. Hainque, and M. Komajda**, Hypertrophic cardiomyopathy: distribution of disease genes, spectrum of mutations, and implications for a molecular diagnosis strategy. *Circulation*, 2003. **107**(17): p. 2227-32.
111. **Ritz-Gold, C.J., R. Cooke, D.K. Blumenthal, and J.T. Stull**, Light chain phosphorylation alters the conformation of skeletal muscle myosin. *Biochemical and biophysical research communications*, 1980. **93**(1): p. 209-14.
112. **Rodriguez, E.K., W.C. Hunter, M.J. Royce, M.K. Leppo, A.S. Douglas, and H.F. Weisman**, A method to reconstruct myocardial sarcomere lengths and orientations at transmural sites in beating canine hearts. *The American journal of physiology*, 1992. **263**(1 Pt 2): p. H293-306.
113. **Rosenfeld, S.S., J. Xing, M. Whitaker, H.C. Cheung, F. Brown, A. Wells, R.A. Milligan, and H.L. Sweeney**, Kinetic and spectroscopic evidence for three actomyosin:ADP states in smooth muscle. *The Journal of biological chemistry*, 2000. **275**(33): p. 25418-26.
114. **Ruegg, C., C. Veigel, J.E. Molloy, S. Schmitz, J.C. Sparrow, and R.H. Fink**, Molecular motors: force and movement generated by single myosin II molecules. *News in physiological sciences : an international journal of physiology produced jointly by the International Union of Physiological Sciences and the American Physiological Society*, 2002. **17**: p. 213-8.
115. **Sanbe, A., J.G. Fewell, J. Gulick, H. Osinska, J. Lorenz, D.G. Hall, L.A. Murray, T.R. Kimball, S.A. Witt, and J. Robbins**, Abnormal cardiac structure and function in mice expressing nonphosphorylatable cardiac regulatory myosin light chain 2. *The Journal of biological chemistry*, 1999. **274**(30): p. 21085-94.
116. **Sarshar, M., W.T. Wong, and B. Anvari**, Comparative study of methods to calibrate the stiffness of a single-beam gradient-force optical tweezers over various laser trapping powers. *Journal of biomedical optics*, 2014. **19**(11): p. 115001.
117. **Schwartz, K., Y. Lecarpentier, J.L. Martin, A.M. Lompre, J.J. Mercadier, and B. Swynghedauw**, Myosin isoenzymic distribution

correlates with speed of myocardial contraction. *Journal of molecular and cellular cardiology*, 1981. **13**(12): p. 1071-5.

118. **Scruggs, S.B., A.C. Hinken, A. Thawornkaiwong, J. Robbins, L.A. Walker, P.P. de Tombe, D.L. Geenen, P.M. Buttrick, and R.J. Solaro**, Ablation of ventricular myosin regulatory light chain phosphorylation in mice causes cardiac dysfunction in situ and affects neighboring myofilament protein phosphorylation. *The Journal of biological chemistry*, 2009. **284**(8): p. 5097-106.
119. **Scruggs, S.B., R. Reisdorph, M.L. Armstrong, C.M. Warren, N. Reisdorph, R.J. Solaro, and P.M. Buttrick**, A novel, in-solution separation of endogenous cardiac sarcomeric proteins and identification of distinct charged variants of regulatory light chain. *Molecular & cellular proteomics : MCP*, 2010. **9**(9): p. 1804-18.
120. **Scruggs, S.B. and R.J. Solaro**, The significance of regulatory light chain phosphorylation in cardiac physiology. *Archives of biochemistry and biophysics*, 2011. **510**(2): p. 129-34.
121. **Seidman, C.E. and J.G. Seidman**, Identifying sarcomere gene mutations in hypertrophic cardiomyopathy: a personal history. *Circulation research*, 2011. **108**(6): p. 743-50.
122. **Sheikh, F., R.C. Lyon, and J. Chen**, Getting the skinny on thick filament regulation in cardiac muscle biology and disease. *Trends in cardiovascular medicine*, 2014. **24**(4): p. 133-41.
123. **Sheikh, F., K. Ouyang, S.G. Campbell, R.C. Lyon, J. Chuang, D. Fitzsimons, J. Tangney, C.G. Hidalgo, C.S. Chung, H. Cheng, N.D. Dalton, Y. Gu, H. Kasahara, M. Ghassemian, J.H. Omens, K.L. Peterson, H.L. Granzier, R.L. Moss, A.D. McCulloch, and J. Chen**, Mouse and computational models link Mlc2v dephosphorylation to altered myosin kinetics in early cardiac disease. *The Journal of clinical investigation*, 2012. **122**(4): p. 1209-21.
124. **Siemankowski, R.F., M.O. Wiseman, and H.D. White**, ADP dissociation from actomyosin subfragment 1 is sufficiently slow to limit the unloaded shortening velocity in vertebrate muscle. *Proceedings of the National Academy of Sciences of the United States of America*, 1985. **82**(3): p. 658-62.
125. **Sobieszek, A.a.J., P.**, Urea-glycerol-acrylamide gel electrophoresis of acidic low molecular weight muscle proteins: Rapid determination of

- myosin light chain phosphorylation in myosin, actomyosin and whole muscle samples. *Electrophoresis*, 1986. **7**(9): p. 417-425.
126. **Sowerby, A.J., C.K. Seehra, M. Lee, and C.R. Bagshaw**, Turnover of fluorescent nucleoside triphosphates by isolated immobilized myosin filaments. Transient kinetics on the zeptomole scale. *Journal of molecular biology*, 1993. **234**(1): p. 114-23.
 127. Spring, K., and Michael Davidson. Introduction to Fluorescence Microscopy
<http://www.microscopyu.com/articles/fluorescence/fluorescenceintro.html>
May 1, 2015].
 128. **Spudich, J.A.**, Hypertrophic and dilated cardiomyopathy: four decades of basic research on muscle lead to potential therapeutic approaches to these devastating genetic diseases. *Biophysical journal*, 2014. **106**(6): p. 1236-49.
 129. **Spudich, J.A., S.E. Rice, R.S. Rock, T.J. Purcell, and H.M. Warrick**, Optical traps to study properties of molecular motors. *Cold Spring Harbor protocols*, 2011. **2011**(11): p. 1305-18.
 130. **Stelzer, J.E., J.R. Patel, and R.L. Moss**, Acceleration of stretch activation in murine myocardium due to phosphorylation of myosin regulatory light chain. *The Journal of general physiology*, 2006. **128**(3): p. 261-72.
 131. **Stewart, M.**, The location of the troponin binding site on tropomyosin. *Proc R Soc Lond B Biol Sci*, 1975. **190**(1099): p. 257-66.
 132. **Sugi, H.**, In Vitro Motility Assay, in *Current Methods in Muscle Physiology: Advantages, Problems and Limitations*. 1998, Oxford University Press: Oxford.
 133. **Sun, Y.B., K. Hilber, and M. Irving**, Effect of active shortening on the rate of ATP utilisation by rabbit psoas muscle fibres. *The Journal of physiology*, 2001. **531**(Pt 3): p. 781-91.
 134. **Sweeney, H.L., B.F. Bowman, and J.T. Stull**, Myosin light chain phosphorylation in vertebrate striated muscle: regulation and function. *The American journal of physiology*, 1993. **264**(5 Pt 1): p. C1085-95.
 135. **Sweeney, H.L. and J.T. Stull**, Phosphorylation of myosin in permeabilized mammalian cardiac and skeletal muscle cells. *The American journal of physiology*, 1986. **250**(4 Pt 1): p. C657-60.

136. **Sweeney, H.L. and J.T. Stull**, Alteration of cross-bridge kinetics by myosin light chain phosphorylation in rabbit skeletal muscle: implications for regulation of actin-myosin interaction. *Proceedings of the National Academy of Sciences of the United States of America*, 1990. **87**(1): p. 414-8.
137. **Sweeney, H.L., Z. Yang, G. Zhi, J.T. Stull, and K.M. Trybus**, Charge replacement near the phosphorylatable serine of the myosin regulatory light chain mimics aspects of phosphorylation. *Proceedings of the National Academy of Sciences of the United States of America*, 1994. **91**(4): p. 1490-4.
138. **Szczesna-Cordary, D., G. Guzman, S.S. Ng, and J. Zhao**, Familial hypertrophic cardiomyopathy-linked alterations in Ca²⁺ binding of human cardiac myosin regulatory light chain affect cardiac muscle contraction. *The Journal of biological chemistry*, 2004. **279**(5): p. 3535-42.
139. **Szczesna, D., D. Ghosh, Q. Li, A.V. Gomes, G. Guzman, C. Arana, G. Zhi, J.T. Stull, and J.D. Potter**, Familial hypertrophic cardiomyopathy mutations in the regulatory light chains of myosin affect their structure, Ca²⁺ binding, and phosphorylation. *The Journal of biological chemistry*, 2001. **276**(10): p. 7086-92.
140. **Tajsharghi, H.**, Thick and thin filament gene mutations in striated muscle diseases. *International journal of molecular sciences*, 2008. **9**(7): p. 1259-75.
141. **Takagi, Y., R.E. Farrow, N. Billington, A. Nagy, C. Batters, Y. Yang, J.R. Sellers, and J.E. Molloy**, Myosin-10 produces its power-stroke in two phases and moves processively along a single actin filament under low load. *Proceedings of the National Academy of Sciences of the United States of America*, 2014. **111**(18): p. E1833-42.
142. **Toepfer, C., V. Caorsi, T. Kampourakis, M.B. Sikkil, T.G. West, M.C. Leung, S.A. Al-Saud, K.T. MacLeod, A.R. Lyon, S.B. Marston, J.R. Sellers, and M.A. Ferenczi**, Myosin regulatory light chain (RLC) phosphorylation change as a modulator of cardiac muscle contraction in disease. *The Journal of biological chemistry*, 2013. **288**(19): p. 13446-54.
143. **Tyska, M.J., D.E. Dupuis, W.H. Guilford, J.B. Patlak, G.S. Waller, K.M. Trybus, D.M. Warshaw, and S. Lowey**, Two heads of myosin are better than one for generating force and motion. *Proceedings of the National Academy of Sciences of the United States of America*, 1999. **96**(8): p. 4402-7.

144. **Tyska, M.J. and D.M. Warshaw**, The myosin power stroke. *Cell motility and the cytoskeleton*, 2002. **51**(1): p. 1-15.
145. **Uyeda, T.Q., P.D. Abramson, and J.A. Spudich**, The neck region of the myosin motor domain acts as a lever arm to generate movement. *Proceedings of the National Academy of Sciences of the United States of America*, 1996. **93**(9): p. 4459-64.
146. **van der Velden, J., Z. Papp, R. Zaremba, N.M. Boontje, J.W. de Jong, V.J. Owen, P.B. Burton, P. Goldmann, K. Jaquet, and G.J. Stienen**, Increased Ca²⁺-sensitivity of the contractile apparatus in end-stage human heart failure results from altered phosphorylation of contractile proteins. *Cardiovascular research*, 2003. **57**(1): p. 37-47.
147. **VanBuren, P., D.E. Harris, N.R. Alpert, and D.M. Warshaw**, Cardiac V1 and V3 myosins differ in their hydrolytic and mechanical activities in vitro. *Circulation research*, 1995. **77**(2): p. 439-44.
148. **Veigel, C., M.L. Bartoo, D.C. White, J.C. Sparrow, and J.E. Molloy**, The stiffness of rabbit skeletal actomyosin cross-bridges determined with an optical tweezers transducer. *Biophysical journal*, 1998. **75**(3): p. 1424-38.
149. **Veigel, C., L.M. Coluccio, J.D. Jontes, J.C. Sparrow, R.A. Milligan, and J.E. Molloy**, The motor protein myosin-I produces its working stroke in two steps. *Nature*, 1999. **398**(6727): p. 530-3.
150. **Wang, L., J.G. Seidman, and C.E. Seidman**, Narrative review: harnessing molecular genetics for the diagnosis and management of hypertrophic cardiomyopathy. *Annals of internal medicine*, 2010. **152**(8): p. 513-20, W181.
151. **Wang, Y., K. Ajtai, and T.P. Burghardt**, Ventricular myosin modifies in vitro step-size when phosphorylated. *Journal of molecular and cellular cardiology*, 2014. **72**: p. 231-7.
152. **Wang, Y., Y. Xu, W.G. Kerrick, Y. Wang, G. Guzman, Z. Diaz-Perez, and D. Szczesna-Cordary**, Prolonged Ca²⁺ and force transients in myosin RLC transgenic mouse fibers expressing malignant and benign FHC mutations. *Journal of molecular biology*, 2006. **361**(2): p. 286-99.
153. **Wang, Y.P. and F. Fuchs**, Osmotic compression of skinned cardiac and skeletal muscle bundles: effects on force generation, Ca²⁺ sensitivity and Ca²⁺ binding. *Journal of molecular and cellular cardiology*, 1995. **27**(6): p. 1235-44.

154. **Warren, S.A., L.E. Briggs, H. Zeng, J. Chuang, E.I. Chang, R. Terada, M. Li, M.S. Swanson, S.H. Lecker, M.S. Willis, F.G. Spinale, J. Maupin-Furlowe, J.R. McMullen, R.L. Moss, and H. Kasahara,** Myosin light chain phosphorylation is critical for adaptation to cardiac stress. *Circulation*, 2012. **126**(22): p. 2575-88.
155. **Warshaw, D.M., J.M. Desrosiers, S.S. Work, and K.M. Trybus,** Smooth muscle myosin cross-bridge interactions modulate actin filament sliding velocity in vitro. *The Journal of cell biology*, 1990. **111**(2): p. 453-63.
156. **Watkins, H., J.G. Seidman, and C.E. Seidman,** Familial hypertrophic cardiomyopathy: a genetic model of cardiac hypertrophy. *Human molecular genetics*, 1995. **4 Spec No**: p. 1721-7.
157. **Whittaker, M., E.M. Wilson-Kubalek, J.E. Smith, L. Faust, R.A. Milligan, and H.L. Sweeney,** A 35-A movement of smooth muscle myosin on ADP release. *Nature*, 1995. **378**(6558): p. 748-51.
158. **Zhi, G., B.P. Herring, and J.T. Stull,** Structural requirements for phosphorylation of myosin regulatory light chain from smooth muscle. *The Journal of biological chemistry*, 1994. **269**(40): p. 24723-7.

CURRICULUM VITAE

Anastasia Smaro Karabina

Address: Department of Biological Sciences
University of Massachusetts, Lowell
198 Riverside St., Lowell MA 01854

Phone: 810-348-3316

Email: anastasia.karabina@gmail.com

Year of Birth: 1987

EDUCATION

B.S., Physics. University of Michigan, Ann Arbor, MI.

April 2008

Ph.D., Biophysics. Boston University, Boston, MA.

August 2015

RESEARCH EXPERIENCE

Boston University School of Medicine, Boston MA

May 2009 - Aug 2015

Graduate Researcher

Laboratory of Dr. Jeffrey Moore, Department of Physiology and Biophysics

- Used fluorescence microscopy to investigate the effects of familial hypertrophic cardiomyopathy mutations and myosin regulatory light chain phosphorylation on cardiac myosin contractility
- Used molecular dynamics (MD) simulations to investigate tertiary and quaternary structure of smooth muscle tropomyosin heterodimers

University of Michigan, Ann Arbor MI

May 2006 - Apr 2008

Undergraduate Researcher

Laboratory of Dr. Wolfgang Lorenzon, Department of Physics

- Hardware design and system optimization to measure the uniformity and quantum efficiency of near-infrared CCDs for use in a space-based telescope
- Thesis: "Characterizing the Absolute Quantum Efficiency of SNAP Near-IR Photodetectors"

Centre for Research and Technology-Hellas (CERTH), Themi, Greece

May - Jul 2005

Research Intern

Aerosol & Particle Technology Laboratory (APTL), Dr. Athanasios Konstandopoulos

- Digitally reconstructed the microstructure of ceramic foam material for use in diesel engine emission filters
- Database Entry

PUBLICATIONS

Karabina A, Kazmierczak K, Szczesna-Cordary D, Moore J. (2015) *Myosin Regulatory Light Chain Phosphorylation Enhances Cardiac β -myosin In Vitro Motility Under Load*. Archives of Biochemistry and Biophysics 580:14-21.

GRANTS AND AWARDS

American Heart Association Founders Affiliate Predoctoral Fellowship
Jul 2012 - Jun 2014

20th Annual Henry I. Russek Student Achievement Day - First Place Award
May 2, 2014

Dean's List University Honors
Fall 2004, Fall 2006

INVITED TALKS

Myofilament Meeting: Modulators and Modifiers of Myofilament Function *Jun 2014*
Madison, WI
Myosin Bearing Familial Hypertrophic Cardiomyopathy Mutations Respond to Regulatory Light Chain Phosphorylation

PRESENTATIONS

Biophysical Society 59th Annual Meeting, Baltimore, MD *Feb 2015*
Poster presentation:
The Effects of Myosin Regulatory Light Chain Phosphorylation on Cardiac Myosin Mechanics in Health and Disease

Washington State University, Pullman, WA *Oct 2014*
Washington Center for Muscle Biology Seminar (Invited Speaker):
The Effect of Regulatory Light Chain Phosphorylation on Mutant and Wild-type Cardiac Myosin Mechanochemistry

Biophysical Society 58th Annual Meeting, San Francisco, CA *Feb 2014*
Poster presentation:
The Effect of Myosin Regulatory Light Chain Phosphorylation on Mutant Myosin Mechanics

Biophysical Society 57th Annual Meeting, Philadelphia, PA *Feb 2013*
Poster presentation:
The Effect of the Regulatory Light Chain Phosphorylation on Myosin Bearing Familial Hypertrophic Cardiomyopathy-linked Mutations

Gordon Research Conference: Muscle & Molecular Motors, New London, NH *Jul 2011*
Poster presentation:
Molecular Dynamics Simulations of Smooth Muscle Tropomyosin Heterodimers

Biophysical Society 55th Annual Meeting, Baltimore, MD *Mar 2011*
Poster presentation:
Molecular Dynamics Simulations of Smooth Muscle Tropomyosin Heterodimers

UNIVERSITY SERVICE

BU Graduate Medical Sciences Student Organization (GMSSO) *Jul 2011 - Dec 2014*
Department of Biophysics and Physiology Representative

Commonwealth Avenue Reconstruction Project *May 2014 - Nov 2014*
Boston University Subcommittee

Professional Development Award Committee *Oct 2011 - Oct 2014*
Designed criteria for award selection, selected winners each semester

Hellenic Student Association (HSA) *Sep 2004 - Apr 2008*
Member, Secretary

K-grams *Sep 2005 - Sep 2006*
Write to elementary pen-pal monthly

PROFESSIONAL MEMBERSHIPS

Biophysical Society *Jan 2010 - Present*

American Heart Association *Jan 2012 - Dec 2014*